J. Mech. Phys. Solids 175 (2023) 105291

Contents lists available at ScienceDirect

Journal of the Mechanics and Physics of Solids

journal homepage: www.elsevier.com/locate/jmps

# Constitutive modelling of fibre networks with stretch distributions, Part II: Alternative representation, affine distribution and anisotropy

Ben R. Britt *, Alexander E. Ehret *

*Empa, Swiss Federal Laboratories for Materials Science and Technology, Überlandstrasse 129, CH-8600 Dübendorf, Switzerland*
*ETH Zurich, Institute for Mechanical Systems, Leonhardstrasse 21, CH-8092 Zürich, Switzerland*

ARTICLE INFO

*Keywords:*
Random fibre network
Multiscale modelling
Affine deformation
Anisotropy
Statistical moments
Generalised structural tensors

ABSTRACT

In this paper, the concept for modelling materials with fibre network microstructures introduced in Part I of this series is reconsidered. At first, an alternative representation of the theory is provided that entails advantages in terms of numerical implementation. Next, the new constitutive approach is applied to affine networks, whose fibre stretches are distributed according to the affine distribution. Despite the tremendously widespread use of this model, it seems that the general form of the corresponding distribution has remained largely unexplored to date. The thus obtained reformulation of the affine full network model provides deep insight into this concept, and may help overcoming well-known numerical problems with the associated spherical integration, e.g. when highly non-linear or piece-wise defined fibre laws are used. The latter case is typical for applications in biomechanics, where fibres are frequently assumed to have negligible compressive resistance. While the developments of our theory thus far had focused on isotropic networks, we here showcase for the affine case how the anisotropy caused by non-uniform directional distributions of the fibres can be incorporated in the novel approach. Finally, it is shown that several earlier approaches to model networks of affinely deforming fibres or polymer chains result as special cases of our theory.

## 1. Introduction

In Part I of this work we proposed a new method to model the homogenised behaviour of materials with random fibre network microstructure, based on the distribution of stretch among the fibres within the network.

The stretch distribution was assumed to be characterised through its probability density function. While this seems the natural choice, averaging over the latter can become cumbersome since it may contain essential discontinuities. Even arguably just a technical detail, the density function formally does not even need to exist (see e.g. Durrett, 2019). For this reason, the first goal of this paper is to reformulate the new modelling strategy in terms of the cumulative distribution function, which in some cases might represent the favourable choice.

One of these cases concerns affine kinematics. Although the method proposed in Part I applies to central force networks in general and is in particular *not* restricted to affine networks, it clearly includes the latter as a special case. Even if the discussion on whether affine or non-affine kinematics better apply to network materials is ongoing (see e.g. Chandran and Barocas, 2006; Fan and Sacks, 2014; Amores et al., 2021; Stracuzzi et al., 2022), and most probably conclusions can only be drawn on a material-specific

* Corresponding authors at: Empa, Swiss Federal Laboratories for Materials Science and Technology, Überlandstrasse 129, CH-8600 Dübendorf, Switzerland.
*E-mail addresses:* ben-rudolf.britt@empa.ch (B.R. Britt), alexander.ehret@empa.ch (A.E. Ehret).

https://doi.org/10.1016/j.jmps.2023.105291
Received 9 December 2022; Received in revised form 21 March 2023; Accepted 27 March 2023
Available online 5 April 2023

basis, the affine network is still of paramount interest in many fields of mechanics including rubber-elasticity and biomechanics, where the corresponding modelling approaches are frequently referred to as 'affine full network' (Treloar et al., 1979; Wu and Van Der Giessen, 1993) and 'structural approach' (Lanir, 1979; Billiar and Sacks, 2000; Kassab and Sacks, 2016), respectively. These concepts have become a state-of-the art method in soft material constitutive modelling, and it is therefore even more surprising that the corresponding distribution of stretch among the fibres of an affine network has apparently never been studied rigorously, notwithstanding some special cases and visual representations discussed later. A comprehensive analysis and representation of the affine stretch distribution thus forms the second goal of this paper.

Effectively, the affine network is used as an averaging operation to deduce the mechanical response of a large ensemble of polymer chains or biological fibres, which form the macroscopic material, from the mechanical behaviour of the individual ones. The behaviour of the latter is typically considered in terms of their 'axial' properties, i.e. their response to a change in end-to-end distance. Therefore, the averaging not only generalises from one to many fibres, but also from one to two or three-dimensional space, in which the fibre ensemble forms a macroscopic body. The single chain or fibre – and for simplicity, we will restrict to the latter term – is associated with a direction in space, so that the implementation of the averaging operation is based on an integral over the set of unit vectors in $d$-dimensional Euclidean space, i.e. the unit sphere. In many relevant cases the integrand, i.e. the strain-energy density of the fibre expressed in terms of measures of axial strain, does not allow for analytical integration, and the integral is approximated by numerical cubature, so that the integral turns into a finite sum of terms evaluated for a set of spatial directions. Although these 'discretised' versions of the concept have proven excellent applicability in various fields, the method is not free of problems. Evidently, these quadrature rules on the sphere only approximate the exact solution, and for many types of quadrature, the limits can be expressed by the degree of spherical polynomials up to which the integration rule is exact (see e.g. Freeden and Gutting, 2017). While a certain numerical error might be acceptable, it was noted regularly that the corresponding discretisation of the sphere with fixed positions of the integration points also induces (additional) anisotropy (e.g. Bažant and Oh, 1986; Badel and Leblond, 2004; Alastrué et al., 2009a; Ehret et al., 2010; Verron, 2015; Itskov, 2016). Both refined integration methods as, e.g., non-linear transformations (Alastrué et al., 2009b; Goldberg and Ihlemann, 2017), as well as the steady increase in available computational power may serve to overcome these problems inherent to numerical quadrature. Nevertheless, the spherical integration of constitutive equations has also been addressed in alternative ways. For isotropic networks Itskov et al. (2010) proposed a method based on a Taylor series expansion of the integrand whose single terms can be integrated over the sphere in closed form. In this way, the approximated integral was solved analytically and expressed in terms of isotropic strain invariants. Independently, several authors have used Taylor series expansions of the integrand in models for soft biological tissues with non-uniformly distributed fibres, and included terms up to order 2 in their formulations (Pandolfi and Vasta, 2012; Vasta et al., 2014; Gizzi et al., 2014). Cortes and Elliott (2014) developed models up to a general order $n$, including the components of the corresponding 'generalised higher order structural tensors' (Cortes and Elliott, 2014), essentially 'fabric tensors' (Kanatani, 1984; Ken-Ichi, 1984) that characterise the anisotropy. A further rigorous analysis of the series expansion-based approach for distributed fibres was elaborated by Hashlamoun et al. (2016), who developed the series with respect to different arguments. In the present contribution we will show that these approaches for tissues with non-uniformly distributed fibres and the analytic isotropic full network approach (Itskov et al., 2010) are closely related if interpreted in terms of the statistics of stretch.

While the mentioned concepts to include non-uniformly distributed fibres were all based on integrating the terms of the series over the unit sphere, Gizzi et al. (2016) noted that the integral can be re-expressed in special deformation states by a change of variables in terms of the probability density of an invariant that represents the squared fibre stretch. The associated benefit when using models that exclude compressed fibres was discussed and the approach was further elaborated for more general isochoric states of deformation (Vasta et al., 2018). The results can be interpreted as special cases of the theory presented in Part I (Britt and Ehret, 2022), when the probability density of the affine model is used and applied to a particular class of materials. We will show in the present Part II of this work that this special case can be generalised and that the full affine network – isotropic or anisotropic – can be integrated by use of the probability density of stretch. However, we also explain why this formulation comes with computational disadvantages and therefore adapt the new strategy, based on the cumulative distribution function, to the affine case.

Hence the third goal of the present work is resuming and extending the strategies at hand to integrate full network and structural models.

The paper is organised as follows: In Section 2 the key aspects of the approach proposed in Part I of this work (Britt and Ehret, 2022) will be resumed. Section 3 then focuses on an alternative representation of the concept in terms of the cumulative distribution function of the stretch in the general non-affine case, and introduces the distribution of squared stretch. Sections 4 and 5 are dedicated to the affine distribution of stretch and square stretch, and to the moments of the latter. After an intermediate summary in Section 6, we discuss and exemplify reformulations of affine full-network models in terms of these moments (Section 7) and the cumulative distribution function (Section 8). The paper closes with summarising conclusions and several appendices with supporting and additional content.

## 2. Modelling with stretch distributions

Microstructurally motivated models that account for the mechanical behaviour of fibre network materials typically consider two length-scales: The macroscopic length scale at which the network appears as a continuous material since each macroscopic material 'point' comprises a sufficiently large region of the network, and the microscopic length scale, associated with the behaviour of single fibres or their end-to-end links within the network. Further length scales of relevance may occur, e.g. when, in turn, the behaviour of the single fibres is explained in terms of their internal structure, but such considerations are beyond the scope of the present paper. Therefore, we briefly resume in this section the description of kinematics and free energy at the two length scales of interest, and how the two scales were bridged in the approach proposed in Part I of this work.

### 2.1. Macroscopic kinematics and constitutive theory

At the macroscopic length scale, the kinematics and properties of the network material are expressed in terms of the framework of rational continuum mechanics (see e.g. Truesdell and Noll, 2004). The deformation of a material body from the reference to the current configuration $\mathcal{B}_0$ and $\mathcal{B}_t$, respectively, is described through the motion $\boldsymbol{x} = \boldsymbol{\varphi}(\boldsymbol{X}, t)$ at fixed time $t$ of its material points with referential and current position vectors $\boldsymbol{X}$ and $\boldsymbol{x}$, respectively. Let $\mathbf{F} = \partial\boldsymbol{\varphi}/\partial\boldsymbol{X}$ denote the corresponding deformation gradient with determinant $J = \det\mathbf{F} > 0$, based on which one defines the right Cauchy–Green tensor $\mathbf{C} = \mathbf{F}^{\mathrm{T}}\mathbf{F}$. The latter has the spectral representation

$$\mathbf{C} = \sum_{i=1}^{3} \Lambda_i \, \boldsymbol{N}_i \otimes \boldsymbol{N}_i \tag{1}$$

with eigenvalues $\Lambda_i$ and eigenvectors $\boldsymbol{N}_i$, and its invariants are given by

$$I_1 = \mathrm{tr}\mathbf{C} = \Lambda_1 + \Lambda_2, \quad I_2 = \det\mathbf{C} = \Lambda_1\Lambda_2 \tag{2}$$

in 2D space ($d = 2$) and

$$I_1 = \mathrm{tr}\mathbf{C} = \Lambda_1 + \Lambda_2 + \Lambda_3, \quad I_2 = \frac{1}{2}\left(I_1^2 - \mathrm{tr}\mathbf{C}^2\right) = \Lambda_1\Lambda_2 + \Lambda_2\Lambda_3 + \Lambda_3\Lambda_1, \quad I_3 = \det\mathbf{C} = \Lambda_1\Lambda_2\Lambda_3 \tag{3}$$

in 3D space ($d = 3$). For a macroscopically hyperelastic network material arguments of material frame indifference (Truesdell and Noll, 2004, Sec. 10) suggest to express the free energy $\Psi$ per unit reference volume of the network material at $\boldsymbol{X}$ in terms of a scalar valued tensor function of $\mathbf{C}$. Since in the present work the heterogeneity of the network material at the macroscopic length scale is irrelevant, we omit the potential explicit dependence of $\Psi$ on $\boldsymbol{X}$ in writing and define the function $\hat{\Psi} : \mathbf{C} \mapsto \Psi$, which defines the free energy density for any given state of strain expressed in terms of $\mathbf{C}$. For a hyperelastic unconstrained material the second Piola–Kirchhoff stress $\mathbf{S}$ and the fourth-order tangent tensor $\mathbb{C}$ calculate as

$$\mathbf{S} = 2\frac{\partial\hat{\Psi}}{\partial\mathbf{C}}, \quad \mathbb{C} = 2\frac{\partial\mathbf{S}}{\partial\mathbf{C}} = 4\frac{\partial^2\hat{\Psi}}{\partial\mathbf{C}\partial\mathbf{C}}. \tag{4}$$

We assume that the reference configuration $\mathcal{B}_0$ is associated with an energy- and stress-free state of the material, i.e. $\hat{\Psi}(\mathbf{I}) = 0$ and $\mathbf{S}(\mathbf{I}) = \mathbf{0}$.

### 2.2. Fibre-scale kinematics and constitutive theory

At the microscopic length scale, we assume that the material properties are determined through a constitutive function that represents the free energy density $\psi(\omega)$ of a fibre characterised through its deformation state $\omega$, which in turn may be characterised through a set of state variables such as the fibre's stretch, curvature etc. In general, this state may depend on the past history of deformation, but here we will restrict to the elastic case and thus assume that $\omega$ is defined by the current state of fibre deformation. We further remark that fibres are often represented as one-dimensional rather than bulky structures in modelling, and that $\psi$ has the dimension of energy per length in this case.

### 2.3. Micro–macro transition based on micro-kinematic distributions

In Part I (Britt and Ehret, 2022) of this series of papers the fibre network energy density was identified to be proportional to the expected value of the fibre energy

$$\bar{\psi} = \mathrm{E}[\psi] = \int_{\Omega} \psi(\omega)\,\mathrm{d}P(\omega), \tag{5}$$

where $\psi(\omega)$ is the energy density associated with a state $\omega \in \Omega$ of deformed fibre element with elemental probability $\mathrm{d}P(\omega)$.

In order to obtain the free energy density of the network material, we considered a representative volume element (RVE) of the network with reference configuration $\mathcal{B}_0$, and corresponding reference volume $|\mathcal{B}_0| = V_{\mathrm{RVE}}$. This RVE typically contains void regions and a certain amount of fibres, that can be quantified by its cumulative generalised $d$-dimensional (referential) volume $|C_0|$. If fibres are considered one-dimensional structures, for example, $|C_0|$ amounts to the total fibre length ($L_{\mathrm{tot}}$). Since energy is only stored in the fibres and not in the void regions of the RVE, the homogenised free energy density $\Psi$ of the network material results from the average (5) formed over the fibres within the RVE, multiplied by the 'fibre volume fraction' $\nu_{\mathrm{f}} = |C_0|/|\mathcal{B}_0|$, i.e. the ratio between fibre and RVE (referential) volume, so that

$$\Psi = \nu_{\mathrm{f}}\,\bar{\psi} = \nu_{\mathrm{f}}\,\mathrm{E}[\psi]\,. \tag{6}$$

We emphasise that $\nu_{\mathrm{f}}$ is not a dimensionless quantity in general, but accounts for the different 'dimensionality' associated with the fibres and RVE.

There is generally a difference between the (potentially curved) fibres and the straight links connecting their ends at which they are connected (cf. Britt and Ehret, 2022). In central force networks, the fibre response is typically lumped into a relation between its end-to-end distance and the force acting along this line, and the terms 'link' and 'fibre' are used synonymously. As in Part I, we will restrict to central force networks, so that the free energy density $\psi$ of a fibre can be completely expressed in terms of the fibre

stretch $\lambda$ along the link between two cross-links of a fibre, i.e. the straight line joining the fibre ends, so that $\psi = \psi_\lambda \circ \lambda$. Accordingly, $|C_0|$ represents the total link length in what follows, i.e. the sum of length of all end-to-end vectors between the cross-links. The relevant kinematic state $\omega$ of a fibre (or link) element is thus entirely characterised through the stretch $\lambda$ that is naturally defined on $(0, \infty)$, i.e. the positive reals $\mathbb{R}_{>0}$. Correspondingly, by combination of Eqs. (5) and (6) we obtained a universal expression for the free energy density of a central force network as (Britt and Ehret, 2022)

$$\boxed{\Psi = \nu_\mathrm{f} \int_{\mathbb{R}_{>0}} \psi_\lambda(z)\, \mathrm{d}P_\lambda(z)\,,} \tag{7}$$

where $P_\lambda((0,z]) = P[\{\omega : \lambda(\omega) \leq z\}]$ (see e.g. Durrett, 2019) is the stretch distribution. If the corresponding probability density function (PDF) $p_\lambda(z) = \mathrm{PDF}_\lambda(z)$ exists, this is equivalent to (Britt and Ehret, 2022)

$$\Psi = \nu_\mathrm{f} \int_{\mathbb{R}_{>0}} \psi_\lambda(z)\, \mathrm{PDF}_\lambda(z)\, \mathrm{d}z\,. \tag{8}$$

Next, we resume a particular result for the important special case, where the fibre free energy density $\psi_\lambda$ is given in terms of an analytic function, so that it can be expressed in terms of a Taylor series about an expansion point $\lambda_0$. Linearity of the expectation operator then allows to rewrite $\bar{\psi}$ in terms of the Taylor series coefficients of $\psi_\lambda$ and the moments of the stretch distribution, and one obtains (Britt and Ehret, 2022)

$$\bar{\psi} = \mathrm{E}\left[\psi\right] = \mathrm{E}\left[\sum_{k=0}^{\infty} \frac{1}{k!} \frac{\partial^k \psi_\lambda}{\partial \lambda^k}\bigg|_{\lambda_0} (\lambda - \lambda_0)^k\right] = \sum_{k=0}^{\infty} \frac{1}{k!} \frac{\partial^k \psi_\lambda}{\partial \lambda^k}\bigg|_{\lambda_0} \mu_{\lambda_0,k}\,, \tag{9}$$

where $\mu_{\lambda_0,k} = \mathrm{E}\left[(\lambda - \lambda_0)^k\right]$ is the $k$th moment of the stretch $\lambda$ with respect to $\lambda_0$. Eq. (9) entails two important consequences (Britt and Ehret, 2022): At first it proves that for a fibre free energy function of polynomial degree $n$, only the first $n+1$ moments of the distribution are required to fully recover the averaged energy. Second, the contribution of higher moments decreases with increasing $k$ if $|\lambda - \lambda_0| < 1$, and thus underlines the role of the expansion point $\lambda_0$. In fact, upon a thoughtful choice of the latter, a truncated form of the series (9) may be sufficient to obtain a good approximation of the averaged energy in a stretch range of interest.

### 2.4. Comparison with directional averaging

In Part I we opposed Eq. (7) to the 'canonical' averaging over the fibre orientation distribution with elemental probability $\mathrm{d}P_{\boldsymbol{N}}(\boldsymbol{z})$ on the unit sphere $\mathcal{S}$

$$\boxed{\Psi = \nu_\mathrm{f}\, \bar{\psi} = \nu_\mathrm{f} \int_{\mathcal{S}} \psi_\lambda\big(\lambda_{\boldsymbol{N}}(\boldsymbol{z})\big)\, \mathrm{d}P_{\boldsymbol{N}}(\boldsymbol{z})\,,} \tag{10}$$

which is inherent to many common techniques in literature (see Britt and Ehret, 2022), and in which the fibre stretch $\lambda$ is assumed to be deterministically defined in terms of the mapping[1] $\lambda_{\boldsymbol{N}} : \mathbf{F}, \boldsymbol{N} \mapsto \lambda$ of the macroscopic deformation $\mathbf{F}$ and the unit vector $\boldsymbol{N}$ characterising the orientation of a fibre link in the reference configuration. We noted that Eq. (10) is clearly another embodiment of Eq. (5), in which $\boldsymbol{N}$ is the only quantity defining the kinematic state of a fibre element for a given $\mathbf{F}$. However, it is a special case dependent on the existence of the mapping $\lambda_{\boldsymbol{N}}$. The most prominent example of such a mapping is the affine relation $\lambda_{\boldsymbol{N}} = \|\mathbf{F}\boldsymbol{N}\|$, which is at the basis of e.g. the affine full-network model of rubber elasticity (Treloar et al., 1979; Wu and Van Der Giessen, 1993) or the structural approach in soft tissue biomechanics (Lanir, 1979; Billiar and Sacks, 2000). Notably, the more general formulation of the average (7) also holds in this case. It will be one of the goals of the present work to elaborate this representation and study some properties of the corresponding 'affine stretch distribution' that results from the reformulation of the affine model. Before this distribution is studied in Section 4, we first present in the next section alternative formulations of Eq. (7) in terms of the cumulative distribution function (CDF), and in terms of the square stretch, which will both turn out to be advantageous in the analysis of the affine model.

## 3. Alternative representations

### 3.1. Averaged free energy in terms of the CDF

The representation of the averaged free energy (7) for a specific distribution in terms of the PDF according to Eq. (8) represents the most evident form to evaluate $\bar{\psi}$. However, (7) can be evaluated even if the PDF does not exist, or if its integration is cumbersome, e.g. due to asymptotic behaviour. In general one can alternatively express $\bar{\psi}$ (7) in terms of the cumulative distribution function (CDF) of the stretch and one can proof the following statement:

Let $\mathrm{CDF}_\lambda$ represent the cumulative distribution function

$$\mathrm{CDF}_\lambda(z) = P(\lambda \leq z) = \int_{(0,z]} \mathrm{d}P_\lambda(z)\,, \tag{11}$$

[1] The dependence of $\lambda_{\boldsymbol{N}}$ on the macroscopic state of deformation $\mathbf{F}$ is understood and will be omitted in writing for the sake of brevity.

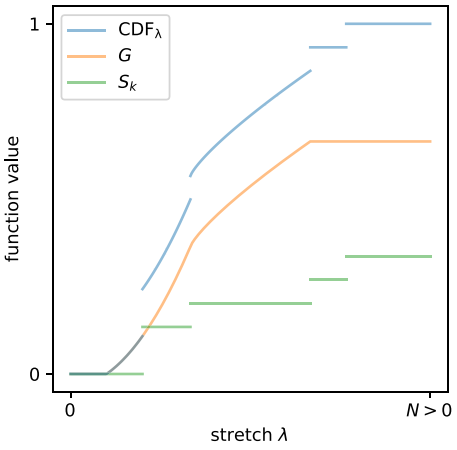


**Fig. 1.** Illustration of a CDF with jump discontinuities as a sum of a continuous function $G$ and multiple step functions $S_k$.

then the averaged free energy $\bar{\psi}$ is obtained as

$$\boxed{\bar{\psi} = \psi_\lambda(a) - \int_0^a \psi'_\lambda \mathrm{CDF}_\lambda \,\mathrm{d}z - \int_a^\infty \psi'_\lambda(\mathrm{CDF}_\lambda - 1)\,\mathrm{d}z\,,} \tag{12}$$

where $a \in (0, \infty)$ is an arbitrary stretch value.

**Proof.** In the general case $\mathrm{CDF}_\lambda$ can have countably but infinitely many jump discontinuities at $\{z_k\}$ so that it can be represented as a superposition of a continuous function $G$ and a linear combination of step functions $\{S_k\}$ representing the jump at each discontinuity $k$ as (Fig. 1)

$$\mathrm{CDF}_\lambda(z) = G(z) + \sum_k S_k(z), \quad S_k = s_k H(z - z_k)\,, \tag{13}$$

where $H$ is the Heaviside function. Correspondingly, $\mathrm{d}P_\lambda$ can be decomposed as

$$\mathrm{d}P_\lambda(z) = G'(z)\,\mathrm{d}z + \sum_k s_k \,\mathrm{d}\eta_{z_k}\,, \tag{14}$$

with density $G'$ and Dirac distributions $\{\eta_{z_k}\}$ centred at $z_k$, so that Eq. (11) is satisfied. Consideration of (14) in (7) and (6) allows rewriting the free energy density as

$$\bar{\psi} = \int_{(0,\infty)} \psi_\lambda \,\mathrm{d}P_\lambda = \int_{(0,\infty)} \psi_\lambda \left[G'\,\mathrm{d}z + \sum_k s_k \,\mathrm{d}\eta_{z_k}\right]. \tag{15}$$

Splitting the integration boundaries of the continuous term into intervals $(0, a]$ and $(a, \infty)$, integrating by parts and rewriting the step term yields

$$\bar{\psi} = \psi_\lambda G\Big|_0^a - \int_0^a \psi'_\lambda G\,\mathrm{d}z + \psi_\lambda\left[G - 1 + \sum_k s_k\right]\Big|_a^\infty - \int_a^\infty \psi'_\lambda\left[G - 1 + \sum_k s_k\right]\mathrm{d}z + \sum_k s_k \psi_\lambda(z_k)\,, \tag{16}$$

where it was used that both $G$ and $G - 1 + \sum_k s_k$ are antiderivatives of $G'$ such that the boundary terms evaluated at 0 and $\infty$ vanish. Further using

$$s_k \psi_\lambda(z_k) = s_k \psi_\lambda(a) + \int_a^0 \psi'_\lambda S_k \,\mathrm{d}z + \int_a^\infty \psi'_\lambda(s_k - S_k)\,\mathrm{d}z\,, \tag{17}$$

the remaining parts can be written as

$$\bar{\psi} = \psi_\lambda(a) - \int_0^a \psi'_\lambda\left(G + \sum_k S_k\right)\mathrm{d}z - \int_a^\infty \psi'_\lambda\left(G - 1 + \sum_k S_k\right)\mathrm{d}z = \psi_\lambda(a) - \int_0^a \psi'_\lambda \mathrm{CDF}_\lambda \,\mathrm{d}z - \int_a^\infty \psi'_\lambda(\mathrm{CDF}_\lambda - 1)\,\mathrm{d}z\,, \tag{18}$$

which is Eq. (12). □

### 3.2. Distribution of the square stretch

In Part I of the work (Britt and Ehret, 2022, Remark 7) we had anticipated that it may be advantageous to study the distribution of other stretch or strain measures. In fact the strictly positive sign of the stretch renders the relation $\Lambda = \lambda^2$ between the simple

and squared stretch one-to-one, so that the probability of a stretch $\lambda$ smaller or equal to $\lambda^*$ must coincide with the probability of a square stretch $\Lambda$ smaller or equal to $\Lambda^* = \lambda^{*2}$, i.e.

$$P[\lambda \leq \lambda^*] = \mathrm{CDF}_\lambda(\lambda^*) = \mathrm{CDF}_\Lambda\left(\lambda^{*2}\right) = P\left[\Lambda \leq \lambda^{*2}\right], \tag{19}$$

and, if the corresponding densities $\mathrm{PDF}_\lambda$ and $\mathrm{PDF}_\Lambda$ exist,[2] it follows that

$$\mathrm{PDF}_\lambda(\lambda^*) = 2\lambda^* \,\mathrm{PDF}_\Lambda\left(\lambda^{*2}\right). \tag{20}$$

Based on the same arguments, one may rewrite the fibre free energy density in terms of the squared stretch, i.e.

$$\psi = \psi_\Lambda(\Lambda) = \psi_\lambda(\lambda). \tag{21}$$

It will be seen in Section 4 that the reformulation of the theory in terms of the squared stretch $\Lambda$, i.e. considering the corresponding distribution $P_\Lambda$, respectively $\mathrm{CDF}_\Lambda(\Lambda)$, is particularly useful to study the affine model. We remark that the equations in Sections 2.3 and 3.1 maintain their validity if interpreted for the squared stretch. Hence, the averaged energy can be given – analogous to Eq. (12) – in terms of the CDF of the squared stretch (19) as

$$\boxed{\bar{\psi} = \psi_\Lambda(A) - \int_0^A \psi'_\Lambda(z)\,\mathrm{CDF}_\Lambda(z)\,\mathrm{d}z - \int_A^\infty \psi'_\Lambda(z)\,(\mathrm{CDF}_\Lambda(z) - 1)\,\mathrm{d}z,} \tag{22}$$

analogous to Eq. (8) in terms of the corresponding PDF (if it exists)

$$\bar{\psi} = \int_0^\infty \psi_\Lambda(z)\,\mathrm{PDF}_\Lambda(z)\,\mathrm{d}z, \tag{23}$$

and – provided the fibre free energy function $\psi_\Lambda$ is analytic – in terms of the moments

$$\mathrm{M}_{\Lambda_0,k} = \mathrm{E}\left[(\Lambda - \Lambda_0)^k\right] \tag{24}$$

of the squared stretch, in analogy to Eq. (9), so that

$$\boxed{\bar{\psi} = \mathrm{E}[\psi] = \mathrm{E}\left[\sum_{k=0}^{\infty} \frac{1}{k!} \frac{\partial^k \psi_\Lambda}{\partial \Lambda^k}\bigg|_{\Lambda_0} (\Lambda - \Lambda_0)^k\right] = \sum_{k=0}^{\infty} \frac{1}{k!} \frac{\partial^k \psi_\Lambda}{\partial \Lambda^k}\bigg|_{\Lambda_0} \mathrm{M}_{\Lambda_0,k}.} \tag{25}$$

Notably, the representations of the free energy Eqs. (12) and (22), Eqs. (8) and (23) as well as Eqs. (9) and (25) only differ with regard to the variable ($\lambda$ or $\Lambda$), i.e. the interpretation of the stretch.

## 4. The affine stretch distribution

Although the affine network model belongs without any doubt to the most widespread concepts for modelling materials with network microstructures, the corresponding distribution of stretch implied by this very particular model has little been studied. Indeed the corresponding PDF has been illustrated in histograms that were obtained from discrete network simulations (Chandran and Barocas, 2006; Zündel et al., 2017; Stracuzzi et al., 2022), as in Part I of this work, to exemplify the mismatch between affine predictions and non-affine computational results. For special cases a mathematical representation of the PDF has been provided by Gizzi et al. (2016) and Vasta et al. (2018), who showed how the PDF of a pseudo-invariant corresponding to the affine stretch square can be obtained from the orientation distribution by a change of variables, and they computed the PDF for a selection of different kinematic states and a von Mises-type transversely isotropic fibre dispersion about a principal direction. As will be seen in this section, affine PDFs contain singularities, which pose a challenge for the numeric integration of the fibre energy (23). Contrariwise, the corresponding CDFs are continuous and monotonically increasing functions with values between 0 and 1. These properties of the affine CDF suggest the use of the alternative representation (12) to compute the averaged free energy and its derivatives in the affine model. To this end, we derive here the CDF of the affine stretch distribution for arbitrary load cases and fibre orientation distributions in what follows.

### 4.1. The affine stretch

The affine model determines the stretch $\lambda_{\boldsymbol{N}}$ and normalised direction vector $\boldsymbol{n}$ of any fibre with referential orientation specified by the unit vector $\boldsymbol{N}$ through the linear mapping

$$\lambda_{\boldsymbol{N}} \boldsymbol{n} = \mathbf{F}\boldsymbol{N} \tag{26}$$

in terms of the deformation gradient $\mathbf{F}$. The corresponding distribution of stretch $P_\lambda$, and thus the cumulative distribution function $\mathrm{CDF}_\lambda$ are therefore fully determined through the macroscopic state of deformation contained in $\mathbf{F}$ and the initial orientation

[2] It will be seen in Section 4 that this requirement is satisfied for the special case of affine deformations if the initial fibre orientation distribution is continuous, unless all stretches are equal (pure dilation).

distribution of the fibres in the network. Specifically the probability of a stretch within the interval $\mathcal{I} \subseteq \mathbb{R}_{>0}$ is identical to the probability of initial orientation vectors which return such stretches $\{\boldsymbol{N}, \lambda_{\boldsymbol{N}} \in \mathcal{I}\}$, i.e.

$$P_\lambda(\mathcal{I}) = P_{\boldsymbol{N}}(\{\boldsymbol{N} : \lambda_{\boldsymbol{N}} \in \mathcal{I}\}), \tag{27}$$

or in integral notation

$$\int_{\mathcal{I}} \mathrm{d}P_\lambda = \int_{\{\boldsymbol{N}:\lambda_{\boldsymbol{N}}\in\mathcal{I}\}} \mathrm{d}P_{\boldsymbol{N}}, \tag{28}$$

for all intervals $\mathcal{I} \subseteq \mathbb{R}_{>0}$.

We will continue the analysis of the affine model in terms of the distribution of the square stretch $\Lambda = \lambda^2$, as introduced in Section 3.2. To this end, we recall at first that the square stretch satisfies

$$\Lambda = \lambda_{\boldsymbol{N}}^2 = \boldsymbol{N} \cdot \mathbf{C}\boldsymbol{N} = \boldsymbol{N} \cdot \left( \sum_{i=1}^{d} \Lambda_i \, \boldsymbol{N}_i \otimes \boldsymbol{N}_i \right) \boldsymbol{N} = \Lambda_i \, (\boldsymbol{N} \cdot \boldsymbol{N}_i)^2, \tag{29}$$

where $\{\boldsymbol{N}_i\}$ denote the eigenvectors of $\mathbf{C}$ corresponding to the eigenvalues $\Lambda_i$. Introducing spherical coordinates $\phi \in (-\pi, \pi]$ and $\theta \in [0, \pi]$ with respect to the material principal axes, the projections of the orientation vector $\boldsymbol{N}$ onto the principal axes $\{\boldsymbol{N}_i\}$ can be expressed as

$$\boldsymbol{N} \cdot \boldsymbol{N}_1 = \cos(\phi), \quad \boldsymbol{N} \cdot \boldsymbol{N}_2 = \sin(\phi) \tag{30}$$

in 2D ($d = 2$), illustrated in Fig. 2a, and

$$\boldsymbol{N} \cdot \boldsymbol{N}_1 = \cos(\phi)\sin(\theta), \quad \boldsymbol{N} \cdot \boldsymbol{N}_2 = \sin(\phi)\sin(\theta), \quad \boldsymbol{N} \cdot \boldsymbol{N}_3 = \cos(\theta) \tag{31}$$

in 3D ($d = 3$), and one finds the well known expressions

$$\Lambda = \begin{cases} \Lambda_1 \cos^2(\phi) + \Lambda_2 \sin^2(\phi) & \text{for } d = 2, \\ \Lambda_1 \cos^2(\phi)\sin^2(\theta) + \Lambda_2 \sin^2(\phi)\sin^2(\theta) + \Lambda_3 \cos^2(\theta) & \text{for } d = 3. \end{cases} \tag{32}$$

Albeit well known, it is emphasised that the minimum and maximum eigenvalue $\Lambda_d$ and $\Lambda_1$, respectively, represent lower and upper bounds of $\Lambda$ in the affine model, as implied by Eq. (32).

### 4.2. Orientation distribution

In line with the common approaches in literature (see e.g Lanir, 1979; Chagnon et al., 2015), it will be assumed that the initial orientation distribution of the fibres in the reference configuration is given in terms of a continuous fibre orientation distribution. This distribution can be expressed in terms of an orientation density function $\rho(\varphi)$ in 2D and $\rho(\varphi, \vartheta)$ in 3D respectively, such that in 2D

$$\frac{1}{2\pi} \int_0^{2\pi} \rho(\varphi) \, \mathrm{d}\varphi = 1 \tag{33}$$

and in 3D

$$\frac{1}{4\pi} \int_0^{2\pi} \int_0^{\pi} \rho(\varphi, \vartheta) \, \sin(\vartheta) \mathrm{d}\vartheta \mathrm{d}\varphi = 1. \tag{34}$$

Here $\varphi$ and $\vartheta$ are spherical angles corresponding to the axes of a Cartesian coordinate system aligned with the orthonormal basis $\{\boldsymbol{e}_i\}, i = 1, \ldots, d$, so that (see Fig. 2a)

$$\boldsymbol{N} \cdot \boldsymbol{e}_1 = \cos(\varphi), \quad \boldsymbol{N} \cdot \boldsymbol{e}_2 = \sin(\varphi), \tag{35}$$

in 2D, and

$$\boldsymbol{N} \cdot \boldsymbol{e}_1 = \cos(\varphi)\sin(\vartheta), \quad \boldsymbol{N} \cdot \boldsymbol{e}_2 = \sin(\varphi)\sin(\vartheta), \quad \boldsymbol{N} \cdot \boldsymbol{e}_3 = \cos(\vartheta) \tag{36}$$

in 3D. It is emphasised that the angles $(\varphi, \vartheta)$ do generally not coincide with $(\phi, \theta)$ introduced in Section 4.1 unless the principal axes of strain $\{\boldsymbol{N}_i\}$ are aligned with the fixed base vectors $\{\boldsymbol{e}_i\}$ that are used to represent the fibre distribution. Moreover, one cannot distinguish between fibres along $\boldsymbol{N}$ and $-\boldsymbol{N}$ which leads to corresponding symmetry conditions on $\rho$, and as a further consequence, it suffices to analyse the distribution on the hemisphere (or semicircle in 2D). Finally, we note that isotropic networks are characterised by a uniform fibre distribution, i.e. $\rho = 1$. In this case, the orientation of $\{\boldsymbol{e}_i\}$ becomes irrelevant and one may formally assume that $(\phi, \theta)$ and $(\varphi, \vartheta)$ coincide.

### 4.3. Stretch distribution in 2D

At first we consider the planar case described by Eqs. (30) and $(32)_1$.

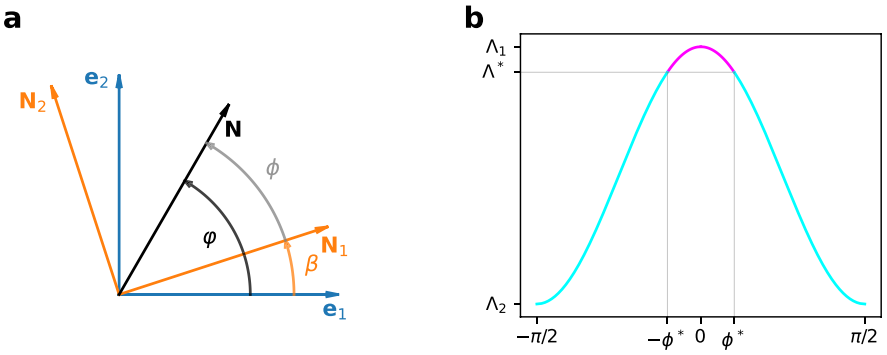


**Fig. 2.** (a) Illustration of the angles relating an arbitrary direction vector $\boldsymbol{N}$ to a set of fixed base vectors $\{\boldsymbol{e}_i\}$ and the principal axes $\{\boldsymbol{N}_i\}$ in 2D. (b) Relation between the angle $\phi$ and the affine square stretch $\Lambda$ in 2D according to Eq. $(32)_1$. The angular domains $|\phi| \geq \phi^*$ (cyan) and $|\phi| < \phi^*$ (magenta), which correspond to square stretches $\Lambda \leq \Lambda^*$ and $\Lambda > \Lambda^*$, respectively, are highlighted.

#### 4.3.1. General (anisotropic) case

In view of the symmetry properties of the trigonometric functions and due to the squares in Eq. $(32)_1$ one can restrict the analysis to the range $\phi \in (-\pi/2, \pi/2]$. Assuming $\Lambda_1 \neq \Lambda_2$ inversion of Eq. $(32)_1$ on $\phi \in [0, \pi/2]$ yields

$$\hat{\phi}(\lambda_\mathrm{n}) = \arccos(\lambda_\mathrm{n}), \quad \lambda_\mathrm{n} = \sqrt{\frac{\Lambda - \Lambda_2}{\Lambda_1 - \Lambda_2}}, \tag{37}$$

where for convenience the notion of a normalised 'stretch' $\lambda_\mathrm{n} \in [0, 1]$ has been introduced.

In order to determine the stretch distribution, we assume without loss of generality $\Lambda_1 \geq \Lambda_2$ and note that the probability $P$ for $\Lambda < \Lambda_2$ is 0 and for $\Lambda \leq \Lambda_1$ it is 1 since the square stretch is limited to $[\Lambda_2, \Lambda_1]$ in the affine case. For the normalised stretch $\lambda_\mathrm{n}$ this implies $P[\lambda_\mathrm{n} < 0] = 0$ and $P[\lambda_\mathrm{n} \leq 1] = 1$. Moreover, for any $\Lambda^*$ in $[\Lambda_2, \Lambda_1)$ or corresponding $\lambda_\mathrm{n}^*$ in $[0, 1)$ one has

$$P\left[\Lambda \leq \Lambda^*\right] = P\left[\lambda_\mathrm{n} \leq \lambda_\mathrm{n}^*\right] = P\left[|\phi| \geq \phi^*\right], \tag{38}$$

where $\phi^* = \hat{\phi}(\lambda_\mathrm{n}^*)$ as illustrated in Fig. 2b, and we note that both domains $\phi \in [\phi^*, \pi/2)$ and $\phi \in (-\pi/2, -\phi^*]$ are included by the absolute value in Eq. (38). Consequently, because we have assumed a continuous fibre initial orientation distribution,[3] one finds

$$\boxed{\mathrm{CDF}_{\lambda_\mathrm{n}}(\lambda_\mathrm{n}^*) = \mathrm{CDF}_\phi(-\phi^*) + 1 - \mathrm{CDF}_\phi(\phi^*),} \tag{39}$$

where the first term on the right hand side relates to the probability $P[\phi \leq -\phi^*]$ and the remaining terms to $P[\phi > \phi^*]$. The CDF of the stretch $\lambda$, its square $\Lambda$ or any other bijective function $f(\lambda_\mathrm{n})$ of $\lambda_\mathrm{n}$ follows as $\mathrm{CDF}_{\lambda_\mathrm{n}}(f^{-1}(z))$. For instance, Eq. $(37)_2$ provides for $\lambda$ and $\Lambda$

$$\mathrm{CDF}_\lambda(z) = \mathrm{CDF}_{\lambda_\mathrm{n}}\left(\sqrt{\frac{z^2 - \Lambda_2}{\Lambda_1 - \Lambda_2}}\right), \quad \mathrm{CDF}_\Lambda(z) = \mathrm{CDF}_{\lambda_\mathrm{n}}\left(\sqrt{\frac{z - \Lambda_2}{\Lambda_1 - \Lambda_2}}\right), \tag{40}$$

and for the normalised square stretch $\Lambda_\mathrm{n} = \lambda_\mathrm{n}^2$ one finds

$$\mathrm{CDF}_{\Lambda_\mathrm{n}}(z) = \mathrm{CDF}_{\lambda_\mathrm{n}}\left(\sqrt{z}\right). \tag{41}$$

Finally, it needs to be taken into account that the angle $\phi = \measuredangle(\boldsymbol{N}_1, \boldsymbol{N})$ measured against the principal axes of strain generally differs from $\varphi = \measuredangle(\boldsymbol{e}_1, \boldsymbol{N})$ given relative to the axes of a fixed Cartesian coordinate system used to represent the non-uniform distribution of fibres in a network. The CDFs of the two angles are simply related through the transformation rule

$$\mathrm{CDF}_\phi(z) = \mathrm{CDF}_\varphi(\beta + z), \tag{42}$$

where

$$\beta = \measuredangle(\boldsymbol{e}_1, \boldsymbol{N}_1) = \begin{cases} \arccos(\boldsymbol{N}_1 \cdot \boldsymbol{e}_1), & \text{if } \boldsymbol{N}_1 \cdot \boldsymbol{e}_2 \geq 0, \\ \arccos(-\boldsymbol{N}_1 \cdot \boldsymbol{e}_1) + \pi, & \text{otherwise.} \end{cases} \tag{43}$$

Here, we understand every CDF to formally satisfy

$$\mathrm{CDF}(z + k\pi) = \mathrm{CDF}(z) + k \tag{44}$$

[3] Notably, in case this distribution is not continuous each discontinuity can in principle be modelled discretely, i.e. by modelling a discrete fibre associated with non-zero probability.

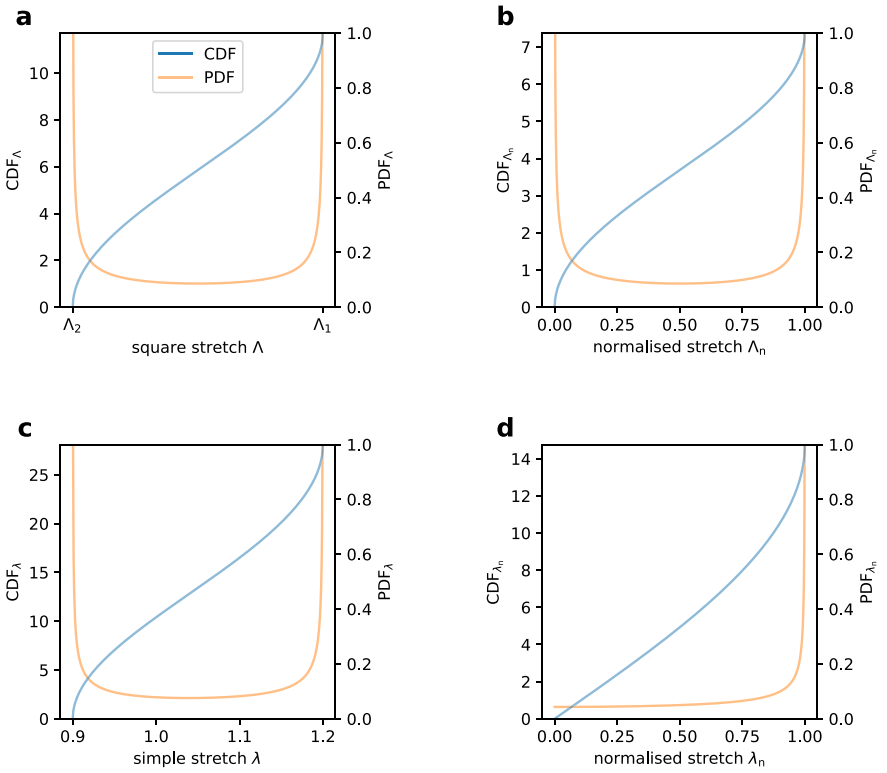


**Fig. 3.** Affine 2D stretch distribution represented in terms of square stretch (a), normalised square stretch (b), simple stretch (c) and normalised simple stretch (d). All graphs correspond to the same deformation ($\lambda_2 = 0.9,\ \lambda_1 = 1.2$).

for any integer $k$, thereby extending its image beyond the original interval $[0, 1]$, such as e.g. in the definition

$$\mathrm{CDF}_{\varphi}(z) = \frac{1}{2\pi}\int_0^z 2\rho(\varphi)\,\mathrm{d}\varphi\,, \tag{45}$$

which highlights the relation to the essential $\pi$-periodicity in $\rho$. We further note that the PDF of the stretch distribution follows by derivation of Eq. (40) since the CDF is absolutely continuous.

#### 4.3.2. *Uniform fibre distribution — isotropic case*

In the special case of a uniform orientation distribution, i.e. $\mathrm{PDF}_{\phi}(z) = 1/\pi$ and $\mathrm{CDF}_{\phi}(z) = z/\pi + 1/2$, Eqs. (39) and (41) yield

$$\mathrm{CDF}_{\Lambda_\mathrm{n}}(z) = \mathrm{CDF}_{\lambda_\mathrm{n}}\big(\sqrt{z}\big) = 1 - \frac{2}{\pi}\arccos\big(\sqrt{z}\big) = \frac{2}{\pi}\arcsin\big(\sqrt{z}\big)\,, \tag{46}$$

for $z \in [0, 1]$, which is the arcsine distribution, and thus a special case of the beta-distribution on $[0, 1]$ (Johnson et al., 1994), with the corresponding density

$$\mathrm{PDF}_{\Lambda_\mathrm{n}}(z) = \frac{1}{\pi\sqrt{(1-z)z}}\,. \tag{47}$$

The CDF and PDF of, e.g., the simple normalised stretch $\lambda_\mathrm{n}$, or the non-normalised variables $\Lambda$ and $\lambda$ can be obtained by a change of variable and are reported in Table 1. They are illustrated in Fig. 3 for a particular state of deformation ($\lambda_2 = 0.9,\ \lambda_1 = 1.2$). The analysis of the plots reveals that the PDF and CDF of $\lambda_\mathrm{n}$ and $\Lambda_\mathrm{n}$ (Fig. 3b, d) are universal, live on the support $[0, 1]$ and are independent of the specific values of $\{\lambda_i\}$. Moreover the shapes of $\mathrm{CDF}_{\Lambda}$ and $\mathrm{CDF}_{\Lambda_\mathrm{n}}$ as well as $\mathrm{PDF}_{\Lambda}$ and $\mathrm{PDF}_{\Lambda_\mathrm{n}}$ match and are therefore universal, although notably the limit values for the squared stretch $\Lambda$ change with $\{\lambda_i\}$. In contrast to that, both the functions and the shapes of $\mathrm{CDF}_{\lambda}$ and $\mathrm{PDF}_{\lambda}$ change with the state of deformation $\{\lambda_i\}$.

We recall that the results above were obtained for two distinct eigenvalues, while the case of equal eigenvalues $\Lambda_1 = \Lambda_2 = \Lambda_\mathrm{D}$ yields

$$\mathrm{CDF}_{\Lambda}(z) = H(z - \Lambda_\mathrm{D})\,, \tag{48}$$

corresponding to the trivial relation $P[\Lambda \le \Lambda_1] = 1$, where $H$ is the Heaviside function.

**Table 1**
Isotropic affine stretch distribution 2D: Representations in terms of CDF and PDF for the square stretch $\Lambda$, simple stretch $\lambda$ and corresponding normalised stretches $\Lambda_\mathrm{n}$ and $\lambda_\mathrm{n}$.

| Stretch | CDF | PDF | Support |
|---|---|---|---|
| $\Lambda = \boldsymbol{N}\cdot\boldsymbol{C}\boldsymbol{N}$ | $2/\pi \arcsin\left(\sqrt{(z-\Lambda_2)/(\Lambda_1-\Lambda_2)}\right)$ | $1/\left(\pi\sqrt{(\Lambda_1-z)(z-\Lambda_2)}\right)$ | $(\Lambda_2,\Lambda_1)$ |
| $\lambda = \sqrt{\Lambda}$ | $2/\pi \arcsin\left(\sqrt{(z^2-\lambda_2^2)/(\lambda_1^2-\lambda_2^2)}\right)$ | $2z/\left(\pi\sqrt{(\lambda_1^2-z^2)(z^2-\lambda_2^2)}\right)$ | $(\lambda_2,\lambda_1)$ |
| $\Lambda_\mathrm{n} = (\Lambda-\Lambda_2)/(\Lambda_1-\Lambda_2)$ | $2/\pi \arcsin\left(\sqrt{z}\right)$ | $1/\left(\pi\sqrt{(1-z)z}\right)$ | $(0,1)$ |
| $\lambda_\mathrm{n} = \sqrt{\Lambda_\mathrm{n}}$ | $2/\pi \arcsin(z)$ | $2/\left(\pi\sqrt{1-z^2}\right)$ | $(0,1)$ |

**Remark 1** (*Chebyshev–Gauss Quadrature*)**.** Interpretation of Eq. (8) in terms of the square stretch, and use of the isotropic density (Table 1) lead to the averaged fibre energy

$$\bar{\psi} = \int_{\Lambda_2}^{\Lambda_1} \psi_\Lambda(z)\,\mathrm{PDF}_\Lambda(z)\,\mathrm{d}z\,. \tag{49}$$

Using the substitution $y = \sqrt{(z-\Lambda_2)/(\Lambda_1-\Lambda_2)} \in [0,1]$ (cp. the definition of $\lambda_\mathrm{n}$ Eq. (37)) and the symmetry of the resulting integrand, the integral can be solved by means of the Chebyshev–Gauss quadrature rule (first kind) (Abramowitz and Stegun, 1972), i.e.

$$\bar{\psi} = \frac{1}{\pi}\int_{-1}^{1} \psi_\Lambda\left(y^2(\Lambda_1-\Lambda_2)+\Lambda_2\right)\frac{\mathrm{d}y}{\sqrt{1-y^2}} \approx \frac{1}{n}\sum_{i=1}^{n}\psi_\Lambda\left(y_i^2(\Lambda_1-\Lambda_2)+\Lambda_2\right)\,, \tag{50}$$

with integration points

$$y_i = \cos\left(\frac{2i-1}{2n}\pi\right)\,. \tag{51}$$

It is now interesting to transform these points back to the equivalent circular domain through Eq. (37), which provides the angles $(2i-1)\pi/(2n)$, i.e. a set of integration points on the (semi-)circle specified by the radial vectors

$$\boldsymbol{y}_i = \cos\left(\frac{2i-1}{2n}\pi\right)\boldsymbol{N}_1 + \sin\left(\frac{2i-1}{2n}\pi\right)\boldsymbol{N}_2. \tag{52}$$

Hence Gauss–Chebyshev integration of the affine model in the square stretch space is equivalent to quadrature on the circle with equidistant points arranged according to Eq. (52) (cp. Chawla and Kaul, 1973).

### 4.4. Square stretch distribution in 3D

To analyse the distribution of the square stretch in 3D affine networks, we first note that the affine square stretch $(32)_2$ is a bivariate function of the two spherical angles. Consequently, the relation cannot be inverted analogously to the 2D case. The problem can formally be addressed by use of a variable transformations, so that an integral expression of the PDF can be obtained (cf. Gizzi et al., 2016; Vasta et al., 2018). Similar as in the 2D case (cf. Fig. 3), the stretch PDF in 3D is characterised through asymptotic behaviour, posing challenges in the integration of expression (23). Therefore, we here directly obtain the CDF, using an analogy with the unit sphere to determine the probability $P[\Lambda \le \Lambda^*]$.

#### 4.4.1. General (anisotropic) case

Let $\{\Lambda_1,\Lambda_2,\Lambda_3\}$ denote the eigenvalues of $\mathbf{C}$, i.e. the squared principal stretches, which – without loss of generality – we assume to be in increasing or decreasing order so that $\Lambda_2$ denotes the mid eigenvalue. Subject to affine deformations the fibre elements will experience stretches $\Lambda$ bounded by $\Lambda_1$ and $\Lambda_3$, and as in the 2D case (Section 4.3) we seek for the probability $P[\Lambda \le \Lambda^*]$ that $\Lambda$ is smaller than a given value $\Lambda^*$. To this end, we consider an analogy with the unit sphere illustrated in Fig. 4. Setting the left hand side of Eq. $(32)_2$ to a constant $\Lambda^*$, it becomes an implicit equation that defines curves on the unit sphere, which are characterised by equal stretch $\Lambda^*$, for any load case specified through $\Lambda_1,\Lambda_2,\Lambda_3$, as illustrated for a set of principal stretches ($\Lambda_3 = 0.8$, $\Lambda_2 = 1$, $\Lambda_1 = 1.5$) and different values of $\Lambda^*$ in Fig. 4.

We further note that $\Lambda \le \Lambda^*$ corresponds to subdomains of the unit (hemi-)sphere (cp. Li et al., 2018a). For example, the case represented by $\Lambda^* = \max\{\Lambda_i\}$ relates to the entire surface of the (hemi-)sphere, as clearly the stretch in any direction is less than or equal to the maximum principal stretch. In the opposite case, where $\Lambda^* = \min\{\Lambda_i\} < \max\{\Lambda_i\}$, the region degenerates to a point if $\Lambda_2 > \min\{\Lambda_i\}$ or a half-circle on the hemisphere if $\Lambda_2 = \min\{\Lambda_i\}$. The corresponding probabilities $P[\Lambda \le \Lambda_{\max}]$ and $P[\Lambda \le \Lambda_{\min} < \Lambda_{\max}]$, respectively, are[4] 1 and 0. For any other value of $\Lambda^*$, the probability $P[\Lambda \le \Lambda^*]$ depends on the area[5] of the surface specified through the set of spherical angles

$$\{\phi,\theta : \Lambda \le \Lambda^*\}, \tag{53}$$

[4] This result formally assumes a continuous fibre orientation distribution.

[5] For non-uniform initial fibre orientation distributions this area needs to be weighted.

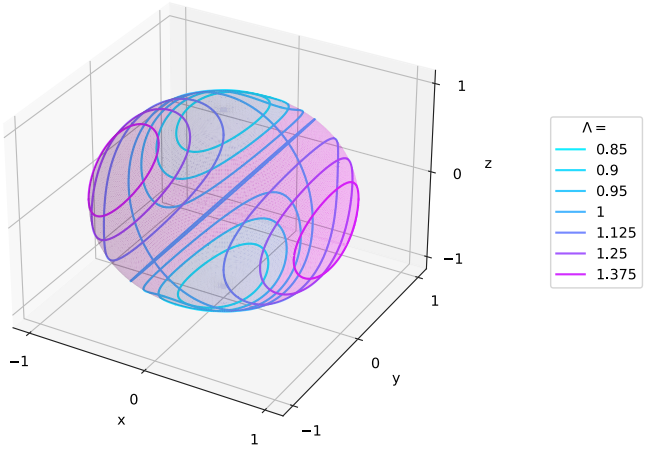


**Fig. 4.** Curves of equal affine (square) stretch on a sphere. The specific state of deformation shown is characterised through the three squared principal stretches $\Lambda_3 = 0.8$, $\Lambda_2 = 1$ and $\Lambda_1 = 1.5$. Regions corresponding to $\{\Lambda < 0.9\}$ and $\{\Lambda > 0.9\}$ are shaded in cyan and magenta, respectively.

which are defined through Eq. $(32)_2$. For $\Lambda^* = 0.9$ the corresponding region is exemplified in Fig. 4. In order to determine the surface areas of these regions, and thus $P[\Lambda \leq \Lambda^*]$, it is convenient to consider an Archimedean projection of the hemisphere $(-\pi/2, \pi/2] \times [0, \pi]$ onto an open half-cylinder, further unwrapped onto the rectangle $(-\pi/2, \pi/2] \times [-1, 1]$ through the transformation $u = \cos(\theta)$ (cf. e.g. Hannay and Nye, 2004). The affine square stretch $(32)_2$ thus takes the form

$$\Lambda = \Lambda_1 \cos^2(\phi)(1-u^2) + \Lambda_2 \sin^2(\phi)(1-u^2) + \Lambda_3 u^2 \,, \tag{54}$$

where $\phi \in (-\pi/2, \pi/2]$ and $\theta \in [0, \pi]$. Setting the left hand side of Eq. (54) to a constant $\Lambda^*$, one finds the corresponding $\Lambda^*$-isolines on the rectangle by solving the resulting implicit equation.

Let us at first assume $\Lambda_2 \neq \Lambda_3$. In this case the upper half ($u \in [0, 1]$) of the symmetric $\Lambda^*$-isolines follows from Eq. (54) as (cf. Fig. 5a)

$$\hat{u}(\Lambda, \phi) = \sqrt{\frac{\Lambda - \Lambda_2 + (\Lambda_2 - \Lambda_1)\cos^2(\phi)}{\Lambda_3 - \Lambda_2 + (\Lambda_2 - \Lambda_1)\cos^2(\phi)}} \,, \quad \Lambda_2 \neq \Lambda_3 \,, \tag{55}$$

which is a univariate function of the angle $\phi$ for any fixed value of $\Lambda = \Lambda^*$.

The Archimedean projection is area preserving so that areas on the (hemi-)sphere $\Lambda \leq \Lambda^*$ can be directly evaluated on the rectangle. In Fig. 5a the probability $P[\Lambda \leq \Lambda_1]$ corresponds to the entire rectangular domain, whereas $P[\Lambda \leq \Lambda_3]$ corresponds to the upper and lower boundary. The probability for any other stretch $\Lambda^* \in (\Lambda_3, \Lambda_1]$ corresponds to the area not 'enclosed' by the corresponding isoline $\Lambda = \Lambda^*$, and can be identified by integration.

Eventually, we need to take into account the fibre initial orientation density $\rho(\varphi, \vartheta)$, which weights the areas corresponding to $\Lambda \leq \Lambda^*$ by the fraction of fibres experiencing those stretches. Expressing the probability in terms of the CDF, this finally yields

$$\mathrm{CDF}_\Lambda(\Lambda^*) = P[\Lambda \leq \Lambda^*] = 1 - \frac{1}{2\pi} \int_{-\phi^*}^{\phi^*} \int_{-u^*(\phi)}^{u^*(\phi)} \hat{q}(u, \phi) \, \mathrm{d}u \, \mathrm{d}\phi \,, \quad \Lambda_2 \neq \Lambda_3 \,, \tag{56}$$

where $u^*(\phi) = \hat{u}(\Lambda^*, \phi)$, $\phi^*$ is the root of $u^*(\phi)$ if it exists or $\pi/2$ otherwise, and $\hat{q}(u(\varphi, \vartheta), \theta(\varphi, \vartheta)) = \rho(\varphi, \vartheta)$ is the fibre initial orientation density.

For reasons that will become clear soon, we repeat the steps that led to Eqs. (54)–(56) using another parametrisation of the sphere in terms of the angles $\tilde{\phi}$ and $\tilde{\theta}$, so that $\tilde{u} = \cos(\tilde{\theta})$ (cp. Fig. 2b), this time assuming $\Lambda_1 \neq \Lambda_2$. In essence, the polar angle $\tilde{\theta}$ is now measured from the principal axis $\boldsymbol{N}_1$ (associated with the principal stretch $\Lambda_1$), so that $\tilde{u} = \boldsymbol{N} \cdot \boldsymbol{N}_1$, and $\tilde{\phi}$ is in the plane spanned by $\boldsymbol{N}_2$ and $\boldsymbol{N}_3$. Analogous to Eq. (54) one can thus express the affine square stretch as

$$\Lambda = \Lambda_1 \tilde{u}^2 + \Lambda_2 \sin^2(\tilde{\phi})(1-\tilde{u}^2) + \Lambda_3 \cos^2(\tilde{\phi})(1-\tilde{u}^2) \,. \tag{57}$$

One finds for $\tilde{u} \in [0, 1]$ the curves of equal stretch $\Lambda$ analogous to (55)

$$\check{u}(\Lambda, \phi) = \sqrt{\frac{\Lambda - \Lambda_2 + (\Lambda_2 - \Lambda_3)\cos^2(\tilde{\phi})}{\Lambda_1 - \Lambda_2 + (\Lambda_2 - \Lambda_3)\cos^2(\tilde{\phi})}} \,, \quad \Lambda_1 \neq \Lambda_2 \,. \tag{58}$$

The corresponding isolines of constant $\Lambda$ are illustrated in Fig. 5b for the same state of deformation as in Fig. 5a, and by use of the same colour scheme. Following the same reasoning as above in Eq. (56), the CDF can thus alternatively be expressed as

$$\mathrm{CDF}_\Lambda(\Lambda^*) = P[\Lambda \leq \Lambda^*] = \frac{1}{2\pi} \int_{-\tilde{\phi}^*}^{\tilde{\phi}^*} \int_{-\tilde{u}^*(\tilde{\phi})}^{\tilde{u}^*(\tilde{\phi})} \check{q}(\tilde{u}, \tilde{\phi}) \, \mathrm{d}\tilde{u} \, \mathrm{d}\tilde{\phi} \,, \quad \Lambda_1 \neq \Lambda_2 \,, \tag{59}$$

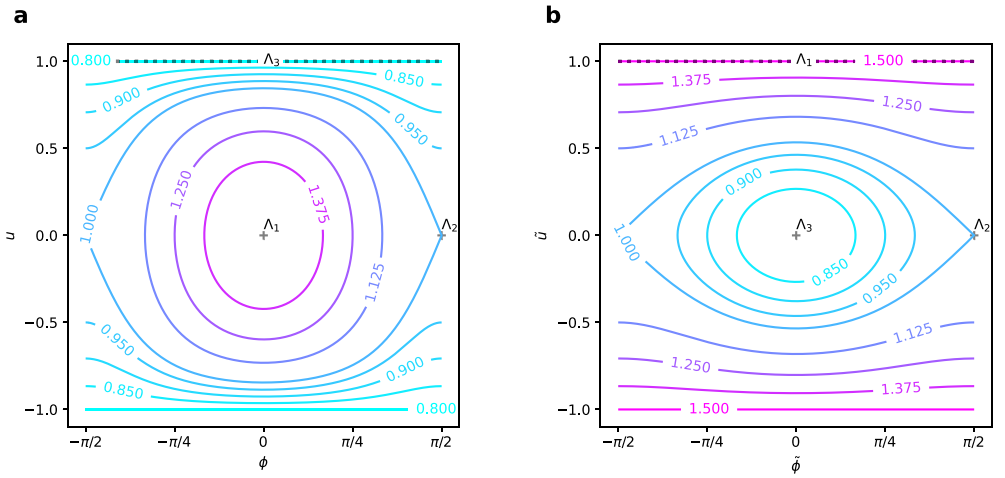


**Fig. 5.** Curves of equal affine (square) stretch: $\pm\hat{u}$ (a) and $\pm\check{u}$ (b) in $(\phi, u)$ and $(\tilde{\phi}, \tilde{u})$ coordinates, respectively. The specific state of deformation shown is characterised through the three squared principal stretches $\Lambda_3 = 0.8$, $\Lambda_2 = 1$ and $\Lambda_1 = 1.5$.

where $\tilde{u}^*(\tilde{\phi}) = \check{u}(\Lambda^*, \tilde{\phi})$, $\tilde{\phi}^*$ is the root of $\tilde{u}^*(\tilde{\phi})$ if it exists or $\pi/2$ otherwise, and $\check{q}(\tilde{u}(\varphi, \vartheta), \tilde{\theta}(\varphi, \vartheta)) = \rho(\varphi, \vartheta)$.

The case of two equal eigenvalues $\Lambda_2 = \Lambda_1$ and $\Lambda_2 = \Lambda_3$ are included in Eqs. (56) and (59), respectively. Finally, the definition of the CDF is completed by the case of eigenvalues with triple coalescence, for which the CDF can be written in terms of the Heaviside function $H$.

To resume the representations of the CDF, without loss of generality let us assume $\Lambda_3 \le \Lambda_2 \le \Lambda_1$ and $\Lambda_3 \neq \Lambda_1$, which only excludes the case, where all stretches are equal. Inspection of the two graphs in Fig. 2b indicates that in one of the two representations, the curve belonging to a given $\Lambda$ spans the entire domain $(-\pi/2, \pi/2]$. Hence, to avoid the determination of $\phi^*$ and $\tilde{\phi}^*$ one can distinguish between the cases $\Lambda_3 < \Lambda^* \le \Lambda_2$ and $\Lambda_2 \le \Lambda^* < \Lambda_1$ to simplify the integration, and to use Eq. (56) in the first case, and Eq. (59) in the latter with bounds $(-\pi/2, \pi/2]$ for the outer integration. With these considerations, the CDF is represented by

$$\mathrm{CDF}_{\Lambda}(\Lambda^*) = \begin{cases} \dfrac{1}{2\pi} \int_{-\pi/2}^{\pi/2} \int_{-u^*(\phi)}^{u^*(\phi)} \hat{q}(u, \phi)\, \mathrm{d}u\, \mathrm{d}\phi & \text{if} \quad \Lambda_3 < \Lambda^* \le \Lambda_2 \\ \dfrac{1}{2\pi} \int_{-\pi/2}^{\pi/2} \int_{-\tilde{u}^*(\tilde{\phi})}^{\tilde{u}^*(\tilde{\phi})} \check{q}(\tilde{u}, \tilde{\phi})\, \mathrm{d}\tilde{u}\, \mathrm{d}\tilde{\phi} & \text{if} \quad \Lambda_2 \le \Lambda^* < \Lambda_1 \\ H(\Lambda^* - \Lambda_{\mathrm{T}}) & \text{if} \quad \Lambda_1 = \Lambda_2 = \Lambda_3 = \Lambda_{\mathrm{T}}\,. \end{cases} \tag{60}$$

*4.4.2. Uniform fibre distribution — isotropic case*

For a uniform orientation distribution $\phi$ and $u = \cos(\theta)$ as well as $\tilde{\phi}$ and $\tilde{u} = \cos(\tilde{\theta})$ are uniformly distributed, i.e. $\hat{q}(u, \phi) = 1$ and likewise $\check{q}(\tilde{u}, \tilde{\phi}) = 1$. For three or two distinct eigenvalues, and $\Lambda^* \in (\Lambda_3, \Lambda_1)$ this allows to write

$$\mathrm{CDF}_{\Lambda}(\Lambda^*) = \begin{cases} 1 - \frac{1}{\pi} \int_{-\pi/2}^{\pi/2} \hat{u}(\Lambda^*, \phi)\, \mathrm{d}\phi & \text{if } \Lambda_3 < \Lambda^* \le \Lambda_2, \\ \\ \frac{1}{\pi} \int_{-\pi/2}^{\pi/2} \check{u}(\Lambda^*, \tilde{\phi})\, \mathrm{d}\tilde{\phi} & \text{if } \Lambda_2 \le \Lambda^* < \Lambda_1. \end{cases} \tag{61}$$

Introducing the parameter

$$\alpha = \frac{\Lambda_1 - \Lambda_2}{\Lambda_1 - \Lambda_3}, \tag{62}$$

the functions $\hat{u}$ (55) and $\check{u}$ (58) can be expressed using the normalised stretch $\Lambda_{\mathrm{n}} = (\Lambda - \Lambda_3)/(\Lambda_1 - \Lambda_3)$. For example, $\hat{u}$ reads

$$\hat{u}((\Lambda_1 - \Lambda_3)\Lambda_{\mathrm{n}} + \Lambda_3, \phi) = \sqrt{\frac{1 - \alpha - \Lambda_{\mathrm{n}} + \alpha \cos^2(\phi)}{1 - \alpha \sin^2(\phi)}}\,, \tag{63}$$

which reveals that the shape of $\mathrm{CDF}_{\Lambda}$ only depends on the parameter $\alpha$, i.e. the relative position of $\Lambda_2$ between $\Lambda_3$ and $\Lambda_1$. $\mathrm{CDF}_{\Lambda}$ and the corresponding $\mathrm{PDF}_{\Lambda}$, which follows by differentiation, are illustrated in Fig. 6. For three distinct eigenvalues Eq. (61) can be expressed in terms of the complete elliptic integral $f(x, y)$ of the third kind (cp. Eqs. (131) and (132))

$$\mathrm{CDF}_{\Lambda}(\Lambda^*) = \begin{cases} 1 - f\left(\dfrac{\Lambda_2 - \Lambda^*}{\Lambda_1 - \Lambda_3}, \alpha\right) & \text{if } \Lambda_3 < \Lambda^* < \Lambda_2, \\ \\ f\left(\dfrac{\Lambda^* - \Lambda_2}{\Lambda_1 - \Lambda_3}, 1 - \alpha\right) & \text{if } \Lambda_2 < \Lambda^* < \Lambda_1, \end{cases} \tag{64}$$

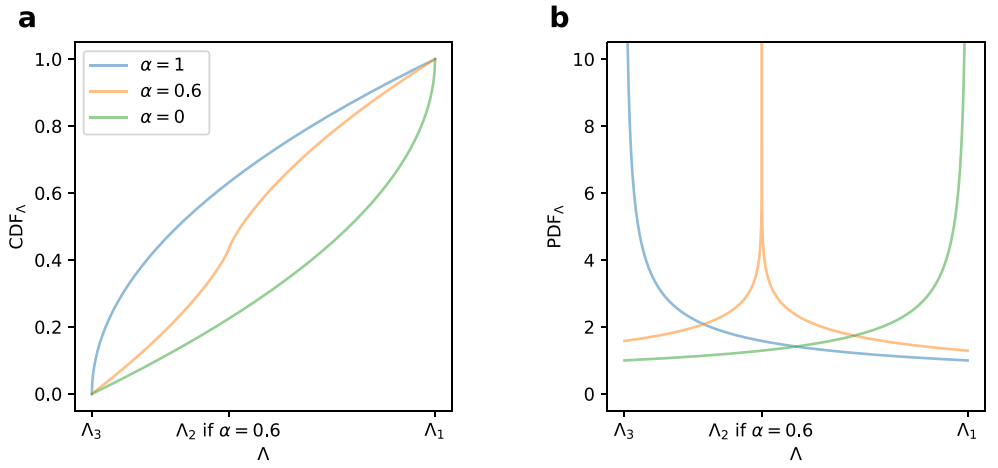


**Fig. 6.** Representation of the square stretch distribution in an isotropic affine network in terms of the CDF (a) and PDF (b). All stretches are distributed between the minimal ($\Lambda_3$) and maximal principal stretch ($\Lambda_1$). The PDF has a singularity at $\Lambda = \Lambda_2$ and the relative position of this pole between $\Lambda_3$ and $\Lambda_1$ is characterised through the ratio $\alpha = (\Lambda_1 - \Lambda_2)/(\Lambda_1 - \Lambda_3)$, which is illustrated for the cases $\alpha = 1$, i.e. $\Lambda_2 = \Lambda_3$ (blue), $\alpha = 0.6$ (orange) and $\alpha = 0$, i.e. $\Lambda_2 = \Lambda_1$ (green) in the plots.

as will be discussed in Section 8.1. For two distinct eigenvalues Eq. (61) simplifies to

$$\mathrm{CDF}_{\Lambda}(\Lambda^*) = \sqrt{\frac{\Lambda^* - \Lambda_\mathrm{D}}{\Lambda_\mathrm{S} - \Lambda_\mathrm{D}}}\,, \tag{65}$$

and finally, the triple coalescence of eigenvalues once again results in the Heaviside function $(60)_3$.

## 5. Moments of the affine stretch distribution

In Part I of this work (Britt and Ehret, 2022), we showed that the statistical moments of the stretch distribution can be used to efficiently compute the network free energy according to Eq. (9). As we will show in what follows, analogous considerations for the affine distribution of the stretch square are strongly related to the concept of generalised structural tensors (Advani and Tucker, 1987; Kanatani, 1984) and their application (e.g. Freed et al., 2005; Gasser et al., 2006; Pandolfi and Vasta, 2012; Holzapfel et al., 2015; Hashlamoun et al., 2016) and thus provide a new interpretation of these tensor-valued quantities and their scalar products with strain measures. In fact, starting from Eq. (25) we can reconcile our theory with structural tensor approaches for materials with non-uniformly distributed fibres proposed by Cortes and Elliott (2014) and Hashlamoun et al. (2016), and finally propose a computationally beneficial reformulation of the method (Section 7.2). What is more, in the isotropic case the moments reduce to a finite set of scalar isotropic tensor functions proposed by Itskov and co-workers (Itskov et al., 2010) for analytical integration of the full-network model over the unit sphere (Section 7.1). The analysis thus not only identifies the close relation between the three approaches, but also provides closed-form representations of the isotropic tensor functions in terms of dedicated invariants of $\mathbf{C}$.

### 5.1. General (anisotropic) 2D and 3D case

The deterministic relation (29) between fibre orientation $\boldsymbol{N}$ and the fibre square stretch in the affine case allows to equivalently express the $n$th moment of the square stretch (24) $\Lambda$ with respect to $\Lambda_0$ in terms of the square stretch or orientation distribution, $P_\Lambda$ or $P_{\boldsymbol{N}}$, respectively, so that

$$\mathrm{M}_{\Lambda_0,n} = \mathrm{E}\big[(\Lambda - \Lambda_0)^n\big] = \int_{[\Lambda_d,\Lambda_1]} (z - \Lambda_0)^n \,\mathrm{d}P_\Lambda(z) = \int_S (\Lambda_{\boldsymbol{N}}(\boldsymbol{z}) - \Lambda_0)^n \,\mathrm{d}P_{\boldsymbol{N}}(\boldsymbol{z})\,. \tag{66}$$

Using notation (A.8) and the tensor contractions (A.3) and (A.1) the right-hand side can be expressed in terms of the $2n$th order tensor $\boldsymbol{N}^{\otimes 2n}$, as

$$(\Lambda - \Lambda_0)^n = ((\mathbf{C} - \Lambda_0\mathbf{I}) : \boldsymbol{N}\otimes\boldsymbol{N})^n = (\mathbf{C} - \Lambda_0\mathbf{I})^{\otimes n\,\vdots^{2n}}\,\boldsymbol{N}^{\otimes 2n} = \big\langle (\mathbf{C} - \Lambda_0\mathbf{I})^{\otimes n}, \boldsymbol{N}^{\otimes 2n}\big\rangle, \tag{67}$$

where it was considered that $\mathbf{I} : \boldsymbol{N}\otimes\boldsymbol{N} = \boldsymbol{N}\cdot\boldsymbol{N} = 1$. Making use of the linearity of the expectation operator, inserting (67) into (66) one thus finds

$$\boxed{\mathrm{M}_{\Lambda_0,n} = \mathrm{E}\left[\big\langle (\mathbf{C} - \Lambda_0\mathbf{I})^{\otimes n}, \boldsymbol{N}^{\otimes 2n}\big\rangle\right] = \big\langle (\mathbf{C} - \Lambda_0\mathbf{I})^{\otimes n}, \mathbb{H}_n\big\rangle,} \tag{68}$$

where the generalised structural tensors (Kanatani, 1984; Ken-Ichi, 1984)

$$\mathbb{H}_n = \mathrm{E}\left[\boldsymbol{N}^{\otimes 2n}\right] = \int_S \boldsymbol{z}^{\otimes 2n} \,\mathrm{d}P_{\boldsymbol{N}}(\boldsymbol{z}) \tag{69}$$

have been introduced. As important examples, the choice $\Lambda_0 = 0$ in Eqs. (66) or (68) yields the raw moments $\{\mathrm{M}_{0,n}\}$, and $\Lambda_0 = \bar{\Lambda} = \mathrm{E}[\Lambda]$, i.e. the average square stretch resulting as

$$\bar{\Lambda} = \mathbf{C} : \mathbb{H}_1 \,, \quad \bar{\Lambda} = \mathbf{C} : \frac{1}{d}\,\mathbf{I} = \frac{1}{d}\,I_1 = \frac{1}{d}\sum_{k=1}^{d} \Lambda_k \,, \tag{70}$$

in the general and isotropic cases, respectively, leads to the central moments $\{\mathrm{M}_{\bar{\Lambda},n}\}$.

**Remark 2** (*Efficient Calculation of Moments*). The computation of the moments in terms of the generalised structural tensors according to Eq. (68) is numerically advantageous compared to the direct evaluation of Eq. (66) by quadrature. This is because the generalised structural tensors only need to be evaluated once for a certain fibre distribution $P_{\boldsymbol{N}}$, and thus Eq. (68) requires less computational operations than Eq. (66). Moreover, for special cases such as isotropic[6] and transversely isotropic fibre distributions there exist efficient techniques to compute the generalised structural tensors themselves (cf. Section 5.4 and Hashlamoun and Federico (2017), respectively). Albeit not identified as moments of the stretch distribution, equivalent expressions to Eq. (68) have been presented earlier in Cortes and Elliott (2014, Eq. 27) and Hashlamoun et al. (2016, Eq. 31) with fixed expansion point $\Lambda_0 = \bar{\Lambda}$ and $\Lambda_0 = I_3^{1/3}$, respectively (see Section 7.2). With adjustments in notation those expressions can be formulated as

$$\mathrm{E}\left[(\Lambda - \Lambda_0)^n\right] = \sum_{k=0}^{n} \binom{n}{k} \mathrm{E}\left[\Lambda^k\right] (-\Lambda_0)^{n-k} = \sum_{k=0}^{n} \binom{n}{k} \left\langle \mathbf{C}^{\otimes k}, \mathbb{H}_k \right\rangle (-\Lambda_0)^{n-k} \,, \tag{71}$$

where by linearity of the integral the expectation operator was included in the binomial expansion sum, and the last equality follows from (67). The computational advantage of the new formulation (68) becomes apparent when comparing the single scalar product therein with the sum of scalar products in (71).

### 5.2. Derivatives of the moments

For the calculation of stress and stiffness, according to Eq. (4), the first and second derivatives of $\Psi$ with respect to $\mathbf{C}$ are required. When using the moment representation of the free energy density (25), this requires the corresponding derivatives of the moments.

With the properties defined in Appendix A, the differentiation of Eq. (68) with respect to $\mathbf{C}$ leads to

$$\begin{aligned} \frac{\partial \mathrm{M}_{\Lambda_0,n}}{\partial \mathbf{C}} &= \mathrm{E}\left[(\Lambda - \Lambda_0)^n\right]_{,\mathbf{C}} = \mathrm{E}\left[n(\Lambda - \Lambda_0)^{n-1}\left(\boldsymbol{N}\otimes\boldsymbol{N} - \Lambda_{0,\mathbf{C}}\right)\right] n\,\mathrm{E}\left[\left((\mathbf{C} - \Lambda_0\mathbf{I}) : \boldsymbol{N}\otimes\boldsymbol{N}\right)^{n-1}\left(\boldsymbol{N}\otimes\boldsymbol{N} - \Lambda_{0,\mathbf{C}}\right)\right] \\ &= n(\mathbf{C} - \Lambda_0\mathbf{I})^{\otimes n-1\ 2(n-1)\cdot} \mathbb{H}_n - n\,\mathrm{M}_{\Lambda_0,n-1}\,\Lambda_{0,\mathbf{C}} \,, \end{aligned} \tag{72}$$

valid for $n \geq 1$. For the second derivative, the analysis yields

$$\begin{aligned} \frac{\partial^2 \mathrm{M}_{\Lambda_0,n}}{\partial \mathbf{C}\partial \mathbf{C}} &= \mathrm{E}\left[n(\Lambda - \Lambda_0)^{n-1}\left(\boldsymbol{N}\otimes\boldsymbol{N} - \Lambda_{0,\mathbf{C}}\right)\right]_{,\mathbf{C}} = \mathrm{E}\left[n(n-1)(\Lambda - \Lambda_0)^{n-2}\left(\boldsymbol{N}\otimes\boldsymbol{N} - \Lambda_{0,\mathbf{C}}\right)^{\otimes 2}\right] - n\,\mathrm{M}_{\Lambda_0,n-1}\,\Lambda_{0,\mathbf{CC}} \\ &= n(n-1)\,\mathrm{E}\left[\left((\mathbf{C} - \Lambda_0\mathbf{I}) : \boldsymbol{N}\otimes\boldsymbol{N}\right)^{n-2}(\boldsymbol{N}^{\otimes 4} - \boldsymbol{N}\otimes\boldsymbol{N}\otimes\Lambda_{0,\mathbf{C}} - \Lambda_{0,\mathbf{C}}\otimes\boldsymbol{N}\otimes\boldsymbol{N} + \Lambda_{0,\mathbf{C}}\otimes\Lambda_{0,\mathbf{C}})\right] - n\,\mathrm{M}_{\Lambda_0,n-1}\,\Lambda_{0,\mathbf{CC}} \\ &= n(n-1)\left[(\mathbf{C} - \Lambda_0\mathbf{I})^{\otimes n-2\ 2(n-2)\cdot} \mathbb{H}_n - (\mathbf{C} - \Lambda_0\mathbf{I})^{\otimes n-2\ 2(n-2)\cdot} \mathbb{H}_{n-1}\otimes\Lambda_{0,\mathbf{C}} - \Lambda_{0,\mathbf{C}}\otimes(\mathbf{C} - \Lambda_0\mathbf{I})^{\otimes n-2\ 2(n-2)\cdot} \mathbb{H}_{n-1}\right. \\ &\qquad \left. + \mathrm{M}_{\Lambda_0,n-2}\,\Lambda_{0,\mathbf{C}}\otimes\Lambda_{0,\mathbf{C}}\right] - n\,\mathrm{M}_{\Lambda_0,n-1}\,\Lambda_{0,\mathbf{CC}} \end{aligned} \tag{73}$$

for $n \geq 2$. The case $n = 0$ is trivial and for $n = 1$ one obtains

$$\frac{\partial \mathrm{M}_{\Lambda_0,1}}{\partial \mathbf{C}} = \mathbb{H}_1 - \Lambda_{0,\mathbf{C}} \,, \quad \frac{\partial^2 \mathrm{M}_{\Lambda_0,1}}{\partial \mathbf{C}\partial \mathbf{C}} = -\Lambda_{0,\mathbf{CC}} \,. \tag{74}$$

We emphasise that the Eqs. (72)–(74) are valid both in the anisotropic and isotropic case.

For the specific choice of $\Lambda_0 = \bar{\Lambda}$ (70) one has

$$\bar{\Lambda} = \mathbf{C} : \mathbb{H}_1, \quad \frac{\partial \bar{\Lambda}}{\partial \mathbf{C}} = \mathbb{H}_1, \quad \frac{\partial^2 \bar{\Lambda}}{\partial \mathbf{C}\partial \mathbf{C}} = \mathbb{O}, \tag{75}$$

where $\mathbb{O}$ is the fourth-order zero tensor, and in the $d$-dimensional isotropic case $\mathbb{H}_1 = \mathbf{I}/d$.

### 5.3. Cartesian components of $\mathbb{H}_n$

In this section we make use of the known representation of the $n$th even order generalised structural tensors $\mathbb{H}_n$ (69) in terms of Cartesian components with respect to bases formed by an arbitrary set of orthonormal unit vectors $\{\boldsymbol{e}_i\}$. As a direct consequence of the definition (69) the Cartesian components $\mathbb{H}_{n|ij\ldots mn}$ of $\mathbb{H}_n$ satisfy

$$\mathbb{H}_{n|ij\ldots mn} = \mathrm{E}\left[N_i N_j \ldots N_m N_n\right] , \tag{76}$$

[6] In the isotropic case the moments can be computed as polynomials of invariants of $\mathbf{C}$ as elaborated in Section 5.4.

where $N_i = \boldsymbol{N} \cdot \boldsymbol{e}_i$ denote the Cartesian components of $\boldsymbol{N}$ with respect to $\{\boldsymbol{e}_i\}$. Due to the high degree of symmetry of $\mathbb{H}_n$, its components are defined by the number of occurrences of the indices from 1 to $d$, e.g. 1 and 2 in the 2D case (Ken-Ichi, 1984; Kanatani, 1984; Hashlamoun and Federico, 2017). We here focus on the 3D case ($d = 3$), and note that the 2D case can be treated analogously (Appendix B). Using the spherical angles $\varphi$ and $\vartheta$ defined in Eq. (36), the components of $\mathbb{H}_n$ read (cp. Hashlamoun and Federico, 2017)

$$\mathbb{H}_{n|p,q,r} = \mathrm{E}\left[(\boldsymbol{N} \cdot \boldsymbol{e}_1)^p (\boldsymbol{N} \cdot \boldsymbol{e}_2)^q (\boldsymbol{N} \cdot \boldsymbol{e}_3)^r\right] = \mathrm{E}\left[\cos^p(\varphi) \sin^{p+q}(\vartheta) \sin^q(\varphi) \cos^r(\vartheta)\right], \tag{77}$$

denoting the value of each component of $\mathbb{H}_n$ that has $p, q, r$ times the indices $1, 2, 3$, respectively. We note that for a given orientation distribution density $\rho(\varphi, \vartheta)$ (cp. Eq. (34)), this can be evaluated as (Hashlamoun and Federico, 2017)

$$\mathbb{H}_{n|p,q,r} = \frac{1}{4\pi} \int_0^{2\pi} \int_0^{\pi} \rho(\varphi, \vartheta) \cos^p(\varphi) \sin^{p+q}(\vartheta) \sin^q(\varphi) \cos^r(\vartheta) \sin\vartheta \, \mathrm{d}\vartheta \mathrm{d}\varphi \,. \tag{78}$$

Another important characteristic of the generalised structural tensors is the recursiveness between tensors of subsequent order. Indeed, from a generalised structural tensor of order $n + k$ all generalised structural tensors of lower order can be obtained by suitable contractions, viz.

$$\mathbb{H}_n = \mathbb{H}_{n+k} \overset{2k}{\cdot} \mathbf{I}^{\otimes k} \,, \tag{79}$$

which is a direct consequence of the contraction rule (A.4), when applied to the $k$-fold dyad of the second-order identity tensor $\mathbf{I}^{\otimes k} = \mathbf{I} \otimes \cdots \otimes \mathbf{I}$. Specifically, for $k = 1$ one obtains (Kanatani, 1984)

$$\mathbb{H}_n = \mathrm{E}\left[\boldsymbol{N}^{\otimes 2n}\right] = \mathrm{E}\left[\boldsymbol{N}^{\otimes 2n} (\boldsymbol{N} \cdot \boldsymbol{N})\right] = \mathbb{H}_{n+1} : \mathbf{I} \,, \tag{80}$$

which in Cartesian coordinates reads $\mathbb{H}_{n|ij\ldots kl} = \mathbb{H}_{n+1|ij\ldots klmn} \delta_{mn}$, where $\delta_{mn}$ denotes the Kronecker delta. In terms of the notation introduced in Eq. (77) this property reads

$$\mathbb{H}_{n|p,q,r} = \mathbb{H}_{n+1|p+2,q,r} + \mathbb{H}_{n+1|p,q+2,r} + \mathbb{H}_{n+1|p,q,r+2} \,. \tag{81}$$

For later use (Appendix D) we note that by means of the spectral representation of $\mathbf{C}$ (Eq. (1)) the expectation in Eq. (66) can be expressed as

$$\mathrm{M}_{\Lambda_0,n} = \mathrm{E}\left[(\Lambda_1 (\boldsymbol{N}_1 \cdot \boldsymbol{N})^2 + \Lambda_2 (\boldsymbol{N}_2 \cdot \boldsymbol{N})^2 + \Lambda_3 (\boldsymbol{N}_3 \cdot \boldsymbol{N})^2 - \Lambda_0)^n\right]. \tag{82}$$

Since the eigenvectors $\boldsymbol{N}_i$ represent a set of orthonormal vectors, they can be used to form another orthonormal basis for the tensors $\mathbb{H}_n$. Let the corresponding components be denoted by $\tilde{\mathbb{H}}_{n|ij\ldots mn}$, and define in analogy to Eq. (77)

$$\tilde{\mathbb{H}}_{n|p,q,r} = \mathrm{E}\left[(\boldsymbol{N} \cdot \boldsymbol{N}_1)^p (\boldsymbol{N} \cdot \boldsymbol{N}_2)^q (\boldsymbol{N} \cdot \boldsymbol{N}_3)^r\right]. \tag{83}$$

Then, by use of trinomial expansion Eq. (82) can be rewritten as

$$\mathrm{M}_{\Lambda_0,n} = \sum_{p+q+r=n} \binom{n}{p,q,r} (\Lambda_1 - \Lambda_0)^p (\Lambda_2 - \Lambda_0)^q (\Lambda_3 - \Lambda_0)^r \, \tilde{\mathbb{H}}_{n|2p,2q,2r} \,, \tag{84}$$

where we note that in the isotropic case the components with respect to any orthonormal bases coincide, i.e. $\tilde{\mathbb{H}}_{n|ij\ldots kl} = \mathbb{H}_{n|ij\ldots kl}$. While Eqs. (68) and (84) hold in the general anisotropic case, we will specify the moments for the important special case of uniform fibre distributions, i.e. isotropic materials in the following section.

### 5.4. Moments and their derivatives for uniform fibre distributions

For the sake of brevity we here consider the 3D case. An independent discussion of the 2D case is given in Appendix C. For a uniform referential fibre orientation distribution the value of $\mathbb{H}_{n|p,q,r}$ is unaffected by any change in the order of $p, q, r$ and zero if the set $\{p, q, r\}$ contains an odd number due the symmetry properties of the trigonometric functions (cp. Hashlamoun and Federico (2017) and Section 5.3). Hence, using binomial expansion together with the identities

$$\frac{1}{2\pi} \int_0^{2\pi} \cos^{2k}(x) \, \mathrm{d}x = \prod_{i=1}^{k} \frac{2i-1}{2i} \,, \quad \frac{1}{2} \int_0^{\pi} \sin^{2k+1}(x) \, \mathrm{d}x = \prod_{i=1}^{k} \frac{2i}{2i+1} \,, \tag{85}$$

that can be found by induction and integration by parts (cf. Eq. (C.3)), the non-zero components can be given as

$$\boxed{\mathbb{H}_{n|2p,2q,2r} = \left(\sum_{m=0}^{r} \binom{r}{m} (-1)^m \prod_{n=1}^{p+q+m} \frac{2n}{2n+1}\right)\left(\sum_{s=0}^{q} \binom{q}{s} (-1)^s \prod_{t=1}^{p+s} \frac{2t-1}{2t}\right).} \tag{86}$$

Table 2 exemplifies these components for the isotropic structural tensors up to order $2n = 10$, i.e. $\mathbb{H}_5$. The moments and their first and second derivatives with respect to $\mathbf{C}$ follow immediately by insertion of the components (86) into (68), (72) and (73), respectively.

**Table 2**
Isotropic structural tensors $\mathbb{H}_n$ of even order $2n$. The non-zero components are given depending on the number of distinct indices $i, j, k$ (from a permutation of $(1, 2, 3)$) represented by $2p, 2q, 2r$ respectively, e.g. $(\mathbb{H}_3)_{112222} = \mathbb{H}_{3|4,2,0}$, where without loss of generality we arrange for $p \geq q \geq r$.

| $n$ | $p, q, r$ | | | $\mathbb{H}_{n\|2p,2q,2r}$ |
|---|---|---|---|---|
| 0 | 0 | 0 | 0 | 1 |
| 1 | 1 | 0 | 0 | 1/3 |
| 2 | 2 | 0 | 0 | 1/5 |
| 2 | 1 | 1 | 0 | 1/15 |
| 3 | 3 | 0 | 0 | 1/7 |
| 3 | 2 | 1 | 0 | 1/35 |
| 3 | 1 | 1 | 1 | 1/105 |
| 4 | 4 | 0 | 0 | 1/9 |
| 4 | 3 | 1 | 0 | 1/63 |
| 4 | 2 | 2 | 0 | 1/105 |
| 4 | 2 | 1 | 1 | 1/315 |
| 5 | 5 | 0 | 0 | 1/11 |
| 5 | 4 | 1 | 0 | 1/99 |
| 5 | 3 | 2 | 0 | 1/231 |
| 5 | 3 | 1 | 1 | 1/693 |
| 5 | 2 | 2 | 1 | 1/1155 |

Alternatively, in Appendix D we provide a closed form solution for the (central) moments $\mathrm{M}_{\bar{\Lambda},n}$ (Eq. (84)) identifying them as polynomials $R_n(A, B)$, so that

$$\boxed{\mathrm{M}_{\bar{\Lambda},n} = R_n(A, B),} \tag{87}$$

of the two dedicated invariants of $\mathbf{C}$ and $\mathbf{C} - \bar{\Lambda}\mathbf{I}$

$$\boxed{A = \frac{3}{2}\sum_{i=1}^{3}(\Lambda_i - \bar{\Lambda})^2 = \frac{3}{2}\mathrm{tr}(\mathbf{C} - \bar{\Lambda}\mathbf{I})^2, \qquad B = \frac{27}{2}\prod_{i=1}^{3}(\Lambda_i - \bar{\Lambda}) = \frac{27}{2}\det(\mathbf{C} - \bar{\Lambda}\mathbf{I}),} \tag{88}$$

that are identical but numerically advantageous to the expressions (cf. Itskov et al., 2010)

$$A = I_1^2 - 3I_2, \qquad B = I_1^3 - \frac{9}{2}I_1 I_2 + \frac{27}{2}I_3, \tag{89}$$

in terms of principal invariants of $\mathbf{C}$ (see example in Appendix E). For $n$ from 0 to 10 the moments $\mathrm{M}_{\bar{\Lambda},n}$ are collected in Table 3.

For the calculation of stress and stiffness, we specify the derivatives of the invariants (89) as

$$A_{,\mathbf{C}} = 3\,(\mathbf{C} - \bar{\Lambda}\mathbf{I}), \quad A_{,\mathbf{CC}} = 3\,\mathbf{I} \boxtimes \mathbf{I} - \mathbf{I} \otimes \mathbf{I} \tag{90}$$

and

$$B_{,\mathbf{C}} = \frac{27}{2}\mathbf{adj}(\mathbf{C} - \bar{\Lambda}\mathbf{I}) + \frac{3}{2}A\,\mathbf{I} = \frac{27}{2}(\mathbf{C} - \bar{\Lambda}\mathbf{I})^2 - 3A\mathbf{I}, \quad B_{,\mathbf{CC}} = \frac{27}{2}((\mathbf{C} - \bar{\Lambda}\mathbf{I}) \boxtimes \mathbf{I} + \mathbf{I} \boxtimes (\mathbf{C} - \bar{\Lambda}\mathbf{I})) - 3(A_{,\mathbf{C}} \otimes \mathbf{I} + \mathbf{I} \otimes A_{,\mathbf{C}}), \tag{91}$$

where $\mathbf{adj}\mathbf{A}$ is the adjugate of a tensor $\mathbf{A}$ defined such that[7] $\mathbf{adj}\mathbf{A}\,\mathbf{A} = \det\mathbf{A}\,\mathbf{I}$. The derivatives of the moments $\mathrm{M}_{\bar{\Lambda},n} = R_n(A, B)$ with respect to $\mathbf{C}$ hence follow by virtue of the chain rule as

$$\frac{\partial \mathrm{M}_{\bar{\Lambda},n}}{\partial \mathbf{C}} = \frac{\partial R_n}{\partial A}A_{,\mathbf{C}} + \frac{\partial R_n}{\partial B}B_{,\mathbf{C}} = \sum_{X \in \{A,B\}}\frac{\partial R_n}{\partial X}X_{,\mathbf{C}}, \tag{92}$$

and

$$\frac{\partial^2 \mathrm{M}_{\bar{\Lambda},n}}{\partial \mathbf{C}\partial \mathbf{C}} = \sum_{\substack{X \in \{A,B\} \\ Y \in \{A,B\}}}\frac{\partial^2 R_n}{\partial Y \partial X}X_{,\mathbf{C}} \otimes Y_{,\mathbf{C}} + \sum_{X \in \{A,B\}}\frac{\partial R_n}{\partial X}X_{,\mathbf{CC}}. \tag{93}$$

Noteworthy, a finite number of terms $R_n(A, B)$ were obtained in an approach for analytic integration of the full-network model (Itskov et al., 2010), but without any reference to statistical moments. In Section 7.1 we readdress this point and reconcile the isotropic special case of our approach with the method in Itskov et al. (2010).

[7] We note that the identity $\mathbf{adj}\mathbf{A} = \det\mathbf{A}\,\mathbf{A}^{-1}$ only holds for invertible tensors $\mathbf{A}$, which is generally not the case here.

**Table 3**
Moments of the affine stretch distribution $\mathrm{M}_{\bar{A},n}$ up to $n = 10$ in terms of the invariants $A, B$ Eq. (89), (cf. Itskov et al., 2010).

| $n$ | $\mathrm{M}_{\bar{A},n}$ |
|---|---|
| 0 | 1 |
| 1 | 0 |
| 2 | $4A/45$ |
| 3 | $16B/945$ |
| 4 | $16A^2/945$ |
| 5 | $128AB/18711$ |
| 6 | $320A^3/81081 + 512B^2/729729$ |
| 7 | $256A^2B/104247$ |
| 8 | $256A\left(63A^3 + 32B^2\right)/15949791$ |
| 9 | $4096B\left(189A^3 + 8B^2\right)/909138087$ |
| 10 | $1024A^2\left(81A^3 + 80B^2\right)/303046029$ |

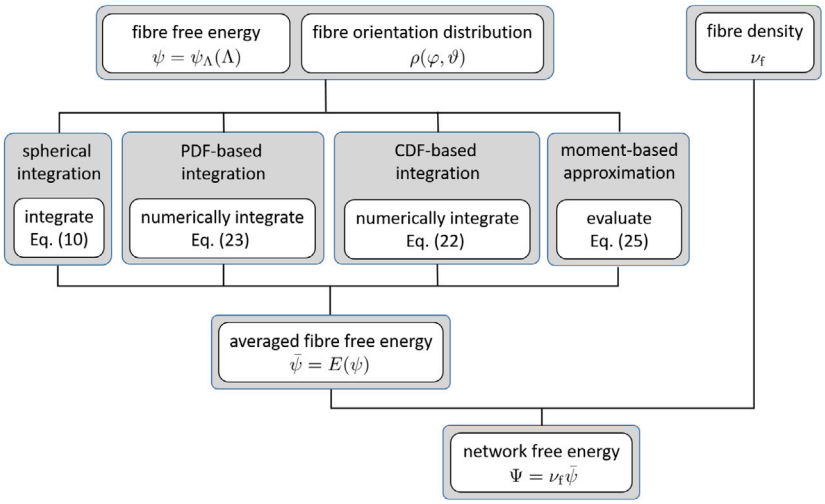


**Fig. 7.** Different methods to integrate the affine full network model.

## 6. Integration of the affine full network model

The results reported thus far have implications for the evaluation of the type of constitutive models that have become known as affine full network models in rubber elasticity, and structural approaches or angular integration models in biomechanics, for all of which the expectation $\mathrm{E}[\psi]$ of the fibre free energy $\psi$ of the form (10) is the essential ingredient. Using the term 'full network model' as a representative for all types of related models, the reformulation of the expectation in terms of the stretch PDF, CDF or corresponding moments demonstrates that there exist different methods to evaluate the full network model, as illustrated in Fig. 7. In particular, the analysis in the previous sections show that spherical integration, even if it represents the canonical strategy, is not the only way of addressing the problem.

Given the stretch PDF treated in Section 4 the *PDF based integration* of the free energy $\psi$ (23) can be adopted to obtain $\Psi$. This concept had been pointed out for the special case of a von-Mises type transversely isotropic fibre distribution by Gizzi et al. (2016). The corresponding stretch PDF was obtained by a change of variables from spherical angles to affine square stretch, and was illustrated for isochoric states of deformation in Gizzi et al. (2016) and Vasta et al. (2018).

Although the switch of the integration domain to the positive reals between the minimum and maximum principal stretch seems to ease the treatment of piece-wise defined fibre free energies, and in particular 'tension-only' fibres (cf. Gizzi et al., 2016), the singularities displayed by the affine stretch PDF (Fig. 6b) pose numerical challenges associated with the evaluation of the integral (23) in the affine case. Therefore, in Section 8 we suggest to use the *CDF based integration* (22) instead, which allows to deal with piecewise-defined fibre strain energies in a similarly straightforward manner, but overcomes the problems associated with the singularities in the PDF, as the CDF is bounded between 0 and 1.

Finally, the *moment-based approximation* (25) turns out to, in fact, include higher-order generalised structural tensor approaches (see e.g. Pandolfi and Vasta, 2012; Cortes and Elliott, 2014; Gizzi et al., 2014; Hashlamoun et al., 2016; Gizzi et al., 2018), and at least formally, also the well-established second-order generalised structure tensor approach (e.g. Freed et al., 2005; Gasser et al., 2006; Holzapfel et al., 2015). This will be elaborated in Section 7.2, where the moment-based representation is applied to

transversely isotropic fibre orientation distributions. Before, in Section 7.1, however, we will show that for uniform fibre orientation distributions, the method complies with the approach in Itskov et al. (2010). What is more, however, we provide closed form representations for the essential functional basis of this approach.

## 7. Moment-based approximation of the affine full-network model

By means of the moment-based representation (25) the free energy $\Psi$ of a network of fibres with analytic fibre free energy $\psi_\Lambda$ can be approximated as

$$\boxed{\Psi \approx \nu_\mathrm{f} \sum_{k=0}^{n} \frac{1}{k!} \frac{\partial^k \psi_\Lambda}{\partial \Lambda^k}\bigg|_{\Lambda=\Lambda_0} \mathrm{M}_{\Lambda_0,k},} \tag{94}$$

where $\nu_\mathrm{f}$ is the fibre volume fraction according to Eq. (6). For a polynomial fibre energy $\psi_\Lambda$ of degree $m \leq n$ the result becomes exact. In view of Eq. (4) the stress and tangent tensors follow by use of the chain rule of differentiation as

$$\mathbf{S} = 2\,\nu_\mathrm{f} \left( \sum_{k=0}^{n} \frac{1}{k!} \frac{\partial^{k+1} \psi_\Lambda}{\partial \Lambda^{k+1}}\bigg|_{\Lambda=\Lambda_0} \mathrm{M}_{\Lambda_0,k} \frac{\partial \Lambda_0}{\partial \mathbf{C}} + \frac{1}{k!} \frac{\partial^k \psi_\Lambda}{\partial \Lambda^k}\bigg|_{\Lambda=\Lambda_0} \frac{\partial \mathrm{M}_{\Lambda_0,k}}{\partial \mathbf{C}} \right) \tag{95}$$

and

$$\begin{aligned} \mathbb{C} = 4\nu_\mathrm{f} \Bigg[ \sum_{k=0}^{n} = \frac{1}{k!} \frac{\partial^{k+2} \psi_\Lambda}{\partial \Lambda^{k+2}}\bigg|_{\Lambda=\Lambda_0} \mathrm{M}_{\Lambda_0,k} \frac{\partial \Lambda_0}{\partial \mathbf{C}} \otimes \frac{\partial \Lambda_0}{\partial \mathbf{C}} \\ + \frac{1}{k!} \frac{\partial^{k+1} \psi_\Lambda}{\partial \Lambda^{k+1}}\bigg|_{\Lambda=\Lambda_0} \left( \frac{\partial \Lambda_0}{\partial \mathbf{C}} \otimes \frac{\partial \mathrm{M}_{\Lambda_0,k}}{\partial \mathbf{C}} + \frac{\partial \mathrm{M}_{\Lambda_0,k}}{\partial \mathbf{C}} \otimes \frac{\partial \Lambda_0}{\partial \mathbf{C}} + \mathrm{M}_{\Lambda_0,k} \frac{\partial^2 \Lambda_0}{\partial \mathbf{C} \partial \mathbf{C}} \right) + \frac{1}{k!} \frac{\partial^k \psi_\Lambda}{\partial \Lambda^k}\bigg|_{\Lambda=\Lambda_0} \frac{\partial^2 \mathrm{M}_{\Lambda_0,k}}{\partial \mathbf{C} \partial \mathbf{C}} \Bigg] . \end{aligned} \tag{96}$$

While for uniform fibre distributions, Eqs. (94)–(96) provide an implementation of the isotropic full network model, non-uniform distributions provide anisotropic full-network models, often employed in the 'structural approach' to model soft biological tissues.

### 7.1. Isotropic full network model

#### 7.1.1. Reconciliation with the analytical method by Itskov et al.

We compare the free energy (94) with a result by Itskov et al. (2010, Eq. 12) who, following ideas by Puso (2003), represented the free energy of an elastic network with fibres whose strain energy density $w(\Lambda)$ is analytic in the vicinity of $\Lambda_0$ as

$$\Psi = \sum_{k=0}^{\infty} \frac{1}{k!} \frac{\partial^k w}{\partial \Lambda^k}\bigg|_{\Lambda=\Lambda_0} W_k(\Lambda_0), \qquad W_k(\Lambda_0) = \frac{1}{4\pi} \int_0^{2\pi} \int_0^{\pi} (\Lambda - \Lambda_0)^k \, \sin\theta \mathrm{d}\theta \, \mathrm{d}\phi \,. \tag{97}$$

Inserting our notation $w = \nu_\mathrm{f}\, \psi_\Lambda$ and identifying the integrals $W_k = \mathrm{M}_{\Lambda_0,k}$ as stretch distribution moments (24) for an isotropic fibre distribution, a truncation of Eq. (97) is identical to our Eq. (94).

#### 7.1.2. Expansion point

Both the fibre strain energy and the state of deformation may favour a special expansion point, e.g. in order to increase the convergence radius of the series approximations (cp. Itskov et al., 2010).

Towards finding a 'generally suitable' expansion point, we first note that the quality of approximation of the truncated Taylor series of $\psi_\Lambda$ generally decreases with increasing distance from the expansion point. Second, we note that approximation errors at higher energies have a larger impact on the computed average, i.e. the value of the integral. Finally, we bear in mind that the fibre energy $\psi_\Lambda$ is a monotonically increasing function of the stretch square for $\Lambda > 1$, and typically asymmetric so that more energy is stored in tension than in compression, at least for slender fibres. Bringing these aspects together one would – loosely speaking – expect a suitable expansion point to lie (i) somewhere in the range of possible stretches, and tending towards higher stretches associated with higher energies. Moreover, letting these energetic considerations aside, (ii) the stretch at which the series is expanded is expected to be 'representative' for the ensemble of fibres. Without additional information, the expectation of the square stretch $\bar{\Lambda}$ itself therefore seems a suitable candidate.

Without prior knowledge about fibre behaviour and state of deformation, we hence suggest to expand the series about the average square stretch, so that $\Lambda_0 = \mathrm{E}[\Lambda] = \bar{\Lambda}$, which at least meets the second criterion (ii). For a uniform fibre distribution one has according to Eq. (75)

$$\bar{\Lambda} = \frac{1}{3}\, \mathbf{C} : \mathbf{I}, \quad \frac{\partial \bar{\Lambda}}{\partial \mathbf{C}} = \frac{1}{3}\, \mathbf{I}, \quad \frac{\partial^2 \bar{\Lambda}}{\partial \mathbf{C} \partial \mathbf{C}} = \mathbb{O}, \tag{98}$$

where $\mathbb{O}$ is the fourth-order zero tensor, so that the expressions (95) and (96) for stress and tangent tensor simplify significantly. Moreover, as discussed in Section 5.4 the corresponding central moments $\mathrm{M}_{\bar{\Lambda},k}$ of the isotropic network can be given as polynomials (87) (Table 3 and Appendix D) of two dedicated invariants (88), so that stress and tangent can be expressed in terms of the derivatives $\partial \mathrm{M}_{\bar{\Lambda},k}/\partial \mathbf{C}$ and $\partial^2 \mathrm{M}_{\bar{\Lambda},k}/(\partial \mathbf{C} \partial \mathbf{C})$, given in Eqs. (92) and (93) respectively.

Notwithstanding, the expansion point may be shifted and non-central moments be used. This procedure, based on binomial expansion, leads to

$$\mathrm{M}_{\Lambda_0,k} = \mathrm{E}\left[(\Lambda-\Lambda_0)^k\right] = \mathrm{E}\left[(\Lambda-\bar{\Lambda}+(\bar{\Lambda}-\Lambda_0))^k\right] = \mathrm{E}\left[\sum_{i=0}^{k}\binom{k}{i}(\Lambda-\bar{\Lambda})^i(\bar{\Lambda}-\Lambda_0)^{k-i}\right] = \sum_{i=0}^{k}\binom{k}{i}\mathrm{M}_{\bar{\Lambda},i}(\bar{\Lambda}-\Lambda_0)^{k-i}\,, \tag{99}$$

as discussed in detail by Itskov et al. (2010).

#### 7.1.3. Advantages of the new formulation

The moment-based integration of the full network model is in full line with the analytical integration proposed in Itskov et al. (2010) and thereby provides an alternative interpretation of this method in terms of the statistics of stretch. Given this equivalence, we omit numerical examples for this method, and refer to the applications in e.g. Itskov et al. (2010) and Itskov and Knyazeva (2016) for an illustration of the performance.

However, the different viewpoint and a detailed mathematical analysis allowed us to reformulate this method. At the one hand, a new, closed form solution for the isotropic moments $W_k(\bar{\Lambda}) = \mathrm{M}_{\Lambda_0,k}$ for arbitrary $k$ was obtained (Appendix D). This clearly brings advantages over the strategy proposed in Itskov et al. (2010) and Itskov (2016) that employs mathematical software to evaluate the integrals $W_k(\bar{\Lambda})$ for individual $k$ and to reformulate the results in terms of the invariants $A$ and $B$. On the other hand, the new formulation of the invariants $A$ and $B$ in terms of invariants of $\mathbf{C}-\bar{\Lambda}\mathbf{I}$ (88) instead of functions of the principal invariants of $\mathbf{C}$ (89) comes with computational advantages, since it reduces the propagation of round-off errors, in particular for nearly pure dilatations, i.e. similar eigenvalues of $\mathbf{C}$. In Appendix E, we illustrate this circumstance in a numerical example.

### 7.2. Moment-based integration of the structural approach

The identification of the essential functions $W_k$ in Eq. (97) with the moments $\mathrm{M}_{\Lambda_0,k}$ allows the natural extension of the analytical integration method reported in Itskov et al. (2010) to the anisotropic case. In fact, the moment-based representation (94) turns out to be the general anisotropic analogue of Eq. (97) if the moments are given by Eq. (68) (or Eq. (84)) for non-uniform referential orientation distributions of the fibres. The network free energy, stress and tangent tensors can be computed according to Eqs. (94)–(96), by use of the anisotropic moments (68) and their derivatives Eqs. (72)–(74).

#### 7.2.1. Approaches for tissues with statistically oriented fibres by Hashlamoun et al.

The moment-based approximation (94) can be brought in agreement with concepts to evaluate the response of tissues reinforced by statistically oriented fibres by Cortes and Elliott (2014) and Hashlamoun et al. (2016). Our analysis therefore reveals a close relation between these approaches and the seemingly distinct method by Itskov et al. (2010).

Hashlamoun et al. (2016, Eq. 7) study free energies for materials reinforced by fibres with orientation distribution $P_{\boldsymbol{N}}$ (associated with a density $\rho$) of the general form (in our notation)

$$\mathcal{F}(\mathbf{C},\mathbf{A}) = \Phi_0\hat{\mathcal{F}}_0(\mathbf{C}) + \Phi_1\int_S \hat{\mathcal{F}}_1(\mathbf{C},\mathbf{A})\,\mathrm{d}P_{\boldsymbol{N}}\,, \tag{100}$$

where $\mathbf{A} = \boldsymbol{N}\otimes\boldsymbol{N}$, $\mathcal{F}_0$ and $\mathcal{F}_1$ represent the elastic energy contributions of the isotropic matrix and the fibres taking the volume fractions $\Phi_0$ and $\Phi_1$, respectively. One can relate the fibre part with our averaged network energy $\Psi$, so that[8]

$$\nu_{\mathrm{f}}\,\psi_{\Lambda}(\mathbf{C}:\mathbf{A}) = \Phi_1\hat{\mathcal{F}}_1(\mathbf{C},\mathbf{A})\,. \tag{101}$$

We note that in Cortes and Elliott (2014, Eqs. 3,10), the volume fraction was lumped into the expression for the energy.

As will be shown next, the moment-based approximation (94), can be aligned with the GHOST method (Cortes and Elliott, 2014), INEX and STEX methods (Hashlamoun et al., 2016) thus identifying the latter as stretch-statistical methods.

We emphasise that despite this quasi-equivalence, the here proposed method (68) to compute the moments and their derivatives (Eqs. (68) and (72)–(74)) comes with computational and numerical advantages (cf. Remark 2).

#### 7.2.2. Comparison with INEX method

At first we align our theory with the INvariant EXpansion (INEX) method proposed in Hashlamoun et al. (2016). This method utilises a representation of the fibre energy in terms of the volume change $J = \sqrt{\det\mathbf{C}}$ and the isochoric stretch $\tilde{I}_4 = J^{-2/3}\Lambda$, which provides the equivalence

$$\Phi_1\check{\mathcal{F}}_1(J,\tilde{I}_4) = \nu_{\mathrm{f}}\,\psi_{\Lambda}(J^{2/3}\tilde{I}_4)\,. \tag{102}$$

In Hashlamoun et al. (2016, Eq. 31) the network energy $\Psi$ is then expressed in terms of the truncated series

$$\Psi = \Phi_1\sum_{j=0}^{n}\frac{1}{j!}\frac{\partial^j\check{\mathcal{F}}_1}{\partial\tilde{I}_4^j}(J,1)\sum_{k=0}^{j}\binom{j}{k}(-1)^k\left(J^{-2/3}\right)^{j-k}\left\langle\mathbf{C}^{\otimes j-k},\mathbb{H}_{j-k}\right\rangle. \tag{103}$$

[8] Note that $\nu_{\mathrm{f}}$ and $\Phi_1$ are not necessarily identical as $\nu_{\mathrm{f}}$ may account for different volumetric concepts, e.g. 1-dimensional fibres in a 3-dimensional network, where $\nu_{\mathrm{f}}$ would quantify to total length of fibre material per volume of the network, see Eq. (6).

Eq. (71) helps to identify the inner sum (slightly rewritten) as

$$J^{-2j/3}\sum_{k=0}^{j}\binom{j}{k}\left(-J^{2/3}\right)^{k}\left\langle \mathbf{C}^{\otimes j-k},\mathbb{H}_{j-k}\right\rangle = J^{-2j/3}\mathrm{M}_{J^{2/3},j}\,, \tag{104}$$

and from (102) it follows that

$$\boldsymbol{\Phi}_1\frac{\partial^j\check{\mathcal{F}}_1}{\partial\tilde{I}_4^j}(J,1) = \nu_{\mathrm{f}}\frac{\partial^j\psi_{\Lambda}}{\partial\Lambda^j}\bigg|_{\Lambda=J^{2/3}}J^{2j/3}\,. \tag{105}$$

Inserting Eqs. (104) and (105) back into the approach (103) yields

$$\Psi = \nu_{\mathrm{f}}\sum_{k=0}^{n}\frac{1}{k!}\frac{\partial^k\psi_{\Lambda}}{\partial\Lambda^k}\bigg|_{\Lambda=J^{2/3}}\mathrm{M}_{J^{2/3},k}, \tag{106}$$

and thus recovers the moment based approximation (94) with expansion point $\Lambda_0 = J^{2/3}$.

### 7.2.3. Comparison with STEX method

We next reconcile the Structure Tensor EXpansion (STEX) method with the moment-based approximation (94). The fibre energy $\hat{\mathcal{F}}_1$ of the STEX method is parametrised in terms of the tensors $\mathbf{C}$ and $\mathbf{A}$, and can therefore be related to the representation $\psi$ used herein as stated in Eq. (101). The STEX free energy is given by the truncated series (Hashlamoun et al., 2016, Eq. 36)

$$\Psi = \boldsymbol{\Phi}_1\sum_{j=0}^{n}\frac{1}{j!}\left\langle\frac{\partial^{(j)}\hat{\mathcal{F}}_1}{\partial\mathbf{A}^{(j)}}(\mathbf{C},\mathbf{A}_0),\sum_{k=0}^{j}\binom{j}{k}(-1)^k\,\mathrm{msym}\left(\mathbb{H}_{j-k}\otimes\mathbf{A}_0^{\otimes k}\right)\right\rangle, \tag{107}$$

i.e. the series is expanded about the structural tensor $\mathbf{A}_0$ associated with the 'dominant' fibre direction of the distribution, and Eq. (101) implies

$$\boldsymbol{\Phi}_1\frac{\partial^{(j)}\hat{\mathcal{F}}_1}{\partial\mathbf{A}^{(j)}}(\mathbf{C},\mathbf{A}_0) = \nu_{\mathrm{f}}\frac{\partial^j\psi_{\Lambda}}{\partial\Lambda^j}\bigg|_{\Lambda=\mathbf{C}:\mathbf{A}_0}\mathbf{C}^{\otimes j}\,. \tag{108}$$

Upon resolving

$$\left\langle\mathbf{C}^{\otimes j},\mathrm{msym}\left(\mathbb{H}_{j-k}\otimes\mathbf{A}_0^{\otimes k}\right)\right\rangle = \left\langle\mathbf{C}^{\otimes j-k},\mathbb{H}_{j-k}\right\rangle(\mathbf{C}:\mathbf{A}_0)^k \tag{109}$$

Eq. (71) reveals the moments about $\Lambda_0 = \mathbf{C}:\mathbf{A}_0$

$$\sum_{k=0}^{j}\binom{j}{k}(-1)^k\left\langle\mathbf{C}^{\otimes j},\mathrm{msym}\left(\mathbb{H}_{j-k}\otimes\mathbf{A}_0^{\otimes k}\right)\right\rangle = \mathrm{M}_{\mathbf{C}:\mathbf{A}_0,j} \tag{110}$$

so that (107) takes the form

$$\Psi = \nu_{\mathrm{f}}\sum_{k=0}^{n}\frac{1}{j!}\frac{\partial^k\psi_{\Lambda}}{\partial\Lambda^k}\bigg|_{\Lambda=\mathbf{C}:\mathbf{A}_0}\mathrm{M}_{\mathbf{C}:\mathbf{A}_0,k}\,. \tag{111}$$

The STEX method (107) hence recovers the moment based approximation (94) with expansion point $\Lambda_0 = \mathbf{C}:\mathbf{A}_0$.

### 7.2.4. Comparison with GHOST method

Cortes and Elliott (2014) investigated strain energy functions with additive isotropic $\Psi_{\mathrm{iso}}$ and anisotropic $\Psi_{\mathrm{ani}}$ contributions, which they associated with the matrix and fibres, respectively. Using a generalised structure tensor approach for the fibre part $\Psi_{\mathrm{ani}}$, which for the sake of comparison we set to $\Psi$, they proposed the approximation (Cortes and Elliott, 2014, Eq. 27)

$$\Psi = \sum_{j=0}^{\infty}\frac{1}{j!}\frac{\partial^j f}{\partial\Lambda^j}\bigg|_{\Lambda=\bar{\Lambda}}\sum_{k=0}^{j}(-1)^k\binom{j}{k}(\bar{\Lambda})^k\left\langle\mathbf{C}^{\otimes j-k},\mathbb{H}_{j-k}\right\rangle, \tag{112}$$

which was adapted here in terms of notation. Setting $f = \nu_{\mathrm{f}}\psi_{\Lambda}$, by virtue of Eq. (71), this coincides with Eq. (94) in case $\Lambda_0 = \bar{\Lambda}$, viz.

$$\Psi = \nu_{\mathrm{f}}\sum_{k=0}^{n}\frac{1}{k!}\frac{\partial^k\psi_{\Lambda}}{\partial\Lambda^k}\bigg|_{\Lambda=\bar{\Lambda}}\mathrm{M}_{\bar{\Lambda},k}\,. \tag{113}$$

However, importantly, Cortes and Elliott (2014) noted the problems associated with neglecting compressed fibres with this method and therefore omitted the fibre switch at $\Lambda = 1$ in the series (112) (cp. their Eq. 20). For a comparison with the STEX and INEX method in Section 7.2.7, we include this switch, and refer to the corresponding method with expansion point $\Lambda_0 = \bar{\Lambda}$ as MEAN method.

*7.2.5. Zero-order term and second-order approximations*

It should be noted that the well-established approaches by Freed et al. (2005) and Gasser et al. (2006) and the elaboration by Pandolfi and Vasta (2012), Vasta et al. (2014) and Gizzi et al. (2014) can also be brought in line with the general approach (94). The formal difference that impedes the direct equivalence is that in these works the fibre free energy was formulated in terms of the isochoric stretch, more precisely as functions $\nu_\mathrm{f}\psi = \psi_\mathrm{aniso}(\tilde{I}_4)$. Provided that either the fibre energy was dependent on $I_4 = \Lambda$ instead, the deformation is isochoric or the material incompressible, the zero-order term of the series

$$\nu_\mathrm{f}\psi_\Lambda(\bar{\Lambda}) = \nu_\mathrm{f}\psi_\Lambda(\mathbf{C} : \mathbb{H}_1) \tag{114}$$

agrees with the contributions of fibres in the popular approaches (Gasser et al., 2006; Freed et al., 2005) for fibre reinforced tissues, where $\Lambda = \bar{\Lambda}$ was chosen as an expansion point. The corresponding second-order approximation

$$\Psi \approx \nu_\mathrm{f}\left(\psi_\Lambda(\bar{\Lambda}) + \frac{1}{2}\frac{\partial^2\psi_\Lambda}{\partial\Lambda^2}\bigg|_{\Lambda=\bar{\Lambda}}\mathrm{M}_{\bar{\Lambda},2}\right) = \nu_\mathrm{f}\left[\psi_\Lambda(\mathbf{C} : \mathbb{H}_1) + \frac{1}{2}\frac{\partial^2\psi_\Lambda}{\partial\Lambda^2}\bigg|_{\Lambda=\bar{\Lambda}}\left(\left\langle\mathbf{C}\otimes\mathbf{C}, \mathbb{H}_2\right\rangle - \left\langle\mathbf{C}, \mathbb{H}_1\right\rangle^2\right)\right] \tag{115}$$

captures the model in Pandolfi and Vasta (2012, Eq. 18), also found in Vasta et al. (2014) and Gizzi et al. (2014), and we emphasise that these authors recognised the meaning of the second term as a statistical variance.

Although the generalised structural tensor approaches (Freed et al., 2005; Gasser et al., 2006) may therefore formally be interpretable as zero-order representations of Eq. (94), the low degree of the series approximation typically endows these models with different characteristics than the affine structural model, unless the fibre energy is proportional to the stretch square (cf. Federico and Herzog, 2008). In the general case, these models may therefore be considered an own class, with typically different parameter sets needed to describe experimental data (see e.g. the discussion in Holzapfel and Ogden, 2017). As noted in Part I of this work (Britt and Ehret, 2022, Eq. 35), these models may likewise be interpreted as anisotropic average-stretch models, in which the relation between fibre stretch and fibre energy is generally non-affine. This view might provide an additional explanation for the differing values of the parameters since affine or non-affine modelling assumptions on fibre-kinematics generally lead to large differences in the fitted material constants while capturing the same tissue-scale experimental data at potentially comparable quality (Stracuzzi et al., 2022).

*7.2.6. Expansion point*

The identification of the GHOST, INEX and STEX methods as moment approaches with different expansion points raises the question about a suitable choice of the latter. As already explained in Section 7.1.2, we suggest to generally use $\Lambda_0 = \mathrm{E}[\Lambda] = \bar{\Lambda}$ as in the GHOST method in the absence of additional information on fibre behaviour and state of deformation that would favour a special choice. The expansion point for a generally anisotropic distribution is thus given by

$$\bar{\Lambda} = \mathrm{E}[\Lambda] = \mathrm{E}\big[\mathbf{C} : \boldsymbol{N}\otimes\boldsymbol{N}\big] = \mathbf{C} : \mathbb{H}_1\,, \tag{116}$$

and the corresponding moments become the central moments $\mathrm{M}_{\bar{\Lambda},n}$ of the distribution.

The expansion point $\Lambda_0 = J^{2/3} = I_3^{1/3}$ of the INEX method generally contradicts our arguments in Section 7.1.2, in particular the energetic argument (i) (Section 7.1.2) as the volume change $J$ does generally not reflect the energetic state of the ensemble of fibres. This issue is particularly evident in application to biological tissues. On the one hand, the corresponding fibres are often considered to work under tension only, on the other hand many of these network materials typically feature a particular kinematic behaviour that leads to volume loss ($J < 1$) not only under compressive but also tensile load states (Ehret et al., 2017). In combination this leads to expansion points $\Lambda_0 = J^{2/3} < 1$, where the fibre energy is negligible and potentially set to zero by definition. Contrary, the expectation $\bar{\Lambda}$ at least reflects the energy state of those fibres that experience the 'average' stretch.

For isotropic fibre distributions, the inequality of arithmetic and geometric means

$$\bar{\Lambda} = I_1/d \geq I_d^{1/d} \tag{117}$$

furthermore implies that $\Lambda_0 = J^{2/3} = I_3^{1/3}$ represents fibres at smaller stretch than $\bar{\Lambda}$. Since for tensile fibre stretches ($\Lambda > 1$), smaller stretch typically implies smaller energy, the energetic consideration (i) on again suggests that $\Lambda_0 = \bar{\Lambda}$ should generally be preferred.

The choice of expansion point is discussed in a numerical example in the next section.

*7.2.7. A numeric example*

The moment-based approach to approximate the full-network model with non-uniform fibre distribution is exemplified for the important special case of fibres symmetrically distributed about a preferred direction $\boldsymbol{N}_0$. We adopt the typically employed fibre orientation density function $\rho(\varphi,\vartheta) = \check{\rho}(\boldsymbol{N}(\varphi,\vartheta))$ (cf. e.g. Gasser et al., 2006, Eq. 4.3)

$$\rho(\varphi,\vartheta) = K\exp(b(\cos(2\measuredangle(\boldsymbol{N}(\varphi,\vartheta),\boldsymbol{N}_0)) + 1)) = K\exp\left(2b(\boldsymbol{N}(\varphi,\vartheta)\cdot\boldsymbol{N}_0)^2\right) \tag{118}$$

of the von Mises distribution (Fig. 8a), where $b$ is a concentration parameter, here selected as $b = 1$, $K = 2\sqrt{2b/\pi}\,/\mathrm{erfi}(\sqrt{2b})$ is a normalisation constant in terms of the imaginary error function $\mathrm{erfi}(z)$ to ensure condition (34), and the parametrisation of $\boldsymbol{N}$ in spherical coordinates follows (36). The preferred fibre direction was set to $\boldsymbol{N}_0 = (\boldsymbol{e}_1 + \boldsymbol{e}_2)/\sqrt{2}$. The fibre strain-energy density is assumed to take the likewise common, exponential form (cf. Holzapfel, 2000)

$$\psi_\Lambda(\Lambda) = \begin{cases} 0 & \text{if } \Lambda < 1, \\ \frac{c}{2k_2}\left(\exp\left(\left(k_2(\Lambda-1)^2\right)\right) - 1\right) & \text{otherwise,} \end{cases} \tag{119}$$

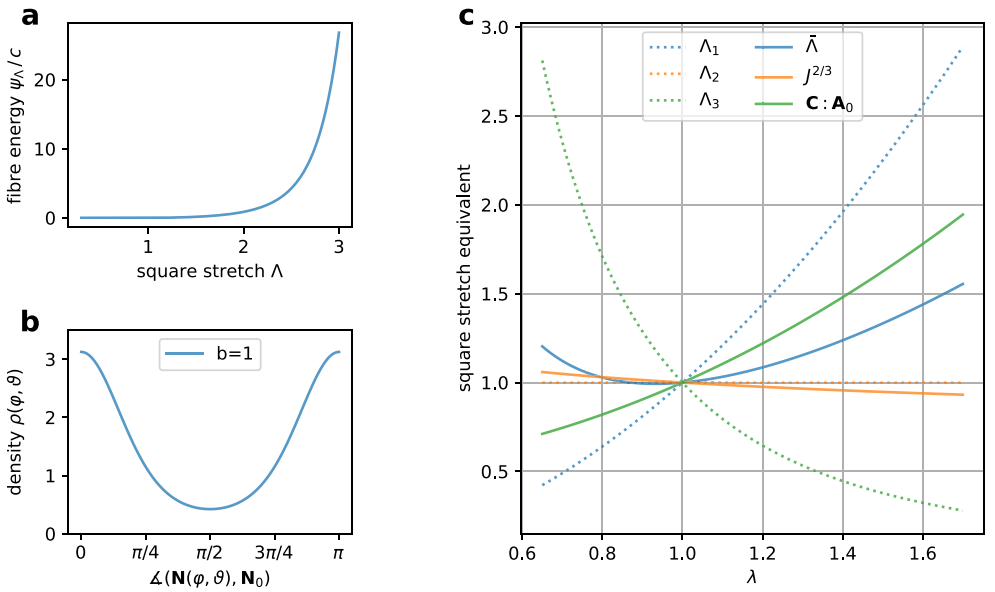


**Fig. 8.** Fibre free energy (a) and orientation distribution density (b) used in the numerical example. The deformation history is defined by the course of the three squared principal stretches (not ordered) $\{\Lambda_1 = \lambda^2, \Lambda_2 = 1, \Lambda_3\}$ (c). Solid lines in (c) show the trajectories of potential expansion points $\Lambda_0 = \bar{\Lambda}$ (MEAN), $\Lambda_0 = J^{2/3}$ (INEX) and $\Lambda_0 = \mathbf{C} : \mathbf{A}_0$ (STEX) of the moment approach (94).

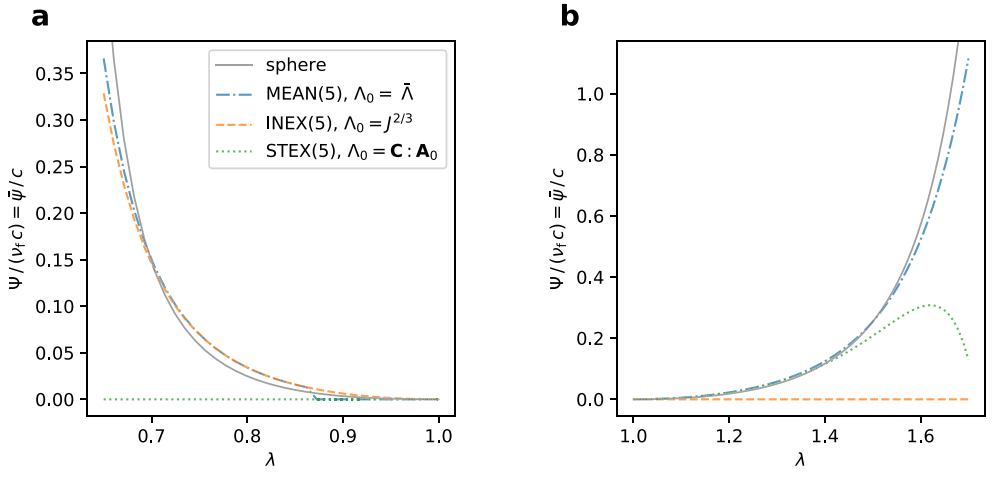


**Fig. 9.** Effect of expansion points for the moment approach (94) in the example in Fig. 8 for tensile (a) and compressive (b) range of $\lambda = \sqrt{\Lambda_1}$. Results are shown for series expanded up to $n = 5$, with expansion points $\Lambda_0 = \bar{\Lambda}$ (MEAN), $\Lambda_0 = J^{2/3}$ (INEX) and $\Lambda_0 = \mathbf{C} : \mathbf{A}_0$ (STEX). The trajectories of the respective expansion points are illustrated in Fig. 8c.

with parameters $c$ with the dimension of a force[9] and $k_2$, which was chosen as $k_2 = 1$ for illustration (Fig. 8b). The piecewise definition with zero contribution from fibres under compression ($\Lambda < 1$) is known to complicate the evaluation of both the structural

[9] We note that this dimension is due to defining $\psi_\Lambda$ as energy per fibre length (see Section 2.3).

and generalised structural tensor approach, and has caused extended discussions in the recent past (Li et al., 2018a; Holzapfel and Ogden, 2017; Pandolfi and Vasta, 2012).

To establish a numerical ground truth for comparison the classical spherical quadrature (10) was implemented based on a $N = 5810$ node Lebedev integration scheme (Burkardt, 2010) integrating exactly polynomials of up to order 131 in $\{x, y, z\}$, i.e. in $\Lambda = x^2 + y^2 + z^2$ up to order $\lfloor 131/2 \rfloor = 65$

$$\bar{\psi} \approx \sum_{i=1}^{N} \psi_\Lambda(\mathbf{C} : \boldsymbol{M}_i \otimes \boldsymbol{M}_i)\, w_i, \tag{120}$$

where $\{\boldsymbol{M}_i\}$ specify the positions of the integration points and $\{w_i\}$ are the corresponding weights.

To highlight interesting differences caused by the choice of expansion point, we consider a plane strain stretch history given by the three principal stretches $\{\lambda_k\} = \{\lambda, 1, \lambda^{-1.2}\}$ along the directions $\{\boldsymbol{N}_k\} = \{\boldsymbol{N}_1, \boldsymbol{N}_2, \boldsymbol{N}_3\}$, which in our example coincide with the fixed basis $\{\boldsymbol{e}_1, \boldsymbol{e}_2, \boldsymbol{e}_3\}$, and $\lambda$ was varied between 0.65 and 1.7 in 99 equidistant steps (100 points) (Fig. 8c).

We compared the 5th order moment-based method with expansion point $\Lambda_0 = \bar{\Lambda}$ (MEAN(5)) against those with expansion points $\Lambda_0 = J^{2/3}$ (INEX(5)) and $\Lambda_0 = \boldsymbol{N}_0 \cdot \mathbf{C} \boldsymbol{N}_0 = \mathbf{C} : \mathbf{A}_0$ (STEX(5)), and the 5810-point Lebedev scheme (sphere). The history of the different expansion points is illustrated in Fig. 8c, and the results in terms of the averaged energy $\bar{\psi}$ are shown in Fig. 9.

The figure reveals a general drawback of moment-based methods associated with a Taylor expansion of the fibre energy if the latter features discontinuous derivatives, observable here as a jump in Fig. 9a for the case MEAN(5) at $\lambda \approx 0.87$. The occurrence of such discontinuities was already pointed out in Melnik et al. (2015), Latorre and Montáns (2016) and Horgan and Murphy (2020) for special cases of order $n = 0$ models. In the present case, energy and stress are zero and continuous at the fibre switch ($\Lambda = 1$) while the second derivative (stiffness) as well as higher ones are not. Moments of order $k \geq 2$ therefore generally contribute to the approximated $\Psi$ when approaching the switch point from the right hand side ($\Lambda_0 \to 1^+$) whereas all derivatives are zero by definition for $\Lambda_0 < 1$ and hence $\Lambda_0 \to 1^-$. Generally, let $\psi_\Lambda$ be $m$ times continuously differentiable, i.e. have zero derivatives at the switch point, according to Eqs. (94) and (95) one has

$$\Lambda_0 \to 1^+ : \Psi(\mathbf{C}) = \nu_\mathrm{f} \sum_{k=m+1}^{n} \frac{1}{k!} \frac{\partial^k \psi_\Lambda}{\partial \Lambda^k}\bigg|_{\Lambda=1} \mathrm{M}_{1,k}\,, \qquad \Lambda_0 \to 1^- : \Psi(\mathbf{C}) = 0, \tag{121}$$

as well as

$$\Lambda_0 \to 1^+ : \frac{\partial \Psi}{\partial \mathbf{C}}(\mathbf{C}) = \nu_\mathrm{f} \sum_{k=m}^{n} \frac{1}{k!} \left( \frac{\partial^{k+1} \psi_\Lambda}{\partial \Lambda^k}\bigg|_{\Lambda=1} \mathrm{M}_{1,k} \frac{\partial \Lambda_0}{\partial \mathbf{C}} + \frac{\partial^k \psi_\Lambda}{\partial \Lambda^k}\bigg|_{\Lambda=1} \frac{\partial \mathrm{M}_{\Lambda_0,k}}{\partial \mathbf{C}} \right), \qquad \Lambda_0 \to 1^- : \frac{\partial \Psi}{\partial \mathbf{C}}(\mathbf{C}) = \mathbf{0}, \tag{122}$$

that cause the jump discontinuities in energy and stress respectively, and in our numerical example $m = 1$ and $n = 5$. These unphysical energy and stress discontinuities can only be avoided if $n < m$, which either limits the quality of approximation or the choice of the functional form of $\psi_\Lambda$. While the same problem can occur for the STEX and INEX methods, their plots in Fig. 9 reveal a second issue: When applied to a material that undergoes volumetric compression, all fibres in the STEX method are switched off if $J < 1$ by definition. Hence, the averaged free energy is zero in this case, independent of the actual stretch in the fibres (Fig. 9b, dashed line). On the other hand, for the STEX method, it suffices that the dominant fibre direction comes under compression to neglect the contribution of all fibres, and set the corresponding average zero (Fig. 9a, dotted line). Moreover, this method shows relatively early divergence also in Fig. 9b (dotted line), an observation that was already discussed by Hashlamoun et al. (2016).

## 8. CDF-based integration of the affine full network model

In this section we exemplify the use of the CDF representation of the stretch distribution to integrate the affine full network model. The network free energy in this case results from Eq. (22)

$$\Psi = \nu_\mathrm{f} \bar{\psi} = \nu_\mathrm{f} \left[ \psi_\Lambda(A) - \int_0^A \psi'_\Lambda(z)\, \mathrm{CDF}_\Lambda(z)\, \mathrm{d}z - \int_A^\infty \psi'_\Lambda(z)\, (\mathrm{CDF}_\Lambda(z) - 1)\, \mathrm{d}z \right] \tag{123}$$

upon insertion of the affine CDF, which in the general anisotropic case is given by Eq. (60). Although by this means the integration of the anisotropic affine full network model is therefore possible, we here restrict to the isotropic case in both 2D and 3D, in which the CDF can be given in closed form by means of essential functions. We put special emphasis on fibre laws characterised by a tension–compression switch, as this typically complicates the common spherical integration due to a deformation-dependent integration domain on the sphere (see e.g. Holzapfel and Ogden, 2015; Gizzi et al., 2016; Li et al., 2018b).

To simplify the analysis, we will assume the case of mutually distinct eigenvalues of $\mathbf{C}$, and note that this case can always be enforced numerically by adding a small perturbations to the eigenvalues if needed, and that the effect on the result should be acceptable in a stable problem. The eigenvalues are denoted by $\Lambda_2 < \Lambda_1$ in 2D and $\Lambda_3 < \Lambda_2 < \Lambda_1$ in 3D. As a consequence of mutual distinctness, the eigenvalues $\{\Lambda_i\}$ and eigenprojections $\{\mathbf{P}_i\}$, for which $\mathbf{C} = \Lambda_i \mathbf{P}_i$, are differentiable, and case distinctions can be omitted in this case, i.e.

$$\frac{\partial \Lambda_i}{\partial \mathbf{C}} = \mathbf{P}_i\,, \quad \frac{\partial \mathbf{P}_i}{\partial \mathbf{C}} = \sum_{\substack{j=1 \\ j \neq i}}^{d} \frac{\mathbf{P}_i \boxtimes \mathbf{P}_j + \mathbf{P}_j \boxtimes \mathbf{P}_i}{\Lambda_i - \Lambda_j}\,. \tag{124}$$

By this means, the stress and tangent tensor in the isotropic case are found by use of the chain rule of differentiation as

$$\mathbf{S} = 2\frac{\partial \check{\Psi}}{\partial \Lambda_i}\mathbf{P}_i\,, \quad \mathbb{C} = 4\frac{\partial^2 \check{\Psi}}{\partial \Lambda_j \partial \Lambda_i}\mathbf{P}_i \otimes \mathbf{P}_j + 4\frac{\partial \check{\Psi}}{\partial \Lambda_i}\frac{\partial \mathbf{P}_i}{\partial \mathbf{C}}\,, \tag{125}$$

respectively, where $\check{\Psi}(\{\Lambda_i\}) = \hat{\Psi}(\Lambda_i \mathbf{P}_i)$. A general derivation of Eq. (124) for non-symmetric tensors can be found in Itskov (2019, Sec. 7).[10] Moreover, for $d = 3$, a specific derivation leading to an analogue version of Eq. $(124)_2$ is given in Miehe (1998, Eq. 17).

Finally, we will make use of the essential property of the affine assumption that no fibre can experience a stretch outside the interval spanned by the smallest and largest principal stretch, i.e. $[\Lambda_d, \Lambda_1]$, which predetermines $\mathrm{CDF}_\Lambda$ to be zero for arguments strictly smaller than $\Lambda_d$ and one for arguments strictly larger $\Lambda_1$. As a consequence the lower and upper integration bounds of Eq. (123) change from zero and infinity to $\Lambda_d$ and $\Lambda_1$, respectively. In the main body of this paper we concentrate on the 3D case, the 2D case is treated in Appendix G.

### 8.1. Isotropic 3D case

In view of the special integration bounds of the affine case, it is appropriate to express Eq. (22) as

$$\bar{\psi} = \psi_\Lambda(\Lambda_2) - \int_{\Lambda_3}^{\Lambda_2} \psi'_\Lambda \mathrm{CDF}_\Lambda \,\mathrm{d}z - \int_{\Lambda_2}^{\Lambda_1} \psi'_\Lambda (\mathrm{CDF}_\Lambda - 1)\,\mathrm{d}z\,, \tag{126}$$

where the affine stretch distribution (Eqs. (56), (59)) is to be inserted for $\mathrm{CDF}_\Lambda$. Continuing with the isotropic case (61) of the latter one obtains

$$\bar{\psi} = \psi_\Lambda(\Lambda_1) + \psi_\Lambda(\Lambda_3) - \psi_\Lambda(\Lambda_2) + \int_{\Lambda_3}^{\Lambda_2} \psi'_\Lambda(z)\,\frac{1}{\pi}\int_{-\pi/2}^{\pi/2} \hat{u}(z,y)\,\mathrm{d}y\,\mathrm{d}z - \int_{\Lambda_2}^{\Lambda_1} \psi'_\Lambda(z)\,\frac{1}{\pi}\int_{-\pi/2}^{\pi/2} \check{u}(z,y)\,\mathrm{d}y\,\mathrm{d}z\,, \tag{127}$$

where $\hat{u}$ and $\check{u}$ are given in Eqs. (55) and (58), respectively. Introducing the parameter $\alpha = (\Lambda_1 - \Lambda_2)/(\Lambda_1 - \Lambda_3) \in (0,1)$ and using the substitutions

$$z_s : (0,1) \to (\Lambda_3, \Lambda_2), \quad z_s(s) = (\Lambda_3 - \Lambda_2)s + \Lambda_2, \qquad z_t : (0,1) \to (\Lambda_2, \Lambda_1), \quad z_t(t) = (\Lambda_1 - \Lambda_2)t + \Lambda_2, \tag{128}$$

Eq. (127) can be rescaled as

$$\bar{\psi} = \psi_\Lambda(\Lambda_1) + \psi_\Lambda(\Lambda_3) - \psi_\Lambda(\Lambda_2) + (\Lambda_2 - \Lambda_3)\underbrace{\int_0^S \psi'_\Lambda(z_s(s))\, f((1-\alpha)s, \alpha)\,\mathrm{d}s}_{①} - (\Lambda_1 - \Lambda_2)\underbrace{\int_T^1 \psi'_\Lambda(z_t(t))\, f(\alpha t, 1-\alpha)\,\mathrm{d}t}_{②}\,, \tag{129}$$

where $S = 1$ and $T = 0$ to consider energetic contributions of all fibres or

$$S(\Lambda_2, \Lambda_3) = \min\left(\max\left(\frac{1-\Lambda_2}{\Lambda_3 - \Lambda_2}, 0\right), 1\right), \qquad T(\Lambda_1, \Lambda_2) = \min\left(\max\left(\frac{1-\Lambda_2}{\Lambda_1 - \Lambda_2}, 0\right), 1\right) \tag{130}$$

to implement a tension–compression switch that excludes fibres under compression. In both cases, the function $f$ is defined as

$$f : (0,1)\times(0,1) \to \mathbb{R}, \qquad x, y \mapsto \frac{1}{\pi}\int_{-\pi/2}^{\pi/2} \sqrt{\frac{x + y\cos^2(\phi)}{1 - y\sin^2(\phi)}}\,\mathrm{d}\phi\,. \tag{131}$$

The latter can be expressed in terms of elementary functions as (see Appendix H)

$$f : (0,1)\times(0,1) \to \mathbb{R}\,, \qquad x, y \mapsto \frac{2(x+y)}{\pi\sqrt{x}}\,\Pi\left(-\frac{y}{x}\middle|\,\frac{y(x+y-1)}{x}\right), \tag{132}$$

where $\Pi$ is the complete elliptic integral of the third kind (see e.g. Abramowitz and Stegun, 1972), i.e.

$$\Pi(n|m) = \int_0^{\pi/2} \frac{\mathrm{d}\theta}{(1 - n\sin^2(\theta))\sqrt{1 - m\sin^2(\theta)}}\,. \tag{133}$$

For the calculation of stress and stiffness we further note the first and second derivatives

$$\begin{aligned}
\bar{\psi}_{,\Lambda_1} &= \psi'_\Lambda(\Lambda_1) - ② + (\Lambda_2 - \Lambda_3)③\alpha_{,\Lambda_1} - (\Lambda_1 - \Lambda_2)\left[④ + ⑤\alpha_{,\Lambda_1}\right],\\
\bar{\psi}_{,\Lambda_2} &= -\psi'_\Lambda(\Lambda_2) + ① + ② + (\Lambda_2 - \Lambda_3)\left[⑥ + ③\alpha_{,\Lambda_2}\right] - (\Lambda_1 - \Lambda_2)\left[⑦ + ⑤\alpha_{,\Lambda_2}\right],\\
\bar{\psi}_{,\Lambda_3} &= \psi'_\Lambda(\Lambda_3) - ① + (\Lambda_2 - \Lambda_3)\left[⑧ + ③\alpha_{,\Lambda_3}\right] - (\Lambda_1 - \Lambda_2)⑤\alpha_{,\Lambda_3}\,,
\end{aligned} \tag{134}$$

[10] Please note the different use of the symbol "⊗" in this reference.

and

$$
\begin{aligned}
\bar{\psi}_{,\Lambda_1\Lambda_1} &= \psi''_\Lambda(\Lambda_1) - 2\Big(④ + ⑤\alpha_{,\Lambda_1}\Big) + (\Lambda_2-\Lambda_3)\Big[⑨\alpha_{,\Lambda_1}^2 + ③\alpha_{,\Lambda_1\Lambda_1}\Big] \\
&\quad - (\Lambda_1-\Lambda_2)\Big[\ ⑩ + 2⑪\alpha_{,\Lambda_1} + ⑫\alpha_{,\Lambda_1}^2 + ⑤\alpha_{,\Lambda_1\Lambda_1} - \psi''_\Lambda(1)Tf(\alpha T, 1-\alpha)T_{,\Lambda_1}\ \Big], \\
\bar{\psi}_{,\Lambda_1\Lambda_2} &= ③\alpha_{,\Lambda_1} - ⑦ - ⑤\alpha_{,\Lambda_2} + ④ + ⑤\alpha_{,\Lambda_1} + (\Lambda_2-\Lambda_3)\Big[⑬\alpha_{,\Lambda_1} + ⑨\alpha_{,\Lambda_2}\alpha_{,\Lambda_1} + ③\alpha_{,\Lambda_1\Lambda_2}\Big] \\
&\quad - (\Lambda_1-\Lambda_2)\Big[\ ⑭ + ⑪\alpha_{,\Lambda_2} + ⑮\alpha_{,\Lambda_1} + ⑫\alpha_{,\Lambda_2}\alpha_{,\Lambda_1} + ⑤\alpha_{,\Lambda_1\Lambda_2} - \psi''_\Lambda(1)Tf(\alpha T, 1-\alpha)T_{,\Lambda_2}\ \Big], \\
\bar{\psi}_{,\Lambda_1\Lambda_3} &= -⑤\alpha_{,\Lambda_3} - ③\alpha_{,\Lambda_1} + (\Lambda_2-\Lambda_3)\Big[⑯\alpha_{,\Lambda_1} + ⑨\alpha_{,\Lambda_3}\alpha_{,\Lambda_1} + ③\alpha_{,\Lambda_1\Lambda_3}\Big] \\
&\quad - (\Lambda_1-\Lambda_2)\Big[⑪\alpha_{,\Lambda_3} + ⑫\alpha_{,\Lambda_3}\alpha_{,\Lambda_1} + ⑤\alpha_{,\Lambda_1\Lambda_3}\Big], \\
\bar{\psi}_{,\Lambda_2\Lambda_2} &= -\psi''_\Lambda(\Lambda_2) + 2\Big(⑥ + ③\alpha_{,\Lambda_2}\Big) + 2\Big(⑦ + ⑤\alpha_{,\Lambda_2}\Big) \\
&\quad + (\Lambda_2-\Lambda_3)\Big[\ ⑰ + 2⑬\alpha_{,\Lambda_2} + ⑨\alpha_{,\Lambda_2}^2 + \psi''_\Lambda(1)(1-S)f((1-\alpha)S,\alpha)S_{,\Lambda_2}\ \Big] \\
&\quad - (\Lambda_1-\Lambda_2)\Big[\ ⑲ + 2⑮\alpha_{,\Lambda_2} + ⑫\alpha_{,\Lambda_2}^2 - \psi''_\Lambda(1)(1-T)f(\alpha T, 1-\alpha)T_{,\Lambda_2}\ \Big], \\
\bar{\psi}_{,\Lambda_2\Lambda_3} &= ⑧ + ③\alpha_{,\Lambda_3} + ⑤\alpha_{,\Lambda_3} - ⑥ - ③\alpha_{,\Lambda_2} \\
&\quad + (\Lambda_2-\Lambda_3)\Big[\ ⑱ + ⑬\alpha_{,\Lambda_3} + ⑯\alpha_{,\Lambda_2} + ⑨\alpha_{,\Lambda_3}\alpha_{,\Lambda_2} + ③\alpha_{,\Lambda_2\Lambda_3} + \psi''_\Lambda(1)(1-S)f((1-\alpha)S,\alpha)S_{,\Lambda_3}\ \Big] \\
&\quad - (\Lambda_1-\Lambda_2)\Big[⑮\alpha_{,\Lambda_3} + ⑫\alpha_{,\Lambda_3}\alpha_{,\Lambda_2} + ⑤\alpha_{,\Lambda_2\Lambda_3}\Big], \\
\bar{\psi}_{,\Lambda_3\Lambda_3} &= \psi''_\Lambda(\Lambda_3) - 2\Big(⑧ + ③\alpha_{,\Lambda_3}\Big) + (\Lambda_2-\Lambda_3)\Big[\ ⑳ + 2⑯\alpha_{,\Lambda_3} + ⑨\alpha_{,\Lambda_3}^2 + ③\alpha_{,\Lambda_3\Lambda_3} + \psi''_\Lambda(1)Sf((1-\alpha)S,\alpha)S_{,\Lambda_3}\ \Big] \\
&\quad - (\Lambda_1-\Lambda_2)\Big[⑫\alpha_{,\Lambda_3}^2 + ⑤\alpha_{,\Lambda_3\Lambda_3}\Big],
\end{aligned}
\tag{135}
$$

respectively. The required integrals $\{(i)\}_{i=3\ldots,20}$ are specified in Appendix F.

The bottleneck of the presented approach for integration of the fibre constitutive law lies in the evaluation of the elliptic function (131), equivalently Eq. (132), and its derivatives.

### 8.2. A numerical example

The CDF-based integration approach is illustrated in application to an isotropic network, i.e. $\rho(\varphi,\vartheta) = 1$, with the previously defined exponential-type fibre energy (119). The specific load case was defined by a pure stretch history $\{\lambda_k\} = \{1.1, \lambda, 0.8\}$ with 100 equidistant points $\lambda \in [0.95, 1.05]$ so that the amount of fibres under tension varies during the experiment. For comparison again the 5810-point Lebedev scheme (120) was used, which implies

$$
\frac{\partial\bar{\psi}}{\partial\mathbf{C}} \approx \sum_{i=1}^{5810} \psi'_\Lambda(\mathbf{C} : \boldsymbol{M}_i\otimes\boldsymbol{M}_i)\boldsymbol{M}_i\otimes\boldsymbol{M}_i\, w_i \tag{136}
$$

and

$$
\frac{\partial^2\bar{\psi}}{\partial\mathbf{C}\partial\mathbf{C}} \approx \sum_{i=1}^{5810} \psi''_\Lambda(\mathbf{C} : \boldsymbol{M}_i\otimes\boldsymbol{M}_i)\boldsymbol{M}_i\otimes\boldsymbol{M}_i\otimes\boldsymbol{M}_i\otimes\boldsymbol{M}_i\, w_i \tag{137}
$$

for the derivatives.

For the evaluation of the integrals $\{(i)\}_{i=1,\ldots,20}$ in the CDF-based integration approach a $N = 10$ point Gauss–Legendre integration was used, such that, e.g.,

$$
① = \int_0^S \psi'_\Lambda(z_s(s))\, f((1-\alpha)s,\alpha)\,\mathrm{d}s \approx \sum_{i=1}^{10} \psi'_\Lambda(z_s(s_i))\, f((1-\alpha)s_i,\alpha)\, w_i \tag{138}
$$

where $\{s_i\}$ are the Gauss–Legendre integration points adjusted to the interval $[0, S]$ and $\{w_i\}$ the corresponding weights.

As by virtue of Eq. (125) the derivatives of the energy $\bar{\psi}$ with respect to $\mathbf{C}$ follow from the derivatives of $\bar{\psi}$ with respect to the eigenvalues $\{\Lambda_i\}$, for the sake of a compact comparison only the latter derivatives are calculated, and it was used that it must also hold that

$$
\frac{\partial\bar{\psi}}{\partial\mathbf{C}} : \mathbf{P}_i = \frac{\partial\bar{\psi}}{\partial\Lambda_i} \tag{139}
$$

for all $i = 1, 2, 3$ and

$$
\left\langle \frac{\partial^2\bar{\psi}}{\partial\mathbf{C}\partial\mathbf{C}}, \mathbf{P}_i\otimes\mathbf{P}_j \right\rangle = \frac{\partial^2\bar{\psi}}{\partial\Lambda_i\partial\Lambda_j} \tag{140}
$$

due to the orthogonality of the eigenprojections $\{\mathbf{P}_i\}$.

Fig. 10 reports the results in terms of strain-energy and stress (both normalised by $\nu_f c$) and shows excellent agreement between the 10-point CDF-based integration (to be applied twice for the energy and additional 6 times for the stress) and the 5810-point

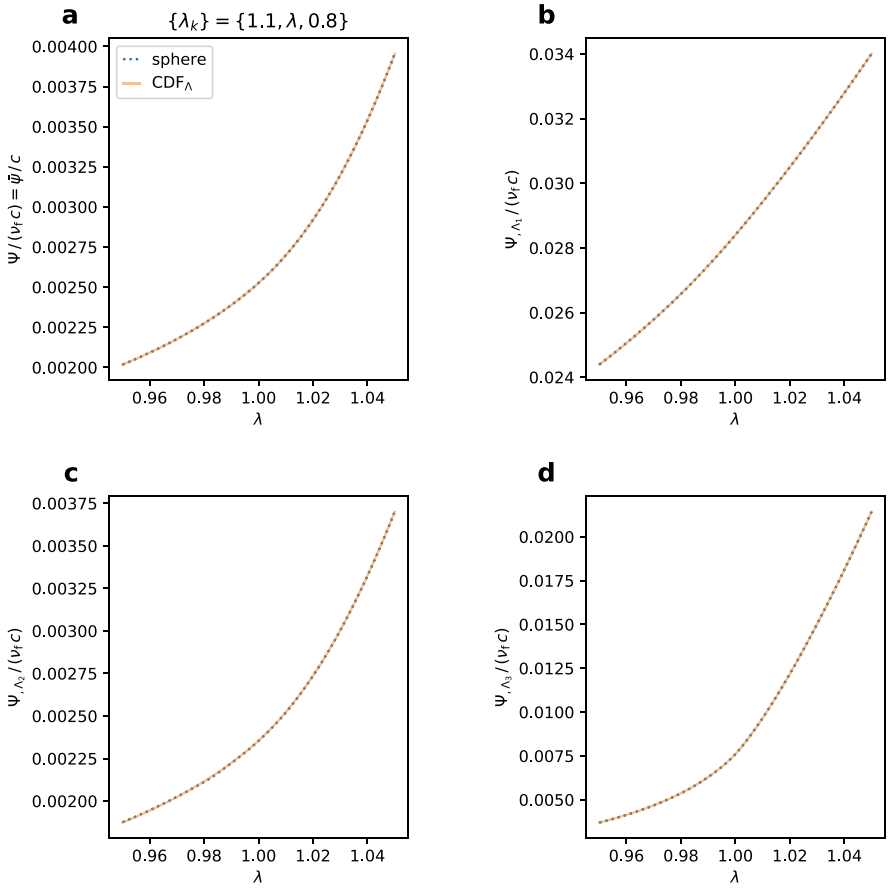


**Fig. 10.** Comparison between CDF-based integration in 3D with 10 integration points (per integral 1–8) and spherical Lebedev integration with 5810 integration points: Averaged fibre energy (a) and first derivatives (b-d) based on Eqs. (134) vs. (136), (139).

spherical quadrature. The advantage in accuracy becomes apparent when comparing the second derivatives (135) against those obtained by spherical integration (Eqs. (137), (140)), which define the tangent tensor $(125)_2$. The smooth curves in Fig. 11 document the insensitivity of the CDF-based approach against fibres switching on and off, compared to the spherical integration, which still displays the switch-associated discontinuities despite the already extremely high-order integration scheme.

### 8.3. Numeric evaluation of stress and tangent tensors

Even if only 10 Gauss points are required, the 6 additional integrals in (134) and 12 additional ones in (135) together with those in the energy add up to 20. Although the implementation of these integrals is merely cumbersome, and does generally not pose a technical obstacle, we provide in the following schemes to determine stress and tangent based on numerical differentiation as often used in the framework of computational inelasticity (e.g. Miehe, 1996; Pérez-Foguet et al., 2000). While in general this will not have less computational cost than evaluating the 20 auxiliary integrals $\{\textcircled{i}\}_{i=1,\dots,20}$, it might be advantageous in view of optimisation techniques that use automatic differentiation schemes, and therefore do not require the implementation of the derivatives.

In the isotropic case $\Psi$ is a function of the eigenvalues of $\mathbf{C}$. Hence the numeric differentiation can be limited to the change of $\Psi$ with respect to the (distinct) eigenvalues, whereas in turn their change with respect to $\mathbf{C}$ is considered in analytic terms, i.e. the numeric forward difference quotient estimates (cp. e.g. Pérez-Foguet et al., 2000)

$$\frac{\partial \check{\Psi}}{\partial \Lambda_i} \approx \frac{\check{\Psi}(\{\Lambda_k + \delta_{ik}\epsilon\}) - \check{\Psi}(\{\Lambda_k\})}{\epsilon} \tag{141}$$

and

$$\frac{\partial^2 \check{\Psi}}{\partial \Lambda_j \partial \Lambda_i} \approx \frac{\check{\Psi}(\{\Lambda_k + (\delta_{ik} + \delta_{jk})\epsilon\}) - \check{\Psi}(\{\Lambda_k + \delta_{jk}\epsilon\}) - \check{\Psi}(\{\Lambda_k + \delta_{ik}\epsilon\}) + \check{\Psi}(\{\Lambda_k\})}{\epsilon^2} \tag{142}$$

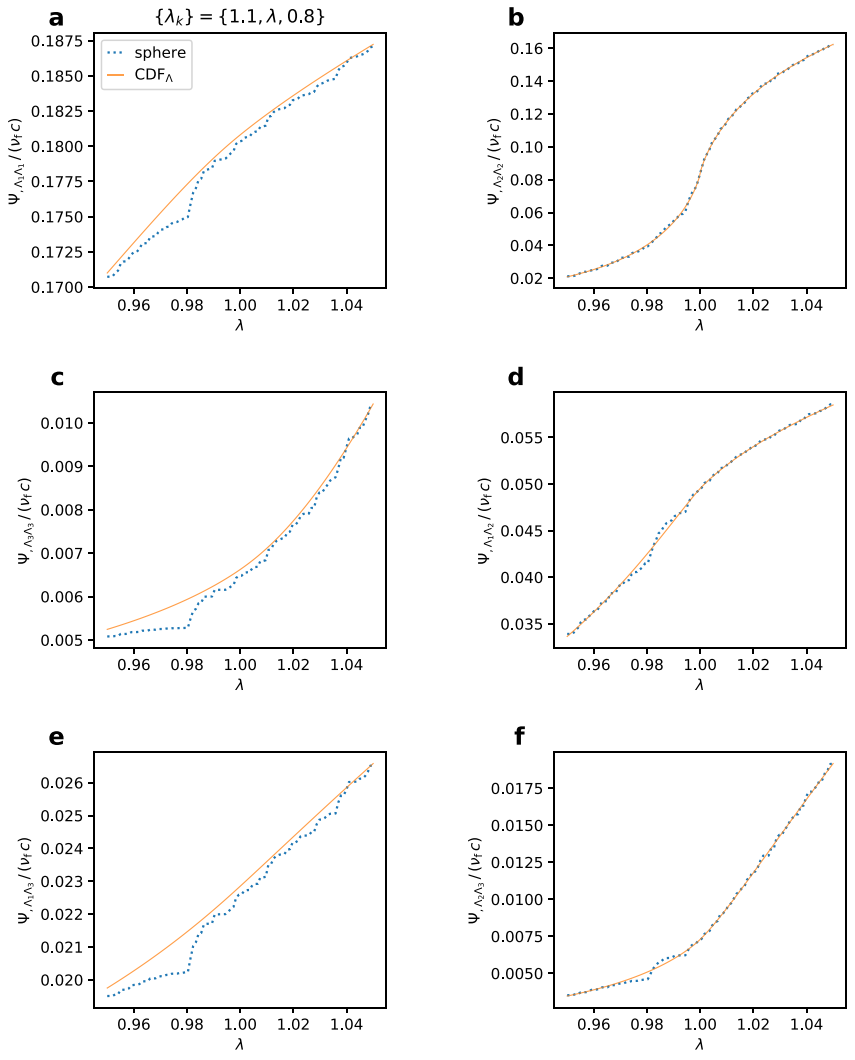


**Fig. 11.** Comparison between CDF-based integration in 3D with 10 integration points (per integral 3–12) and spherical Lebedev integration with 5810 integration points: Second derivatives (a–f) based on Eqs. (135) vs. (137), (140).

can be inserted into Eq. (125). The set notation $\{...\}$ used here includes all elements of the indices $k = 1, \dots, d$, and the Kronecker delta symbol $\delta_{ik} = 1$ if $i = k$ or 0 otherwise. We note that this technique strictly requires the eigenvalues to be distinct, as it relies on the validity of Eq. (124). However, adapting the argumentation in Miehe (1998) this can always be ensured by adding small variations to the eigenvalues when necessary. Given a stable problem this is justifiable because, by definition, it may only cause a small variation of the result. It can be concluded by counting that the required total number of function evaluations for $\hat{\Psi}$ in the expressions (141) and (142) is 6 in the 2D and 10 in the 3D setting.

More generally, in the isotropic or anisotropic case, one can approximate the directional derivative (cf. e.g. Itskov, 2019, Sec. 6) using small $\epsilon$ as

$$\frac{\partial \hat{\Psi}}{\partial \mathbf{C}} : \mathbf{T} = \frac{\mathrm{d}}{\mathrm{d}\epsilon} \hat{\Psi}(\mathbf{C} + \epsilon \mathbf{T}) \Big|_{\epsilon=0} \approx \frac{\hat{\Psi}(\mathbf{C} + \epsilon \mathbf{T}) - \hat{\Psi}(\mathbf{C})}{\epsilon} \tag{143}$$

and, applying this twice, for small $\epsilon_1$ and $\epsilon_2$

$$\left\langle \frac{\partial^2 \hat{\Psi}}{\partial \mathbf{C} \partial \mathbf{C}}, \mathbf{T} \otimes \mathbf{U} \right\rangle = \frac{\mathrm{d}^2}{\mathrm{d}\epsilon_2 \mathrm{d}\epsilon_1} \hat{\Psi}(\mathbf{C} + \epsilon_1 \mathbf{T} + \epsilon_2 \mathbf{U}) \Big|_{\substack{\epsilon_1=0 \\ \epsilon_2=0}} \approx \frac{\hat{\Psi}(\mathbf{C} + \epsilon_1 \mathbf{T} + \epsilon_2 \mathbf{U}) - \hat{\Psi}(\mathbf{C} + \epsilon_1 \mathbf{T}) - \hat{\Psi}(\mathbf{C} + \epsilon_2 \mathbf{U}) + \hat{\Psi}(\mathbf{C})}{\epsilon_1 \epsilon_2}, \tag{144}$$

valid for all suitable symmetric second-order tensors $\mathbf{T}$ and $\mathbf{U}$. For example, choosing $\mathbf{T}$ and $\mathbf{U}$ as $(\boldsymbol{e}_i \otimes \boldsymbol{e}_j + \boldsymbol{e}_j \otimes \boldsymbol{e}_i)/2$ for $i \in \{1, 2, d\}$ and $j \in \{1, 2, d\}$, it can be concluded by counting that all unique components of $\partial\hat{\Psi}/\partial\mathbf{C}$ and $\partial^2\hat{\Psi}/\partial\mathbf{C}\partial\mathbf{C}$ according to Eqs. (143) and (144) can be computed with a total number of 10 and 28 function evaluations for $\hat{\Psi}$ in the 2D and 3D case, respectively.

## 9. Summary and conclusions

In the present contribution the framework to model the mechanical behaviour of materials with network microstructures based on the distribution of stretch as proposed in Part I of this series of papers was further elaborated. At first, (i) an alternative representation in terms of the cumulative distribution function of stretch was developed. This representation brings both conceptional and computational advantages, since it is not dependent on the existence of a probability density function, and it is generally free of essential discontinuities and even bounded between zero and one, in clear contrast to the latter. Next, the approach was applied to model materials with affinely deforming fibres. This procedure led to (ii) a rigorous investigation of the 'affine stretch distribution' in terms of its cumulative distribution function and density. Finally, the special case of affine networks allowed considering (iii) non-uniform initial fibre orientation distributions within the new framework.

These steps provided new perspectives on classical approaches to deal with network and fibre materials such as the affine full-network model of rubber elasticity and the structural approach in biomechanics, including the following aspects:

- The assumption of affine fibre kinematics implies that the stretches within the network obey a particular probability distribution, here referred to as affine distribution, which depends on the network's macroscopic state of deformation.
- Using this distribution as a starting point, the stretch-statistical approach for modelling materials with network microstructure proposed in Part I generally serves to compute the response of materials with affine fibre kinematics.
- The directional averaging over the unit sphere inherent to the full network and structural approaches can be circumvented by three alternative averaging operations based on the stretch distribution, its probability density or its moments.
- While the use of the affine probability density function was omitted due to its essential singularities, the cumulative distribution function proved to be well suited to accurately integrate the isotropic full network model even for highly non-linear 'tension-only' constitutive behaviour of the fibres. Nonetheless, its potential advantage over classical spherical integration in terms of computational cost still needs to be evaluated, and may strongly depend on both the efficiency of the implementation and the specific problem to be solved.
- The presented general moment-based, i.e. higher order structural tensor formulation of the problem includes several approaches proposed in literature as special cases, which can partly be reconciled with each other, or at least be shown to belong to a family of models which actually makes use of the statistical moments of the affine distribution. Several improvements were proposed in terms of either more compact representations or computationally more efficient forms.
- The expansion points about which the moments are formulated have a strong impact on the performance of these higher order structural tensor models. In general, when 'tension-only' fibre laws are considered, the considered moment-based approximations can suffer from discontinuities even in the averaged energy if moments higher than order 0 are used.

In conclusion, this work enhances the theoretical understanding of full network and structural approaches as well-established and widespread averaging strategies in constitutive modelling of fibrous materials and tissues. We anticipate that the alternative perception of these concepts as averages over a known distribution of fibre stretch instead of a known distribution of fibre orientation may open up further alternative routes to efficiently implement these and related approaches in the future.

## CRediT authorship contribution statement

**Ben R. Britt:** Conceptualization, Methodology, Software, Investigation, Formal analysis, Visualization, Validation, Data curation, Writing – original draft, Writing – review & editing. **Alexander E. Ehret:** Conceptualization, Methodology, Formal analysis, Validation, Supervision, Funding acquisition, Project administration, Writing – original draft, Writing – review & editing.

## Declaration of competing interest

The authors declare that they have no known competing financial interests or personal relationships that could have appeared to influence the work reported in this paper.

## Funding

A. E. Ehret and B. R. Britt acknowledge the financial support of this work from the Swiss National Science Foundation (SNSF, Grant No. 182014).

## Data availability

No data was used for the research described in the article

## Appendix A. Definitions

Let the *scalar product* '$\langle\,,\rangle$' between two tensors of arbitrary order $n \geq 1$ be the inner product defined by

$$\langle \boldsymbol{a}_1 \otimes \ldots \otimes \boldsymbol{a}_n, \boldsymbol{b}_1 \otimes \ldots \otimes \boldsymbol{b}_n \rangle = \prod_{i=1}^{d} \boldsymbol{a}_i \cdot \boldsymbol{b}_i \tag{A.1}$$

and, by understanding tensors of order zero as real numbers, we extend this definition by including the common product between real numbers, so that $\langle a, b\rangle = ab$ for $n = 0$. For tensors given as e.g. $\mathbb{A} = A^{i\ldots j}\,\boldsymbol{g}_i \otimes \ldots \otimes \boldsymbol{g}_j$ and $\mathbb{B} = B_{s\ldots t}\,\boldsymbol{g}^s \otimes \ldots \otimes \boldsymbol{g}^t$, with respect to bases formed by the dual sets of base vectors $\{\boldsymbol{g}_i\}$, $\{\boldsymbol{g}^j\}$ so that $\boldsymbol{g}_i \cdot \boldsymbol{g}^j = \delta_i^j$ (Kronecker delta), this definition thus provides

$$\langle \mathbb{A}, \mathbb{B} \rangle = A^{i\ldots j}\,B_{s\ldots t}\,\delta_i^s \ldots \delta_j^t = A^{i\ldots j}\,B_{i\ldots j}, \tag{A.2}$$

and we note that the distinction between super- and subscript indices is not necessary when working with orthonormal bases.

In addition to the 'complete' contraction (A.1), we introduce a *k-contraction* '$\overset{k}{:}$' between two tensors of order $n \geq k$ and $m \geq k$, respectively, as the multi-linear operation defined by (cf. Rubin, 2021)

$$\boldsymbol{a}_1 \otimes \ldots \otimes \boldsymbol{a}_n \overset{k}{:} \boldsymbol{b}_1 \otimes \ldots \otimes \boldsymbol{b}_m = \prod_{i=1}^{k} \left(\boldsymbol{a}_{n-k+i} \cdot \boldsymbol{b}_i\right) \boldsymbol{a}_1 \otimes \ldots \otimes \boldsymbol{a}_{n-k} \otimes \boldsymbol{b}_{k+1} \otimes \ldots \otimes \boldsymbol{b}_m\,. \tag{A.3}$$

Understanding $\mathbb{A}$ and $\mathbb{B}$ as tensors of order $n \geq k$ and $m \geq k$ respectively, analogously to Eq. (A.2) this definition yields

$$\mathbb{A} \overset{k}{:} \mathbb{B} = A^{i\ldots j s\ldots t}\,B_{s\ldots t u\ldots v}\,\underbrace{\boldsymbol{g}_i \otimes \ldots \otimes \boldsymbol{g}_j}_{n-k} \otimes \underbrace{\boldsymbol{g}^u \otimes \ldots \otimes \boldsymbol{g}^v}_{m-k}, \tag{A.4}$$

and the special case $k = 2$ is the double contraction, viz.

$$\mathbb{A} : \mathbb{B} = \mathbb{A} \overset{2}{:} \mathbb{B}\,. \tag{A.5}$$

We define the tensor product '$\boxtimes$' between two second order tensors such that

$$\mathbf{A} \boxtimes \mathbf{B} : \mathbf{X} = \mathbf{A}\frac{\mathbf{X} + \mathbf{X}^{\mathrm{T}}}{2}\mathbf{B} \tag{A.6}$$

for all second order tensors $\mathbf{A}$, $\mathbf{B}$ and $\mathbf{X}$, which implies e.g. for $\mathbf{A} = A^{ij}\,\boldsymbol{g}_i \otimes \boldsymbol{g}_j$ and $\mathbf{B} = B^{ij}\,\boldsymbol{g}_i \otimes \boldsymbol{g}_j$

$$\mathbf{A} \boxtimes \mathbf{B} = \frac{A^{is}\,B^{tj} + A^{it}\,B^{sj}}{2}\,\boldsymbol{g}_i \otimes \boldsymbol{g}_j \otimes \boldsymbol{g}_s \otimes \boldsymbol{g}_t\,. \tag{A.7}$$

The $n$th tensor power of a tensor $\mathbb{A}$ of arbitrary order is defined as (cp. Hashlamoun et al., 2016)

$$\mathbb{A}^{\otimes n} = \underbrace{\mathbb{A} \otimes \ldots \otimes \mathbb{A}}_{n \text{ times}}, \tag{A.8}$$

which is understood to include $\mathbb{A}^{\otimes 0} = 1 \in \mathbb{R}$ by convention.

For two tensors $\mathbb{A}$ and $\mathbb{B}$ of orders $n$ and $m$, where we understand the former to be a function of the latter, i.e. $\mathbb{A} = \mathbb{F}(\mathbb{B})$, the derivative of $\mathbb{A}$ with respect to $\mathbb{B}$ is defined such that

$$\frac{\partial \mathbb{A}}{\partial \mathbb{B}} \overset{m}{:} \mathbb{T} = \frac{\mathrm{d}}{\mathrm{d}\epsilon}\mathbb{F}(\mathbb{B} + \epsilon\mathbb{T})\bigg|_{\epsilon=0} \tag{A.9}$$

for all tensors $\mathbb{T}$ of order $m$ compatible with $\mathbb{B}$. Expressed with the component representations $\mathbb{A} = A_{i\ldots j}\boldsymbol{e}_i \otimes \ldots \otimes \boldsymbol{e}_j$ and $\mathbb{B} = B_{s\ldots t}\boldsymbol{e}_s \otimes \ldots \otimes \boldsymbol{e}_t$, where $\{\boldsymbol{e}_i\}$ forms a fixed orthonormal basis, this yields (without special considerations of potential symmetries)

$$\frac{\partial \mathbb{A}}{\partial \mathbb{B}} = \frac{\partial A_{i\ldots j}}{\partial B_{s\ldots t}}\boldsymbol{e}_i \otimes \ldots \otimes \boldsymbol{e}_j \otimes \boldsymbol{e}_s \otimes \ldots \otimes \boldsymbol{e}_t\,. \tag{A.10}$$

## Appendix B. Generalised structural tensors in the 2D case

The definition of the $n$th even order structural tensor (76) is valid in the $d$-dimensional case. In analogy to the 3D expression (77) one finds for 2D

$$\mathbb{H}_{n|p,q} = \mathrm{E}\left[(\boldsymbol{N} \cdot \boldsymbol{e}_1)^p (\boldsymbol{N} \cdot \boldsymbol{e}_2)^q\right] = \mathrm{E}\left[\cos^p(\varphi)\sin^q(\varphi)\right]. \tag{B.1}$$

The properties (79) and (80) hold for any dimension $d$. While Eq. (80) thus translates into Eq. (81) in the 3D case, its 2D equivalent reads

$$\mathbb{H}_{n|p,q} = \mathbb{H}_{n+1|p+2,q} + \mathbb{H}_{n+1|p,q+2}\,. \tag{B.2}$$

## Appendix C. Moments in the isotropic 2D case

If the referential fibre orientation is uniform, the components of the generalised structural tensors (B.1) drastically simplify, and the moments can be evaluated according to (68). However, in the isotropic case, one may also directly evaluate the defining Eq. (66) by an analytic integration over the unit circle. The representations of the square stretch Eq. $(32)_1$ and its mean Eq. (70) thus allow to write the $n$th moment of the affine stretch distribution (24) as

$$\mathrm{M}_{\bar{\Lambda},n} = \frac{1}{2\pi}\int_0^{2\pi}\left(\Lambda_1\cos^2(\phi)+\Lambda_2\sin^2(\phi)-\frac{\Lambda_1+\Lambda_2}{2}\right)^n \mathrm{d}\phi\,, \tag{C.1}$$

which can be further simplified to

$$\mathrm{M}_{\bar{\Lambda},n} = \left(\frac{\Lambda_1-\Lambda_2}{2}\right)^n \frac{1}{2\pi}\int_0^{2\pi}\cos^n(2\phi)\,\mathrm{d}\phi \tag{C.2}$$

by use of the relations between trigonometric functions and their powers. The first two central moments ($n=0$, $n=1$) are predetermined by definition. For $n\geq 2$, by partial integration and the identity $\sin^2(z)=1-\cos^2(z)$ one finds the recursive formula

$$\int\cos^n(z)\,\mathrm{d}z = \frac{n-1}{n}\int\cos^{n-2}(z)\,\mathrm{d}z+\frac{1}{n}\cos^{n-1}(z)\sin(z)\,, \tag{C.3}$$

which implies identity $(85)_1$ and thus allows to rewrite Eq. (C.2) as

$$\mathrm{M}_{\bar{\Lambda},n} = \begin{cases}\left(\dfrac{\Lambda_1-\Lambda_2}{2}\right)^n\displaystyle\prod_{k=1}^{\frac{n}{2}}\frac{2k-1}{2k} & \text{for } n \text{ is even,}\\[2ex] 0 & \text{for } n \text{ is odd,}\end{cases} \tag{C.4}$$

where in case $n=0$ we use the empty product convention returning $\mathrm{M}_{\bar{\Lambda},0}=1$.

Finally, we address the derivatives of the moments with respect to $\mathbf{C}$, required for the definition of stress and tangent stiffness. To this end, let

$$D := \left(\frac{\Lambda_1-\Lambda_2}{2}\right)^2 = \frac{I_1^2-4I_2}{4} = -\det(\mathbf{C}-\bar{\Lambda}\mathbf{I})\,, \tag{C.5}$$

for which one obtains

$$\frac{\partial D}{\partial\mathbf{C}} = \mathbf{C}-\bar{\Lambda}\mathbf{I}\,,\quad \frac{\partial^2 D}{\partial\mathbf{C}\partial\mathbf{C}} = \mathbf{I}\boxtimes\mathbf{I}-\frac{1}{2}\mathbf{I}\otimes\mathbf{I}\,, \tag{C.6}$$

where $\mathbf{I}\boxtimes\mathbf{I}=\partial\mathbf{C}/\partial\mathbf{C}$ in agreement with the definition (A.6). The derivatives of the non-zero moments in (C.4), i.e. even $n$, thus follow by the chain rule of differentiation, viz.

$$\frac{\partial \mathrm{M}_{\bar{\Lambda},n}}{\partial\mathbf{C}} = \frac{\partial \mathrm{M}_{\bar{\Lambda},n}}{\partial D}\frac{\partial D}{\partial\mathbf{C}}\,,\qquad \frac{\partial^2 \mathrm{M}_{\bar{\Lambda},n}}{\partial\mathbf{C}\partial\mathbf{C}} = \frac{\partial^2 \mathrm{M}_{\bar{\Lambda},n}}{\partial D^2}\frac{\partial D}{\partial\mathbf{C}}\otimes\frac{\partial D}{\partial\mathbf{C}}+\frac{\partial \mathrm{M}_{\bar{\Lambda},n}}{\partial D}\frac{\partial^2 D}{\partial\mathbf{C}\partial\mathbf{C}}\,. \tag{C.7}$$

## Appendix D. Invariant formulation of the moments of the affine isotropic stretch distribution

This appendix provides the moments $\mathrm{M}_{\bar{\Lambda},n}$ of the affine isotropic square stretch distribution of any order $n$ in closed form in terms of the invariants (88). The $n$th moment about $\bar{\Lambda}=\mathrm{E}[\Lambda]$ reads (Eq. (84))

$$\mathrm{M}_{\bar{\Lambda},n} = \sum_{p+q+r=n}\binom{n}{p,q,r}(\Lambda_1-\bar{\Lambda})^p(\Lambda_2-\bar{\Lambda})^q(\Lambda_3-\bar{\Lambda})^r\,\mathbb{H}_{n|2p,2q,2r}\,, \tag{D.1}$$

where in the isotropic case the expression for $\mathbb{H}_{n|2p,2q,2r}$ are given by Eq. (86). Making use of symmetries this can be written as

$$\mathrm{M}_{\bar{\Lambda},n} = \sum_{\substack{p+q+r=n\\ p\leq q\leq r}} w(p,q,r)\binom{n}{p,q,r}\frac{1}{6}\sum_{(i,j,k)\in\mathfrak{S}} a^i b^j c^k\,\mathbb{H}_{n|2p,2q,2r}\,, \tag{D.2}$$

where $\mathfrak{S}$ is the set containing all 6 permutations of $(p,q,r)$, and we abbreviated

$$a=(\Lambda_1-\bar{\Lambda})\,,\quad b=(\Lambda_2-\bar{\Lambda})\,,\quad c=(\Lambda_3-\bar{\Lambda})\,. \tag{D.3}$$

The term $w(p,q,r)$ evaluates to 1,3 or 6 for 3,2 or 1 unique elements in $(p,q,r)$, respectively, and results by considering the symmetries in the $n$th layer of Pascals' pyramid. As the inner sum in Eq. (D.2) is a symmetric polynomial in the eigenvalues of $\mathbf{C}$ it is an invariant of $\mathbf{C}$. One can write

$$\sum_{(i,j,k)\in\mathfrak{S}} a^i b^j c^k = (abc)^p\sum_{(i,j,k)\in\mathfrak{S}} a^{i-p}b^{j-p}c^{k-p}\,, \tag{D.4}$$

where each element of the sum on the right hand side contains at least one exponent that is 0. For the special cases $p = q$ or $q = r$ one has

$$\sum_{(i,j,k)\in\mathfrak{S}} a^i b^j c^k = 2(abc)^p \begin{cases} P_{r-q}, & p = q \\ Q_{q-p}, & q = r \end{cases}, \tag{D.5}$$

with the two power sums

$$P_m = a^m + b^m + c^m, \quad Q_m = (ab)^m + (bc)^m + (ca)^m. \tag{D.6}$$

For the remaining cases Eq. (D.4) can be further decomposed as

$$\begin{aligned} \sum_{(i,j,k)\in\mathfrak{S}} a^i b^j c^k &= (abc)^p \Big( Q_{q-p} P_{r-q} - \big( (ab)^{q-p} c^{r-q} + (bc)^{q-p} a^{r-q} + (ca)^{q-p} b^{r-q} \big) \Big) \\ &= (abc)^p \left( Q_{q-p} P_{r-q} - \begin{cases} (abc)^{q-p} P_{r-2q+p}, & r-q \geq q-p, \\ (abc)^{r-q} Q_{2q-p-r}, & r-q \leq q-p \end{cases} \right). \end{aligned} \tag{D.7}$$

One can now show that Eqs. (D.5) and (D.7) are polynomials of the invariants $A$ and $B$ (88). In fact, one obtains from Eqs. (88) and (D.3) that

$$(abc)^m = \left( \prod_{i=1}^{3} (\Lambda_i - \bar{\Lambda}) \right)^m = \left( \frac{2}{27} B \right)^m. \tag{D.8}$$

The power sums $P_0 = 3$ and $Q_0 = 3$ are directly obtained from (D.6), and the remaining $P_m$ and $Q_m$ can be resolved using Newton's identities as follows: For $P_m$

$$\begin{aligned} P_1 &= E_1, \\ P_2 &= E_1 P_1 - 2E_2, \\ P_3 &= E_1 P_2 - E_2 P_1 + 3E_3, \\ P_4 &= E_1 P_3 - E_2 P_2 + E_3 P_1, \\ P_5 &= E_1 P_4 - E_2 P_3 + E_3 P_2, \\ &\vdots \end{aligned} \tag{D.9}$$

and similarly for $Q_m$

$$\begin{aligned} Q_1 &= F_1, \\ Q_2 &= F_1 Q_1 - 2F_2, \\ &\vdots \end{aligned} \tag{D.10}$$

where

$$E_1 = a + b + c = \sum_{i=1}^{3} (\Lambda_i - \bar{\Lambda}) = 0, \quad E_2 = ab + bc + ca = \sum_{\substack{i,j=1 \\ j>i}}^{3} (\Lambda_i - \bar{\Lambda})(\Lambda_j - \bar{\Lambda}) = -\frac{A}{3}, \quad E_3 = abc = \frac{2}{27} B, \tag{D.11}$$

and

$$F_1 = ab + bc + ca = -\frac{A}{3}, \quad F_2 = abbc + bcca + caab = 0, \quad F_3 = abbcca = \left( \frac{2}{27} B \right)^2. \tag{D.12}$$

## Appendix E. Round-off errors in the computation of $A$ and $B$

The propagation of round-off errors in the computation of the invariants $A$ and $B$ is studied if they are calculated either from their relationship with the principal invariants (89) or as invariants of the tensor $\mathbf{C} - \bar{\Lambda}\mathbf{I}$ (Eq. (88)), respectively. We exemplify this by the states of deformation reflected by

$$\mathbf{C} = \mathbf{I} + a(0.1\, \boldsymbol{e}_1 \otimes \boldsymbol{e}_1 + 0.2\, \boldsymbol{e}_2 \otimes \boldsymbol{e}_2 + 0.4\, \boldsymbol{e}_3 \otimes \boldsymbol{e}_3), \tag{E.1}$$

where $a$ is varied from 0 to 1 in 99 equidistant steps. To illustrate the effect we implemented both formulations using float32 (single precision) and float64 (double precision) format. The difference between the two formulations using float64 was in the order of $10^{-14}$. However, evaluating the errors

$$\varepsilon^{(88)} = X^{(88)}_{\text{float32}} - X^{(88)}_{\text{float64}}, \quad \varepsilon^{(89)} = X^{(89)}_{\text{float32}} - X^{(88)}_{\text{float64}}, \tag{E.2}$$

for $X = A, B$, which are plotted as orange and blue lines in Fig. E.12, reveals the loss of accuracy when changing from float64 to float32. The results indicate that the accumulated error is markedly smaller when using the new formulation (88).

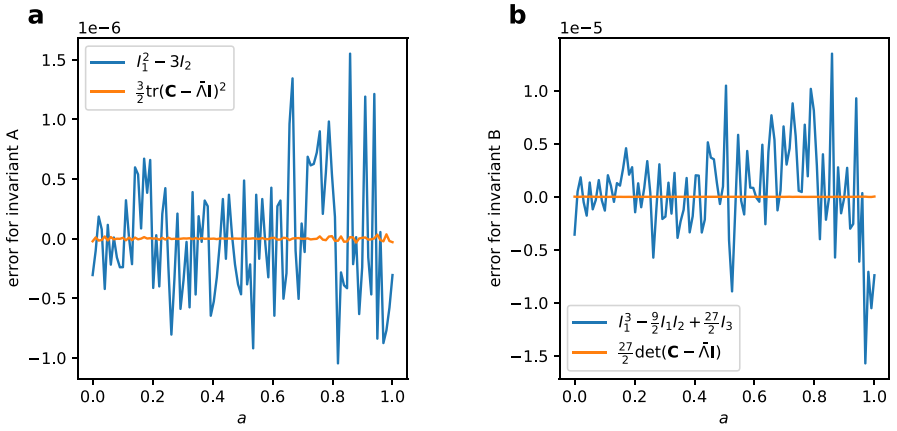


**Fig. E.12.** Error when using float32 compared to float64 in the computation of the invariants $A$ and $B$ from either Eq. (89) (blue) or Eq. (88) (orange).

## Appendix F. Integrals for analytical 3D integration

The integrals $\{\textcircled{i}\}_{i=3,\dots,20}$ are specified as

$$\begin{aligned}
\textcircled{3} &= \int_0^S \psi'_\Lambda(z_s)\, f((1-\alpha)s,\alpha)_{,\alpha}\,\mathrm{d}s, & \textcircled{4} &= \int_T^1 \psi''_\Lambda(z_t)\, t f(\alpha t, 1-\alpha)\,\mathrm{d}t,\\
\textcircled{5} &= \int_T^1 \psi'_\Lambda(z_t)\, f(\alpha t, 1-\alpha)_{,\alpha}\,\mathrm{d}t, & \textcircled{6} &= \int_0^S \psi''_\Lambda(z_s)\,(1-s) f((1-\alpha)s,\alpha)\,\mathrm{d}s,\\
\textcircled{7} &= \int_T^1 \psi''_\Lambda(z_t)\,(1-t) f(\alpha t, 1-\alpha)\,\mathrm{d}t, & \textcircled{8} &= \int_0^S \psi''_\Lambda(z_s)\, s f((1-\alpha)s,\alpha)\,\mathrm{d}s,
\end{aligned} \tag{F.1}$$

and

$$\begin{aligned}
\textcircled{9} &= \int_0^S \psi'_\Lambda(z_s)\, f((1-\alpha)s,\alpha)_{,\alpha\alpha}\,\mathrm{d}s, & \textcircled{10} &= \int_T^1 \psi'''_\Lambda(z_t)\, t^2 f(\alpha t, 1-\alpha)\,\mathrm{d}t,\\
\textcircled{11} &= \int_T^1 \psi''_\Lambda(z_t)\, t f(\alpha t, 1-\alpha)_{,\alpha}\,\mathrm{d}t, & \textcircled{12} &= \int_T^1 \psi'_\Lambda(z_t)\, f(\alpha t, 1-\alpha)_{,\alpha\alpha}\,\mathrm{d}t,\\
\textcircled{13} &= \int_0^S \psi''_\Lambda(z_s)\,(1-s) f((1-\alpha)s,\alpha)_{,\alpha}\,\mathrm{d}s, & \textcircled{14} &= \int_T^1 \psi'''_\Lambda(z_t)\,(1-t) t f(\alpha t, 1-\alpha)\,\mathrm{d}t,\\
\textcircled{15} &= \int_T^1 \psi''_\Lambda(z_t)\,(1-t) f(\alpha t, 1-\alpha)_{,\alpha}\,\mathrm{d}t, & \textcircled{16} &= \int_0^S \psi''_\Lambda(z_s)\, s f((1-\alpha)s,\alpha)_{,\alpha}\,\mathrm{d}s,\\
\textcircled{17} &= \int_0^S \psi'''_\Lambda(z_s)\,(1-s)^2 f((1-\alpha)s,\alpha)\,\mathrm{d}s, & \textcircled{18} &= \int_0^S \psi'''_\Lambda(z_s)\, s(1-s) f((1-\alpha)s,\alpha)\,\mathrm{d}s,\\
\textcircled{19} &= \int_T^1 \psi'''_\Lambda(z_t)\,(1-t)^2 f(\alpha t, 1-\alpha)\,\mathrm{d}t, & \textcircled{20} &= \int_0^S \psi'''_\Lambda(z_s)\, s^2 f((1-\alpha)s,\alpha)\,\mathrm{d}s.
\end{aligned} \tag{F.2}$$

## Appendix G. CDF-based integration of the isotropic 2D full-network

For the 2D case, the averaged energy of the affine full-network model (22) specifies to

$$\bar{\psi} = -\int_{\Lambda_2}^{\Lambda_1} \psi'_\Lambda(\mathrm{CDF}_\Lambda - 1)\,\mathrm{d}z + \psi_\Lambda(\Lambda_2)\,. \tag{G.1}$$

By use of the substitution in Remark 1 this becomes

$$\bar{\psi} = -(\Lambda_1 - \Lambda_2)\int_0^1 \psi'_\Lambda(z_y(y))\big(\mathrm{CDF}_{\lambda_\mathrm{n}}(y) - 1\big)2y\,\mathrm{d}y + \psi_\Lambda(\Lambda_2)\,, \tag{G.2}$$

where we have defined the function $z_y(y)$ such that

$$z_y : [0,1] \to [\Lambda_2, \Lambda_1]\,, \qquad z_y(y) = (\Lambda_1 - \Lambda_2)y^2 + \Lambda_2\,, \tag{G.3}$$

and the isotropic $\mathrm{CDF}_{\lambda_\mathrm{n}}$ is given in Table 1.

An important special case concerns a piece-wise defined $\psi_\Lambda$ that is zero for square stretches $\Lambda < 1$. In this case the lower integration bound in Eqs. (G.1) and (G.2) can be adjusted accordingly from $\Lambda_2$ to 1.

The normalised stretch $\lambda_\mathrm{n}$ and hence the isotropic $\mathrm{CDF}_{\lambda_\mathrm{n}}$ (Table 1) is independent of the specific values of the principal stretches $\{\Lambda_i\}$ and therefore $\mathbf{C}$, so that it is convenient to replace $(\mathrm{CDF}_{\lambda_\mathrm{n}}(y) - 1)2y =: f_2(y)$, and we deduce

$$\bar{\psi} = \psi_\Lambda(\Lambda_2) - (\Lambda_1 - \Lambda_2) \underbrace{\int_Y^1 \psi'_\Lambda(z_y(y)) f_2(y)\,\mathrm{d}y}_{①}, \tag{G.4}$$

where $Y = 0$ to consider all fibre contributions and to exclude fibres under compression

$$Y(\Lambda_1, \Lambda_2) = \begin{cases} 0 & \text{if } \Lambda_2 > 1, \\ \sqrt{\dfrac{1-\Lambda_2}{\Lambda_1 - \Lambda_2}} & \text{if } \Lambda_2 \le 1 < \Lambda_1, \\ 1 & \text{otherwise.} \end{cases} \tag{G.5}$$

To calculate stress, the derivatives

$$\bar{\psi}_{,\Lambda_1} = -① - (\Lambda_1 - \Lambda_2)②, \qquad \bar{\psi}_{,\Lambda_2} = \psi'_\Lambda(\Lambda_2) + ① - (\Lambda_1 - \Lambda_2)③ \tag{G.6}$$

will be needed, where it was used that the Leibniz-rule term for $a$ vanishes as $\psi_\Lambda(z_y(Y)) = 0$. The second derivatives, required for calculation of the tangent tensor, read

$$\begin{aligned} \bar{\psi}_{,\Lambda_1\Lambda_1} &= -2② - (\Lambda_1 - \Lambda_2)\left[④ - \psi''_\Lambda(1) Y^2 f_2(Y) Y_{,\Lambda_1}\right], \\ \bar{\psi}_{,\Lambda_1\Lambda_2} &= -③ + ② - (\Lambda_1 - \Lambda_2)\left[⑤ - \psi''_\Lambda(1) Y^2 f_2(Y) Y_{,\Lambda_2}\right], \\ \bar{\psi}_{,\Lambda_2\Lambda_2} &= \psi''_\Lambda(\Lambda_2) + 2③ - (\Lambda_1 - \Lambda_2)\left[⑥ - \psi''_\Lambda(1)\left(1 - Y^2\right) f_2(Y) Y_{,\Lambda_2}\right]. \end{aligned} \tag{G.7}$$

The integrals $\{(i)\}_{i=2,\dots,6}$ that define Eqs. (G.6) and (G.7) are given by

$$\begin{aligned} ② &= \int_Y^1 \psi''_\Lambda(z_y)\, y^2 f_2(y)\,\mathrm{d}y, & ③ &= \int_Y^1 \psi''_\Lambda(z_y)\,\left(1 - y^2\right) f_2(y)\,\mathrm{d}y, \\ ④ &= \int_Y^1 \psi'''_\Lambda(z_y)\, y^4 f_2(y)\,\mathrm{d}y, & ⑤ &= \int_Y^1 \psi'''_\Lambda(z_y)\, y^2\left(1 - y^2\right) f_2(y)\,\mathrm{d}y, \\ ⑥ &= \int_Y^1 \psi'''_\Lambda(z_y)\,\left(1 - y^2\right)^2 f_2(y)\,\mathrm{d}y. \end{aligned} \tag{G.8}$$

The numerical example shown in Figs. G.13 is analogous to the 3D example in Section 8.2, but uses 20 Gauss–Legendre integration points per required integral $\{(i)\}_{i=1,\dots,6}$ and, for comparison, a spherical integration with $N = 500$ integration points

$$\boldsymbol{M}_i = \cos\left(\frac{(2i+1)\pi}{2N}\right)\boldsymbol{e}_1 + \sin\left(\frac{(2i+1)\pi}{2N}\right)\boldsymbol{e}_2, \quad i = 1, 2, \dots, N \tag{G.9}$$

and equal weights $1/N$.

## Appendix H. Proof concerning elliptic integral Eq. (132)

We prove the equality (132) using three basic observations: First, by means of the incomplete elliptic integral the complete elliptic integral may be expressed as

$$\begin{aligned} \Pi(n|m) &= \Pi\left(n; \frac{\pi}{2}\middle|m\right) - \Pi(n; 0|m) = \Pi\left(n; \arccos\left(\sqrt{\frac{a\,t^2}{a + b(1-t^2)}}\right)\middle|m\right)\Bigg|_0^1 \\ &= \int_0^1 \frac{\mathrm{d}}{\mathrm{d}t}\Pi\left(n; \arccos\left(\sqrt{\frac{a\,t^2}{a + b(1-t^2)}}\right)\middle|m\right)\Bigg|_{t=\tau} \mathrm{d}\tau\,. \end{aligned} \tag{H.1}$$

Second, for the special choice of $n = -b/a$ and $m = b(a + b - 1)/a$ one has

$$\frac{\mathrm{d}}{\mathrm{d}t}\Pi\left(-\frac{b}{a}; \arccos\left(\sqrt{\frac{a\,t^2}{a + b(1-t^2)}}\right)\middle|\frac{b(a+b-1)}{a}\right) = \frac{\sqrt{a}}{a-b}\sqrt{\frac{a + b(1-t^2)}{1 - bt^2}}\frac{1}{\sqrt{1-t^2}}\,. \tag{H.2}$$

Finally, substitution of $t = \sin(\phi)$ and exploiting symmetry of the integrand yields

$$\int_0^1 \sqrt{\frac{a + b(1-\tau^2)}{1 - b\tau^2}}\frac{1}{\sqrt{1-\tau^2}}\,\mathrm{d}\tau = \frac{1}{2}\int_{-\pi/2}^{\pi/2}\sqrt{\frac{a + b\cos^2(\phi)}{1 - b\sin^2(\phi)}}\,\mathrm{d}\phi\,. \tag{H.3}$$

Hence by virtue of Eq. (H.3) insertion of Eq. (H.2) into Eq. (H.1) proves Eq. (132).

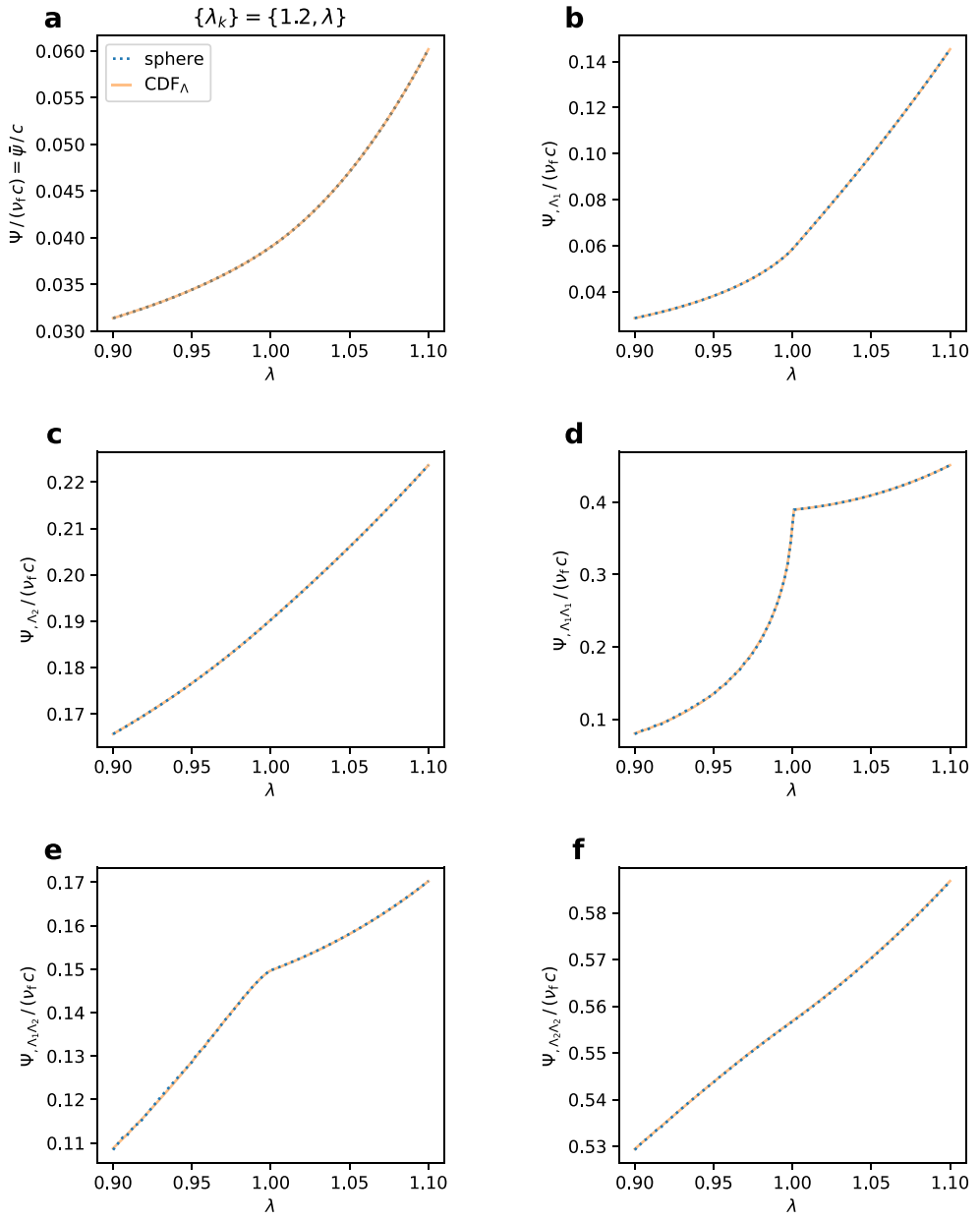


**Fig. G.13.** Comparison between CDF-based integration in 2D with 20 integration points (per integral 1–6) and spherical (circular) integration with 500 points: Averaged fibre energy (a), first (b, c) and second derivatives (d–f) based on Eqs. (G.4)–(G.8) vs. Eqs. (136), (137), (139), (140) specified for 2D.

## References

Abramowitz, M., Stegun, I.A., 1972. Handbook of Mathematical Functions with Formulas, Graphs, and Mathematical Tables. U S Department of Commerce.

Advani, S.G., Tucker, C.L., 1987. The use of tensors to describe and predict fiber orientation in short fiber composites. J. Rheol. 31 (8), 751–784. http://dx.doi.org/10.1122/1.549945.

Alastrué, V., Martínez, M.A., Doblaré, M., Menzel, A., 2009a. Anisotropic micro-sphere-based finite elasticity applied to blood vessel modelling. J. Mech. Phys. Solids 57 (1), 178–203. http://dx.doi.org/10.1016/j.jmps.2008.09.005.

Alastrué, V., Martínez, M.A., Menzel, A., Doblaré, M., 2009b. On the use of non-linear transformations for the evaluation of anisotropic rotationally symmetric directional integrals. Application to the stress analysis in fibred soft tissues. Internat. J. Numer. Methods Engrg. 79 (4), 474–504. http://dx.doi.org/10.1002/nme.2577.

Amores, V.J., Nguyen, K., Montáns, F.J., 2021. On the network orientational affinity assumption in polymers and the micro–macro connection through the chain stretch. J. Mech. Phys. Solids 148, 104279. http://dx.doi.org/10.1016/j.jmps.2020.104279.

Badel, P.-B., Leblond, J.-B., 2004. A note on integration schemes for the microplane model of the mechanical behaviour of concrete. Commun. Numer. Methods Eng. 20 (1), 75–81. http://dx.doi.org/10.1002/cnm.658.

Bažant, P., Oh, B.H., 1986. Efficient numerical integration on the surface of a sphere. ZAMM - J. Appl. Math. Mech. / Z. Angew. Math. Mech. 66 (1), 37–49. http://dx.doi.org/10.1002/zamm.19860660108.

Billiar, K.L., Sacks, M.S., 2000. Biaxial mechanical properties of the native and glutaraldehyde-treated aortic valve cusp: Part II–A structural constitutive model. J. Biomech. Eng. 122 (4), 327–335. http://dx.doi.org/10.1115/1.1287158.

Britt, B.R., Ehret, A.E., 2022. Constitutive modelling of fibre networks with stretch distributions. Part I: Theory and illustration. J. Mech. Phys. Solids 167, 104960. http://dx.doi.org/10.1016/j.jmps.2022.104960.

Burkardt, J., 2010. Sphere_Lebedev_Rule - Quadrature Rules for the Sphere. https://people.sc.fsu.edu/~jburkardt/datasets/sphere_lebedev_rule/sphere_lebedev_rule.html. [Accessed 24 Nov. 2022].

Chagnon, G., Rebouah, M., Favier, D., 2015. Hyperelastic energy densities for soft biological tissues: A review. J. Elasticity 120 (2), 129–160. http://dx.doi.org/10.1007/s10659-014-9508-z.

Chandran, P.L., Barocas, V.H., 2006. Affine versus non-affine fibril kinematics in collagen networks: theoretical studies of network behavior. J. Biomech. Eng. 128 (2), 259–270. http://dx.doi.org/10.1115/1.2165699.

Chawla, M.M., Kaul, V., 1973. Optimal rules for numerical integration round the unit circle. BIT Numer. Math. 13 (2), 145–152. http://dx.doi.org/10.1007/BF01933486.

Cortes, D.H., Elliott, D.M., 2014. Accurate prediction of stress in fibers with distributed orientations using generalized high-order structure tensors. Mech. Mater. 75, 73–83. http://dx.doi.org/10.1016/j.mechmat.2014.04.006.

Durrett, R., 2019. Probability: Theory and Examples, fifth ed. In: Cambridge Series in Statistical and Probabilistic Mathematics, Cambridge University Press, Cambridge, http://dx.doi.org/10.1017/9781108591034.

Ehret, A.E., Bircher, K., Stracuzzi, A., Marina, V., Zündel, M., Mazza, E., 2017. Inverse poroelasticity as a fundamental mechanism in biomechanics and mechanobiology. Nature Commun. 8 (1), 1002. http://dx.doi.org/10.1038/s41467-017-00801-3.

Ehret, A.E., Itskov, M., Schmid, H., 2010. Numerical integration on the sphere and its effect on the material symmetry of constitutive equations—A comparative study. Int. J. Numer. Methods Eng. 81 (2), 189–206. http://dx.doi.org/10.1002/nme.2688.

Fan, R., Sacks, M.S., 2014. Simulation of planar soft tissues using a structural constitutive model: Finite element implementation and validation. J. Biomech. 47 (9), 2043–2054. http://dx.doi.org/10.1016/j.jbiomech.2014.03.014.

Federico, S., Herzog, W., 2008. Towards an analytical model of soft biological tissues. J. Biomech. 41 (16), 3309–3313. http://dx.doi.org/10.1016/j.jbiomech.2008.05.039.

Freed, A.D., Einstein, D.R., Vesely, I., 2005. Invariant formulation for dispersed transverse isotropy in aortic heart valves. Biomech. Model. Mechanobiol. 4 (2), 100–117. http://dx.doi.org/10.1007/s10237-005-0069-8.

Freeden, W., Gutting, M., 2017. Integration and Cubature Methods : a Geomathematically Oriented Course. Chapman and Hall/CRC, http://dx.doi.org/10.1201/9781315195674.

Gasser, T.C., Ogden, R.W., Holzapfel, G.A., 2006. Hyperelastic modelling of arterial layers with distributed collagen fibre orientations. J. R. Soc. Interface 3 (6), 15–35. http://dx.doi.org/10.1098/rsif.2005.0073.

Gizzi, A., Pandolfi, A., Vasta, M., 2016. Statistical characterization of the anisotropic strain energy in soft materials with distributed fibers. Mech. Mater. 92, 119–138. http://dx.doi.org/10.1016/j.mechmat.2015.09.008.

Gizzi, A., Pandolfi, A., Vasta, M., 2018. A generalized statistical approach for modeling fiber-reinforced materials. J. Eng. Math. 109 (1), 211–226. http://dx.doi.org/10.1007/s10665-017-9943-5.

Gizzi, A., Vasta, M., Pandolfi, A., 2014. Modeling collagen recruitment in hyperelastic bio-material models with statistical distribution of the fiber orientation. Internat. J. Engrg. Sci. 78, 48–60. http://dx.doi.org/10.1016/j.ijengsci.2014.02.008.

Goldberg, N., Ihlemann, J., 2017. On an alternative modelling of distributed fibre directions. Int. J. Solids Struct. 126–127, 140–149. http://dx.doi.org/10.1016/j.ijsolstr.2017.07.030.

Hannay, J.H., Nye, J.F., 2004. Fibonacci numerical integration on a sphere. J. Phys. A: Math. Gen. 37 (48), 11591. http://dx.doi.org/10.1088/0305-4470/37/48/005.

Hashlamoun, K., Federico, S., 2017. Transversely isotropic higher-order averaged structure tensors. Z. Angew. Math. Phys. 68 (4), 88. http://dx.doi.org/10.1007/s00033-017-0830-8.

Hashlamoun, K., Grillo, A., Federico, S., 2016. Efficient evaluation of the material response of tissues reinforced by statistically oriented fibres. Z. Angew. Math. Phys. 67 (5), 113. http://dx.doi.org/10.1007/s00033-016-0704-5.

Holzapfel, G.A., 2000. Nonlinear Solid Mechanics: a Continuum Approach for Engineering. Wiley.

Holzapfel, G.A., Niestrawska, J.A., Ogden, R.W., Reinisch, A.J., Schriefl, A.J., 2015. Modelling non-symmetric collagen fibre dispersion in arterial walls. J. R. Soc. Interface 12 (106), 20150188. http://dx.doi.org/10.1098/rsif.2015.0188.

Holzapfel, G.A., Ogden, R.W., 2015. On the Tension–Compression switch in soft fibrous solids. Eur. J. Mech. A Solids 49, 561–569. http://dx.doi.org/10.1016/j.euromechsol.2014.09.005.

Holzapfel, G.A., Ogden, R.W., 2017. On fiber dispersion models: exclusion of compressed fibers and spurious model comparisons. J. Elasticity 129 (1), 49–68. http://dx.doi.org/10.1007/s10659-016-9605-2.

Horgan, C.O., Murphy, J.G., 2020. On the tension-compression switch hypothesis in arterial mechanics. J. Mech. Behav. Biomed. Mater. 103, 103558. http://dx.doi.org/10.1016/j.jmbbm.2019.103558.

Itskov, M., 2016. On the accuracy of numerical integration over the unit sphere applied to full network models. Comput. Mech. 57 (5), 859–865. http://dx.doi.org/10.1007/s00466-016-1265-3.

Itskov, M., 2019. Tensor Algebra and Tensor Analysis for Engineers: with Applications To Continuum Mechanics. In: Mathematical Engineering, Springer International Publishing, Cham, http://dx.doi.org/10.1007/978-3-319-98806-1.

Itskov, M., Ehret, A.E., Dargazany, R., 2010. A full-network rubber elasticity model based on analytical integration. Math. Mech. Solids 15 (6), 655–671. http://dx.doi.org/10.1177/1081286509106441.

Itskov, M., Knyazeva, A., 2016. A rubber elasticity and softening model based on chain length statistics. Int. J. Solids Struct. 80, 512–519. http://dx.doi.org/10.1016/j.ijsolstr.2015.10.011.

Johnson, N.L., Kotz, S., Balakrishnan, N., 1994. Continuous Univariate Distributions, Volume 1. Wiley.

Kanatani, K.-I., 1984. Stereological determination of structural anisotropy. Internat. J. Engrg. Sci. 22 (5), 531–546. http://dx.doi.org/10.1016/0020-7225(84)90055-7.

Kassab, G.S., Sacks, M.S. (Eds.), 2016. Structure-Based Mechanics of Tissues and Organs. Springer US, Boston, MA, http://dx.doi.org/10.1007/978-1-4899-7630-7.

Ken-Ichi, K., 1984. Distribution of directional data and fabric tensors. Internat. J. Engrg. Sci. 22 (2), 149–164. http://dx.doi.org/10.1016/0020-7225(84)90090-9.

Lanir, Y., 1979. A structural theory for the homogeneous biaxial stress-strain relationships in flat collagenous tissues. J. Biomech. 12 (6), 423–436. http://dx.doi.org/10.1016/0021-9290(79)90027-7.

Latorre, M., Montáns, F.J., 2016. On the tension-compression switch of the Gasser–Ogden–Holzapfel model: Analysis and a new pre-integrated proposal. J. Mech. Behav. Biomed. Mater. 57, 175–189. http://dx.doi.org/10.1016/j.jmbbm.2015.11.018.

Li, K., Ogden, R.W., Holzapfel, G.A., 2018a. A discrete fibre dispersion method for excluding fibres under compression in the modelling of fibrous tissues. J. R. Soc. Interface 15 (138), 20170766. http://dx.doi.org/10.1098/rsif.2017.0766.

Li, K., Ogden, R.W., Holzapfel, G.A., 2018b. Modeling fibrous biological tissues with a general invariant that excludes compressed fibers. J. Mech. Phys. Solids 110, 38–53. http://dx.doi.org/10.1016/j.jmps.2017.09.005.

Melnik, A.V., Borja Da Rocha, H., Goriely, A., 2015. On the modeling of fiber dispersion in fiber-reinforced elastic materials. Int. J. Non-Linear Mech. 75, 92–106. http://dx.doi.org/10.1016/j.ijnonlinmec.2014.10.006.

Miehe, C., 1996. Numerical computation of algorithmic (consistent) tangent moduli in large-strain computational inelasticity. Comput. Methods Appl. Mech. Engrg. 134 (3), 223–240. http://dx.doi.org/10.1016/0045-7825(96)01019-5.

Miehe, C., 1998. Comparison of two algorithms for the computation of fourth-order isotropic tensor functions. Comput. Struct. 66 (1), 37–43. http://dx.doi.org/10.1016/S0045-7949(97)00073-4.

Pandolfi, A., Vasta, M., 2012. Fiber distributed hyperelastic modeling of biological tissues. Mech. Mater. 44, 151–162. http://dx.doi.org/10.1016/j.mechmat.2011.06.004.

Pérez-Foguet, A., Rodríguez-Ferran, A., Huerta, A., 2000. Numerical differentiation for local and global tangent operators in computational plasticity. Comput. Methods Appl. Mech. Engrg. 189 (1), 277–296. http://dx.doi.org/10.1016/S0045-7825(99)00296-0.

Puso, M., 2003. Mechanistic Constitutive Models for Rubber Elasticity and Viscoelasticity. Technical Report UCRL-ID-151578, Lawrence Livermore National Lab., CA (US), http://dx.doi.org/10.2172/15004918.

Rubin, M., 2021. Continuum Mechanics with Eulerian Formulations of Constitutive Equations. In: Solid Mechanics and Its Applications, vol. 265, Springer International Publishing, Cham, http://dx.doi.org/10.1007/978-3-030-57776-6.

Stracuzzi, A., Britt, B.R., Mazza, E., Ehret, A.E., 2022. Risky interpretations across the length scales: Continuum vs. Discrete models for soft tissue mechanobiology. Biomech. Model. Mechanobiol. 21 (2), 433–454. http://dx.doi.org/10.1007/s10237-021-01543-4.

Treloar, L.R.G., Riding, G., Gee, G., 1979. A non-Gaussian theory for rubber in biaxial strain. I. Mechanical properties. Proc. R. Soc. Lond. Ser. A Math. Phys. Eng. Sci. 369 (1737), 261–280. http://dx.doi.org/10.1098/rspa.1979.0163.

Truesdell, C., Noll, W., 2004. The non-linear field theories of mechanics. In: Truesdell, C., Noll, W., Antman, S.S. (Eds.), The Non-Linear Field Theories of Mechanics. Springer, Berlin, Heidelberg, pp. 1–579. http://dx.doi.org/10.1007/978-3-662-10388-3_1.

Vasta, M., Gizzi, A., Pandolfi, A., 2014. On three- and two-dimensional fiber distributed models of biological tissues. Probab. Eng. Mech. 37, 170–179. http://dx.doi.org/10.1016/j.probengmech.2014.05.003.

Vasta, M., Gizzi, A., Pandolfi, A., 2018. A spectral decomposition approach for the mechanical statistical characterization of distributed fiber-reinforced tissues. Int. J. Non-Linear Mech. 106, 258–265. http://dx.doi.org/10.1016/j.ijnonlinmec.2018.06.010.

Verron, E., 2015. Questioning numerical integration methods for microsphere (and microplane) constitutive equations. Mech. Mater. 89, 216–228. http://dx.doi.org/10.1016/j.mechmat.2015.06.013.

Wu, P.D., Van Der Giessen, E., 1993. On improved network models for rubber elasticity and their applications to orientation hardening in glassy polymers. J. Mech. Phys. Solids 41 (3), 427–456. http://dx.doi.org/10.1016/0022-5096(93)90043-F.

Zündel, M., Mazza, E., E. Ehret, A., 2017. A 2.5D approach to the mechanics of electrospun fibre mats. Soft Matter 13 (37), 6407–6421. http://dx.doi.org/10.1039/C7SM01241A.